Mechanisms and Modelling of Gas Separations Through Ceramic Membranes in Chemical Reaction Processes

A thesis submitted for the degree of

Doctor of Philosophy

of the University of London

by

Suttichai Assabumrungrat

Department of Chemical Engineering
and Chemical Technology
Imperial College of Science, Technology and
Medicine
LONDON SW7 2BY
UNITED KINGDON

September 1996

BIBL. LONDIN. IMPER.

ABSTRACT

The thesis is concerned with high temperature permeation of some gases and organic vapours through commercially available 'Membralox' ceramic membranes. General information on the membranes, their applications and membrane preparation are discussed. Transport mechanisms through these porous membranes and literature reviews on surface diffusion and membrane reactor are provided. A simple apparatus which requires simple flow measurement was designed and built for experimental studies. Permeation rates of pure nitrogen and hydrogen gases were measured through the membranes with pore diameter of 4 and 10 nm at 5 temperature levels ranging from the room temperature to 200 ^{o}C. A model based on the combination of Knudsen diffusion and viscous flow was developed to describe the transport rate. This model is used to predict gas phase transport rate of other gases.

Permeation of some strongly chemisorbed vapours; such as those of methanol and ethanol, through the alumina membranes with the same pore size were conducted at three temperature levels between 150 to 200 ^{o}C. Their permeabilities were found to be less than those predicted from the previous model and can be described by a new model based on the assumption that the adsorbed film does not make a contribution to the total flow. The validity of the model was checked by permeation studies of mixtures of nitrogen gas with alocohol vapours.

Experimental studies also included the case where adsorption on the membrane was not so strong. Permeation of isopropanol and acetone through the membrane with pore diameter of 4 nm were measured at three temperature levels from 160 to 200 ^{o}C. A model taking into account surface diffusion was developed and checked with the results from the permeation studies of

mixtures of nitrogen gas and the vapour of the organic species. The model was further extended to predict the permeation of mixtures of isopropanol and acetone, and was verified by experimental results.

The models developed to describe the transport rate of the already-mentioned organic vapours can be applied in the prediction of the behaviour of endothermic catalytic reactions occurring within such membranes. In this thesis the modelling of the dehydrogenation of isopropanol to acetone in an alumina membrane is considered.

To my Father in Heaven

and to my family on Earth

ACKNOWLEDGEMENT

I would like to express my sincere gratitude to my supervisor, Dr. D. A. White for his help and guidance throughout my MSc and PhD courses over the last four years. This thesis is an immeasurably better document because of him. I would like also to thank the staff of the Chemical Engineering Department who have helped me in all sorts of ways. My financial support which was provided by the British Council is gratefully acknowledged.

I am very grateful to all my friends in our research group for making my work really pleasant and enjoyable. Special thanks to my colleagues in the 'Nuclear Tech' lab, Ahmad, Guy, Radu, Ed, Rachmann, Solomon, Yinka and Yung; some of whom have already finished their studies.

Finally I would like to take this opportunity to thank all my Thai friends here, especially Sert and Wit for their friendship, help and encouragement and all sort of things.

TABLE OF CONTENTS

	Page
ABSTRACT	2
DEDICATION	4
ACKNOWLEDGEMENT	5
TABLE OF CONTENTS	6
LIST OF FIGURES	9
LIST OF TABLES	13
NOTATION	14
CHAPTER 1 INTRODUCTION	17
1.1 Membrane Definition	18
1.2 Membrane Geometries	19
1.3 Membrane Applications	21
1.3.1 Membranes for Separation Purposes	21
1.3.2 Membranes for Other Purposes	23
1.3.3 Membrane Technologies Under Development	23
1.4 Inorganic Membranes	24
1.4.1 Overview	24
1.4.2 Preparation of Porous Membranes	27
CHAPTER 2 THEORY OF GAS PERMEATION	32
2.1 Transport Mechanisms Through Porous Membranes	33
2.1.1 Viscous Bulk Flow	33
2.1.2 Knudsen Diffusion	35
2.1.3 Surface Diffusion	36
2.1.4 Capillary Condensation	37
2.1.5 Molecular Sieving	39
2.2 Gas Phase Flow Through Alumina Membranes	40

		Page
CHAPTER 3	**LITERATURE REVIEWS**	43
	3.1 Surface Diffusion	44
	3.2 Membrane Reactors	54
CHAPTER 4	**EXPERIMENTAL STUDIES OF PURE GAS PERMEATION**	61
	4.1 Introduction	62
	4.2 Description of Experimental System	62
	4.3 Results and Discussion	64
	4.4 Prediction of Permeability of Other Gases	67
	4.5 Conclusion	69
CHAPTER 5	**EXPERIMENTAL STUDIES OF ETHANOL AND METHANOL VAPOUR PERMEATION**	70
	5.1 Introduction	71
	5.2 Description of Experimental System	71
	5.3 Model Development	73
	5.4 Results and Discussion	77
	5.5 Conclusion	87
CHAPTER 6	**EXPERIMENTAL STUDIES OF ACETONE AND ISOPROPANOL PERMEATION**	88
	6.1 Introduction	89
	6.2 Description of Experimental System	89
	6.3 Model Development	90
	6.4 Results and Discussion	93
	6.5 Prediction of Permeation of Pure Isopropanol and Acetone Vapours	99
	6.6 Prediction of Mixture of Organic Vapour Permeation	101
	6.7 Conclusions	103

	Page
CHAPTER 7 APPLICATION ON THE DEHYDROGENATION OF ISOPROPANOL TO ACETONE IN AN ALUMINA MEMBRANE REACTOR	104
7.1 Introduction	105
7.2 Modelling of a Membrane Reactor	106
7.3 Solving the Rate Equations	110
7.4 Results and Discussion	111
7.5 Conclusion	124
CHAPTER 8 CONCLUSIONS AND SUGGESTIONS FOR FUTURE WORK	125
8.1 Conclusions	126
8.2 Suggestions for Future Work	127
APPENDICES	130
APPENDIX 1 CHARACTERISTICS OF THE MONOTUBE MEMBRALOX MULTILAYER ALUMINA MEMBRANES	131
APPENDIX 2 MOLECULAR DIAMETER AND MEAN FREE PATH OF SOME GASES AND VAPOURS	134
APPENDIX 3 SATURATION PRESSURE OF SOME ORGANIC VAPOURS	136
APPENDIX 4 ERROR ANALYSIS FOR EXPERIMENTAL DATA	138A
REFERENCES	139

LIST OF FIGURES

Figure		Page
2.1	Transport mechanisms through a porous membrane	34
3.1	The apparatus for transient studies and an experimental result	45
3.2	Experimental setup of 'square-pulse' method	46
3.3	Trajectory of a molecule on a solid surface	51
3.4	Membrane reactor configurations	55
4.1	The schematic diagram of experimental setup for gas permeation measurement	63
4.2	Nitrogen gas permeability through the membrane with 4 nm membrane pore size	65
4.3	Nitrogen gas permeability through the membrane with 10 nm membrane pore size	65
4.4	Knudsen parameters from N_2 experiments	66
4.5	Viscous flow parameters from N_2 experiments	67
4.6	Hydrogen gas permeability through the membrane with 4 nm membrane pore size	68
4.7	Hydrogen gas permeability through the membrane with 10 nm membrane pore size	68
5.1	The schematic diagram of experimental setup for vapour permeation measurement	72
5.2	Cross sectional of a membrane pore	75
5.3	Permeability of pure ethanol vapour through the alumina membrane with 10 nm pore size	79
5.4	Permeability of pure ethanol vapour through the alumina membrane with 4 nm pore size	79
5.5	Permeability of pure methanol vapour through the alumina membrane with	

Figure		Page
	10 nm pore size	80
5.6	Permeability of pure methanol vapour through the alumina membrane with 4 nm pore size	80
5.7	The relation between ω and feed pressure (From pure ethanol vapour permeation through the membrane with 10 nm pore size)	82
5.8	The relation between ω and feed pressure (From pure ethanol vapour permeation through the membrane with 4 nm pore size)	82
5.9	The relation between ω and feed pressure (From pure methanol vapour permeation through the membrane with 10 nm pore size)	83
5.10	The relation between ω and feed pressure (From pure methanol vapour permeation through the membrane with 4 nm pore size)	83
5.11	Experimental results from the mixtures of nitrogen gas and ethanol vapour through the membrane with 10 nm pore size	85
5.12	Experimental results from the mixtures of nitrogen gas and ethanol vapour through the membrane with 4 nm pore size	85
5.13	Experimental results from the mixtures of nitrogen gas and methanol vapour through the membrane with 10 nm pore size	86
5.14	Experimental results from the mixtures of nitrogen gas and methanol vapour through the membrane with 4 nm pore size	86

Figure		Page
6.1	Permeability of pure isopropanol through the alumina membrane with 4 nm pore size	94
6.2	Experimental results from the mixtures of nitrogen gas and isopropanol vapour through the membrane with 4 nm pore size (gas phase flow model)	95
6.3	Experimental results from the mixtures of nitrogen gas and isopropanol vapour through the membrane with 4 nm pore size (Fick's law model)	97
6.4	Permeability of pure acetone through the alumina membrane with 4 nm pore size	98
6.5	Experimental results from the mixtures of nitrogen gas and acetone vapour through the membrane with 4 nm pore size (Fick's law model)	99
6.6	Experimental results from the mixtures of isopropanol and acetone vapours through the membrane with 4 nm pore size	102
7.1	The membrane reactor configuration	106
7.2	Effect of reaction side pressure on the performance of membrane reactor	112
7.3	Effect of reactor diameter on the performance of membrane reactor	113
7.4	Effect of sweep ratio on the performance of membrane reactor	114
7.5	Effect of mode of operation on the performance of membrane reactor	116
7.6	Partial pressure of hydrogen along the membrane	117
7.7	Partial pressure of isopropanol along the membrane	117
7.8	Partial pressure of acetone along the membrane	118
7.9	Effect of operating temperature on the performance of membrane reactor	119

Figure		Page
7.10	Effect of rate of reaction on the performance of membrane reactor	120
7.11	Effect of pressure on permeability ratio of hydrogen and isopropanol	122
7.12	Effect of pressure on permeability ratio of hydrogen and acetone	123
7.13	Effect of pressure on permeability ratio of acetone and isopropanol	123
7.14	Effect of temperature on permeability ratio	124

LIST OF TABLES

Table		Page
1.1	Membrane separation processes	22
1.2	Commercially available porous membranes	26
3.1	Some reactions using membrane reactors	57
5.1	Fitting parameters at different temperature from the studies of ethanol permeation	81
5.2	Fitting parameters at different temperature from the studies of methanol permeation	81
6.1	Fitting parameters of gas phase flow model for the permeation of isopropanol	94
6.2	Fitting parameters with the Fick's law model for the permeation of isopropanol	96
6.3	Fitting parameters with the H.I.O. model for the permeation of isopropanol	96
6.4	Fitting parameters with the Fick's law model for the permeation of acetone	98
6.5	Surface diffusion parameters	100
7.1	Summary of input parameters used for membrane reactor model	111
A1.1	Characteristics of a membrane with 4 nm pore size	131
A1.2	Permeability of each membrane layer	132
A2.1	Molecular diameter of some gases and vapours	135
A2.2	Mean free path of some gases and vapours	135
A3.1	Saturation pressure of ethanol	137
A3.2	Saturation pressure of methanol	137
A3.3	Saturation pressure of isopropanol	137
A3.4	Saturation pressure of acetone	138
A4.1	Error analysis of parameters a and b for the membrane with pore size of 4 and 10 nm	138C

Nomenclature

a	Knudsen parameter defined in Equation (2.15) $(mol.g.K)^{1/2}/m.sec.kPa$
b	Viscous parameter defined in Equation (2.15) (mol.K/m.kPa)
C_R	Coefficient in Equation (3.5)
d_n	Membrane pore diameter after adsorption by organic vapour (m)
d_o	Membrane pore diameter before adsorption by organic vapour (m)
d_p	Membrane pore diameter (m)
D_a	Apparent diffusivity (m^2/sec)
D_e	Effective diffusivity (m^2/sec)
D_F	Parameter in Equation (6.10) (mol/m.sec.kPa)
D_F^o	Parameter in Equation (6.17) (mol/m.sec.kPa)
D_H	Parameter in Equation (6.12) (mol/m.sec)
D_I	Inner diameter of membrane reactor (m)
D_K	Knudsen diffusivity (m^2/sec)
D_o	Outer diameter of membrane reactor (m)
D_s	Surface diffusion coefficient (m^2/sec)
D_s^o	Parameter in Equation (6.7) (m^2/sec)
E_s	Activation energy of surface diffusion (kJ/mol)
F_i	Molar flow rate of species i (mol/sec)
J_i	Molar flux of species i ($mol/m^2.sec$)
k_o	Reaction rate constant ($m^3kPa/kg.sec$)
K'	Parameter in Langmuir isotherm (mol/kg.kPa)
K	Parameter in Langmuir isotherm (kPa^{-1})
K_a	Adsorption parameter in Equation (7.12) (kPa^{-1})
K_d	Constant in Equation (2.7)
K_p	Reaction equilibrium constant (kPa)
l	Axial distance (m)
L	Length of the membrane (m)
M_i	Molecular weight of species i
n	Number of membrane pore per unit area (m^{-2})
N_i	Molar flow rate of species i in the feed side (mol/sec)

p	Pressure at any distance in membrane (kPa)
p_c	Capillary suction pressure (kPa)
p_o	Saturation pressure in a planar surface (kPa)
p_p	Saturation pressure in a membrane pore (kPa)
p_i	Partial pressure of species i (kPa)
p_1	Feed side pressure (kPa)
p_2	Permeate side pressure (kPa)
P	Permeability defined in Equation (2.15) (mol/m.sec.kPa)
q_i	Adsorption isotherm of species i (mol/kg)
Q_i	Molar flow rate of species i in the permeate side(mol/sec)
Q_{st}	Heat of adsorption (kJ/mol)
r	Radial distance of the membrane (m)
r_{ace}	Rate of formation of acetone ($mol/m^3.sec$)
r_h	Rate of surface migration ($mol/m^2.sec$)
R	Universal gas constant
R^2	Goodness of fitting
R_K	Parameter defined in Equation (2.9) (mol/sec.m.kPa)
R_V	Parameter defined in Equation (2.9) ($mol/sec.m.kPa^2$)
S_t	Specific surface area of the membrane (m^2/kg)
t	Thickness of the adsorbed film (m)
T	Temperature (K)
v^o	Initial velocity of a molecule on membrane surface (m/sec)
V_t	Specific volume of adsorbate (m^3/mol)
W	Constant in Equation (3.8)
x_i	Composition of species i in the feed side
y_i	Composition of species i in the permeate side
z	Axial distance along the membrane (m)
Z	Thickness of the membrane (m)

Subscripts

alc	Alcohol
ace	Acetone

c	Capillary condensation
iso	Isopropanol
g	Gas phase
K	Knudsen
org	Organic species
s	Surface phase
V	Viscous flow

Greek Letters

α	Separation factor
χ	Parameter in Equation (5.10) (kPa^{-1})
χ°	Constant in Equation (6.16) (kPa^{-1})
ϕ	Fraction of the membrane area blocked by adsorption of organic
φ	Jumping angle of a molecule on membrane surface
λ	Mean free path of a molecule (m)
μ	Viscosity (kPa.s)
ν_i	Stoichiometric coefficient of species i
ω	Dimensionless parameter in equation (5.9)
θ	Surface coverage
ρ	Density of condensate (kg/m^3)
ρ_{app}	Apparent density of the membrane (kg/m^3)
ρ_b	Density of catalyst bed (kg/m^3)
σ	Surface tension (kg/sec^2)
τ_g	Tortuosity of the pores for gas phase flow
τ_s	Tortuosity of the pores for surface flow
ψ	Contact angle of the condensed liquid on the solid
ξ	Relaxation constant

CHAPTER 1

INTRODUCTION

1.1 Membrane Definition

1.2 Membrane Geometries

1.3 Membrane Applications

1.3.1 Membranes for Separation Purposes

1.3.2 Membranes for Other Purposes

1.3.3 Membrane Technologies Under Development

1.4 Inorganic Membranes

1.4.1 Overview

1.4.2 Preparation of Porous Membranes

CHAPTER 1

INTRODUCTION

1.1 Membrane Definition

A membrane is an interface between two bulk phases and it controls the exchange of mass with differing chemical and physical properties between them. The membrane phase can be one or a combination of the following: a nonporous solid, microporous or macroporous solid with a fluid in the pores, a liquid phase with or without a second phase, or a gel (Winston and Sirkar, 1990). The exchange between the two bulk phases across the membrane are caused from the presence of a driving force. The most common of these are chemical potential, pressure, concentration gradients and cell voltage.

Because of the fact that different species move across a membrane with different rates, the membrane is used in many separation processes. A mixture of many species is introduced to one bulk phase called the feed side and each species permeates through the membrane to the other bulk phase or permeate side at different rate. To show the ability of the separation, the parameter 'Selectivity' or 'Separation factor' is defined as follows.

$$\alpha_{ij} = \frac{c_i'' / c_j''}{c_i' / c_j'} \qquad (1.1)$$

where c denotes to concentration, and superscript prime (') and double prime (") show properties of feed side and permeate side, respectively. i and j are the two permeating species.

1.2 Membrane Geometries

Membranes for laboratory and commercial use are available in many geometries. Each one has its own advantages and disadvantages. Matson *et al.* (1983) classified membrane geometries into the following four groups.

1) Ultrathin films
2) Asymmetric membranes
3) Hollow fibres
4) Composites and coated structure

Because the flux across a membrane varies inversely with its thickness, membranes should be manufactured as thin as possible. This, however, means that the membrane has poor mechanical properties. These films are thus applied in two-layer laminates, where the thin selective film is supported by a microporous backing membrane. This support provides mechanical strength and protects the thin separative element. Selection of the support membrane is based on two important principles. Firstly, the transport resistance should be minimised, in other words it must be made sufficiently porous. Nevertheless its pores must be small enough that the bursting strength of the thin membrane is not exceeded where it spans the opening of any pore in the support. The other factor is that the support should have the maximum mechanical strength possible. One early production method involved using a clean glass plate which was immersed in a dilute polymer solution and then withdrawn. After excess solvent had evaporated, a thin coating remained and could be removed from the plate by immersion in water for example. The thin film, floating on the water surface can be carefully picked up on a microporous support. A new technique to improve this method casts the membrane on surface of a fluid rather than on a solid. This can solve the difficulty of separating the film from the plate.

Introduction of small-diameter hollow-fibre membranes in the 1960's represented an important advance in membrane fabrication technology. These membranes provide larger surface area in very small compact devices and packing densities as high as several thousand m^2/m^3 of permeator, whereas plate-and-flame, tubular, and spiral-wounded membrane modules permit packing densities no higher than a few hundred m^2/m^3 of permeator. In capillary modules the feed is normally on the shell side. In addition they are relatively inexpensive since the need for membrane supports, separator screens, and associated hardware is eliminated or reduced. However, substantial pore-side pressure drop occurs, leading to reduction of the transmembrane pressure ratio and the module separation factor. The drawbacks of the hollow fibres are fewer in the case of gas separation than in reverse osmosis and ultrafiltration, where plugging of the fibre lumen and shell-side polarisation are more severe. The earliest fibres had solid walls and their permeability was low. After the combination with asymmetric and composite fibres, the performance of this membrane type is even better.

Compared with membrane geometries discussed above, composites and coated structures show more intimate relationship between the thin coating and the substrate. The coating is frequently found extending some distance into the porous substrate and the two layers are generally inseparable. Preparation of these membrane was first carried by casting a thin layer of solution directly over a microporous support and then allowing the solvent to evaporate. This process had several disadvantages such as the difficulty of controlling the production of uniform thin yet defect-free coatings. A new alternative is to dip one side of the membrane into a solution which contains the monomer and cross-linking agent and allows them to react at elevated temperature. This membrane can be

further categorised according to whether the coating or the substrate controls the permeation properties of the composite.

In a glassy asymmetric membrane, its surface layer typically exhibits surface porosity. Such pores and membrane defects can significantly decrease selectivity, and membrane post-treatments designed to close them are not always satisfactory. This deficiency can be solved by introducing elastomeric coatings on and within the surface of the asymmetric hollow fibres. The elastomer behaves as filler in the surface pores and defects, while glassy and inherently more selective substrate material controls the separation.

1.3 Membrane Applications

This section will deal with applications of membrane which will be classified into the three following groups.

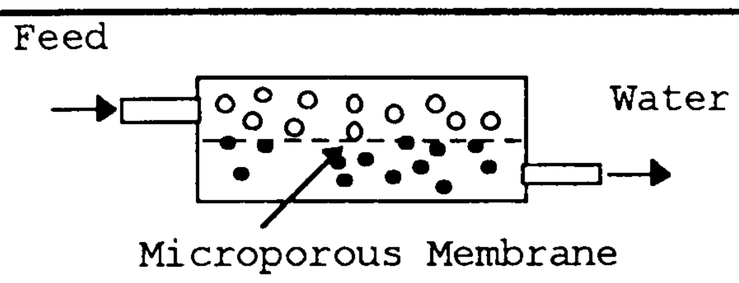
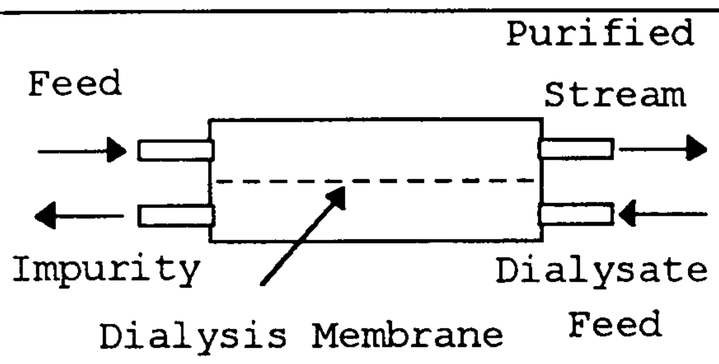
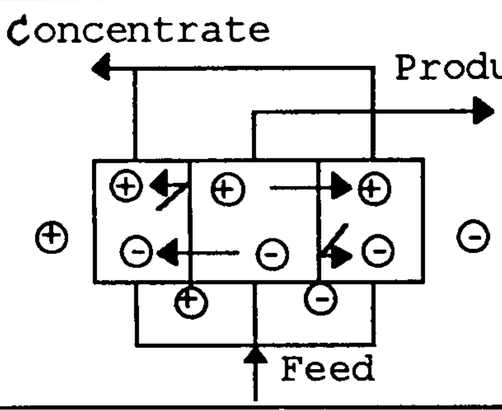
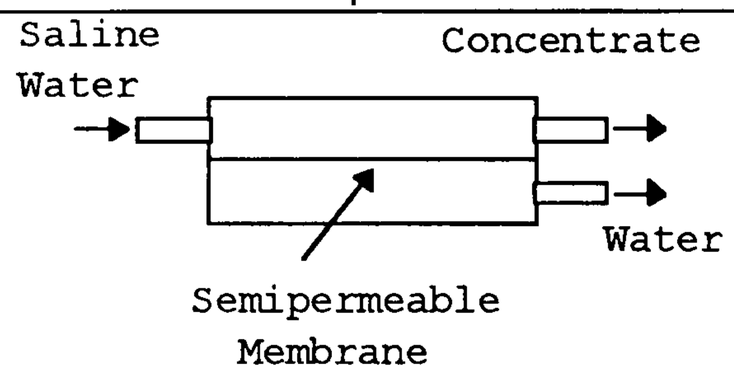
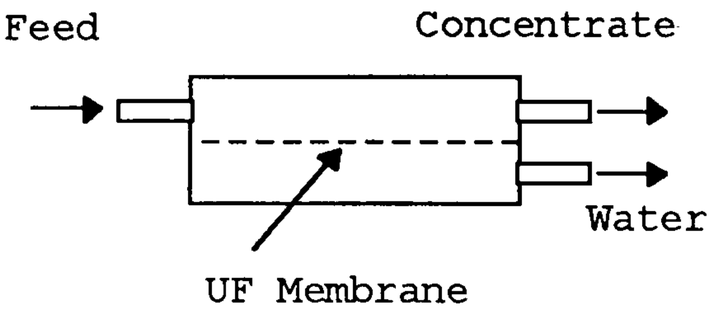
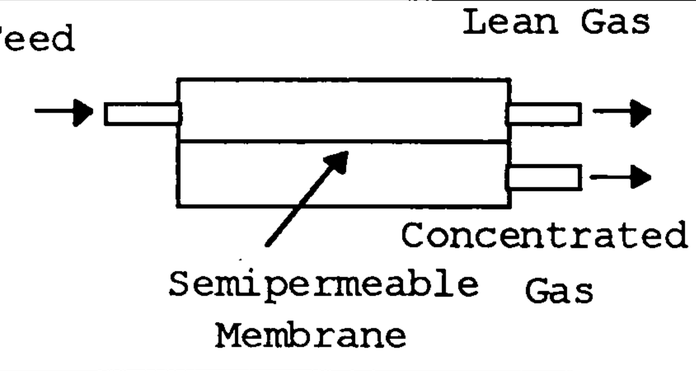
1) Membranes for separation purposes
2) Membranes for other purposes
3) Membrane technologies under development

1.3.1 Membranes for Separation Purposes

Membrane separation processes offer a number of significant advantages. First, energy requirements, and in some cases also capital investment costs, are lower than those of conventional separation processes for a number of important industrial applications. Second, the necessary process equipment is simple, compact, and relatively easy to operate and control. Moreover, this equipment is modular and can be easily scaled up or operated at partial capacity. The commercial membrane separation processes available nowadays are microfiltration, dialysis, electrodialysis, reverse osmosis, ultrafiltration,

pervaporation and gas separation. A summary of the membrane separation processes is presented in Table 1.1 (Lonsdale, 1982).

Table 1.1 Membrane separation processes

Process	Concept	Materials Passed	Driving Force	Material Retained
Micro-filtration		Water and Dissolved Species	Pressure Difference Typically 70 kPa	Suspended Material Variable Particle-Size Cutoffs.
Dialysis		Ions and Low Molecular-Weight Organics (Urea, etc.)	Concentra-tion Difference	Dissolved and Suspended Material with MW>1000
Electro-Dialysis		Ions	Voltage, Typically 1-2 V/cell Pair	All Non-Ionic and Macro molecular Species
Reverse Osmosis		Water	Pressure Difference, Typically 680-5400kPa	Virtually All Suspended and Dissolved Material
Ultra-filtra-tion		Water and Salts	Pressure Difference Typically 70-700 kPa	Biological Colloids and Macro molecules. Variable Molecular Weight Cutoffs
Gas Separa-tion		Gases and Vapours	Pressure Difference, 100-10000 kPa	Membrane-Impermea-ble Gases and Vapours

1.3.2 Membranes for Other Purposes

Apart from the separation advantages, membranes can be utilised in other applications. They can be addressed into two major fields; control release and membrane electrode. The control release technology has been commercialised for more than a decade. The membrane is used to control the rate at which a species is supplied from a reservoir to an environment where it has to be delivered. It shows considerable promise, particularly, in chemical and biochemical fields where some components have to be administered or supplied at low levels continuously or intermittently for an extended period in any application.

The other application of membrane is for membrane electrodes. It is a device used to measure the thermodynamic activity of an ion in an external solution. Three essential elements in a membrane electrode are an ion-specific membrane, an internal aqueous filling solution and a reference electrode. Ion-specific electrodes for many ions have been developed but perhaps the most well-known one is the pH electrode by which the concentration of hydrogen ion is measured.

1.3.3 Membrane Technologies Under Development

The amount of work being devoted to the development of new selective membranes has increased in the last few years. The aim of much of this work is to improve membrane kinetics and selectivity.

Development of new membrane-based equilibrium processes, such as membrane solvent extraction, are being investigated. This development would improve selectivity since it combines a true membrane process with a conventional equilibrium-based separation process. One of

the most active areas of work today is the development of membranes for air separation.

A membrane reactor is a recent application. Because a normal reactor encounters the limitation of an equilibrium conversion, the membrane reactor makes a reaction progress simultaneously with separation of some product species. Consequently, the reaction conversion is shifted forward and the load on the downstream separator is reduced. Membrane reactors are discussed in Chapter 3.

1.4 Inorganic Membranes

1.4.1 Overview

Most of the membranes used in industries are organic membranes; mainly polymeric ones. However, the disadvantages of organic membranes are their low thermal stability, poor mechanical strength, the problems of compacting and swelling, poor resistance toward chemicals and microbiological attack, and cleaning problems. As a result, development of membranes made of inorganic materials such as metals, ceramics, and inorganic polymers has been carried out. This interest has, especially, been accelerated with the introduction of commercial ceramic membranes with consistent quality and small pore sizes. Present commercial inorganic membranes come in three configurations: flat sheets or disks, tubes and multichannel monoliths. The use of disks has been limited to medical and pharmaceutical applications, while tubes and monoliths are used industrially for various applications such as removal of yeast from wine and beer fermentation, oil-water separation, fruit juice concentration and milk processing. The monolithic multichannel configuration represents a technical evolution from single-tube or tube-bundle geometry as it potentially offers high mechanical strength, savings in

installation and maintenance costs, and a higher membrane packing density (more filtration area in a given volume).

Inorganic membranes can be categorised into two groups; dense (nonporous) membranes and porous membranes. Dense membranes are mainly made of thin metal films such as palladium and its alloys, silver and nickel. These membranes have been used mostly for gas separation. Some of the nonporous metallic membranes are known to provide high selectivity since they are selectively permeable to certain gases. For example, hydrogen is selectively permeable through nonporous membranes made of palladium and its alloys whilst oxygen is selectively permeable through nonporous silver membranes. Nickel was used as a membrane in UF_6 processing for uranium enrichment. Nevertheless, industrial use of these dense membranes is limited by their brittleness tendency, high cost and low permeability compared to microporous membrane.

Porous membranes are superior to dense membranes from the point of view of their permeabilities; nevertheless, the selectivities of the porous membranes are not as good as those of the dense membranes. As a result the production of the porous membranes must be based on the compromise between selectivity and permeability. A porosity of 30 to 60 % by volume provides satisfactory compromise. Most porous metallic membranes exhibit single-layer structure while many porous ceramic membranes, on the other hand, are composite or graded in structure. In general, the composites consist of a microporous mechanically strong support a few millimetres thick superimposed with a thin selective membrane layer of a few microns thickness. One or more intermediate layers 'sandwiched' between the membrane and support can be introduced to avoid or reduce penetration of those membrane precursor particles into support pores. Any significant penetration of particles into the pores of the underlying layer may cause pore blockage, thus decreasing

permeability through the membrane-support composite. Commercial porous inorganic membranes are made of metals, zirconia, alumina and glass (silica) as listed in Table 1.2 (Hsieh, 1988). Most of their applications are based on liquid separation. Gas separation using the porous membranes is not so widespread in industry except in the enrichment of uranium. However, after the availability of fine-pore alumina, silica (or glass), and molecular sieves, the porous inorganic membrane appears to be promising in separating specific mixtures of gases, especially under high temperature and corrosive condition.

Table 1.2 Commercially available porous membranes

Manufac-turer	Trade Name	Membrane Material	Support Material	Membrane Pore size	Membrane Configu-ration
Mott		SS,Ni, Au,Ag,Pt, etc.		> 0.5 μm	tube
Pall		SS, Ni, etc.		> 0.5 μm	tube
Osmonics	Hytrex	Ag		0.2-5 μm	disk
Union Carbide	Ucarsep	ZrO_2	C	30 A	tube
SFEC	Carbosep	ZrO_2	C	40 A	tube
CARRE		ZrO_2 (dynamic Membrane)	SS		tube
TDK	Dynaceram	ZrO_2 (dynamic Membrane)	Al_2O_3	100 A	tube
Alcoa/SCT	Membralox	Al_2O_3	Al_2O_3	40-1000 A	Monolith /tube
Norton	Ceraflo	Al_2O_3	Al_2O_3	0.2-1.0 μm	Monolith /tube
NGK		Al_2O_3	Al_2O_3	0.2-5 μm	tube
Anotec /Alcan	Anopore	Al_2O_3	Al_2O_3	250 A	disk
Asahi Glass		Glass		40-500 A	tube/disk
Schott Glass		Glass		100 A	tube
Fuji Filters		Glass		0.25-1.2μm	tube
Ceram Filters		SiC	SiC	0.15-8 μm	tube

1.4.2 Preparation of Porous Membranes

The development of porous membranes with crack free, small pore size and narrow pore size distribution is a new challenge. Several approaches are known for preparation of porous inorganic membranes: phase separation and leaching, particle dispersion and 'slipcasting', anodic oxidation, pyrolysis, thin-film deposition, and track-etched methods. Selection of the preparation techniques is dependant on materials, membrane and support structures, pore size, porosity and membrane thickness. The following discussions provide general concept of each technique.

- Phase Separation and Leaching

This method is usually used to prepare porous glass membranes. Firstly, the mixtures of unleachable components such as silica and leachable components such as Na_2O and B_2O_3 are melted and well mixed. The melt is cooled down at a fast rate to form a homogenous and amorphous material. Then the glass is heat-treated to allow spatial redistribution of the phases to occur. Different temperatures and different periods of time have an effect on controlling the structure of the membrane. When the heat treating process is stopped, the glass is leached by water or acidic solutions to form a fine porous structure in the glass. After leaching, the porous glass is heat treated for compaction. This membrane is suitable for microfiltration, ultrafiltration or gas separation. Some of porous metal membranes can be prepared by this method with a strong acid, base or hydrogen peroxide as the leaching medium.

- Particle Dispersion and 'Slipcasting'

This method is widely applied for making ceramic membranes. The procedure consists of two steps. Firstly a

dispersion of fine particles called a 'slip' is prepared, and then they are deposited on a porous support by a 'slipcasting' method. To form a crack-free ultrafine-pore membrane with narrow-pore size distribution, a special procedure to prepare a stable dispersion of submicron particles is needed. The 'sol-gel' technique is a well established method for making submicron particles for the preparation of the 'slip'. It was firstly introduced in the early 1940's for producing uniformly-sized powders of uranium dioxide pellets for nuclear reactors (Anderson *et al.*, 1988). There are two kinds of 'sol-gel' techniques. The first one is polymerisation of molecular units (PMU) which is based on controlled hydrolysis of alkoxides and condensation-polymerisation reactions. The other is destabilisation of colloidal solutions (DCS) which uses peptisation of inorganic salts or hydrous metal oxides with an electrolyte. Examples of membranes produced by PMU in the past are silica, titania and zirconia membranes, while those of DCS are made of zirconia, alumina, lanthanum oxychloride and palladium doped silica membranes (Julbe *et al.*, 1993). The 'sol-gel' techniques are advantageous compared with other techniques. A ceramic is obtained at a relatively low sintering temperature, the particle size is very homogeneous and thus, the pore size distribution is narrow.

Membrane precursor particles are used to produce an integral and self-supporting membrane by compression or extrusion. To form a composite membrane the 'slipcasting' method is needed. In this method, an organic binder, and, if necessary, viscosity modifiers may be added to the 'slips' to enhance the bonding between them and the support and to control the consistency of the 'slip'. The 'slip' is deposited on one or more layers of support by a dipping or 'slipcasting' procedure. A capillary pressure drop, created by contacting the 'slip' with a microporous ceramic support, is a major driving force in the 'slipcasting' procedure. It forces the dispersion medium

of the 'slip' to flow into the dry pores of the support. The 'slip' particles are retained and concentrated at the entrance of the pores to form a gel layer of particles. It should be noted that drying, sintering and heat treatment strongly affect the final pore size and porosity and that the coefficient of thermal expansion of both 'slip' and support should be the same.

- Anodic Oxidation

In this method, one side of a thin high-porosity metal such as aluminum sheet is anodically oxidised in an acid electrolyte such as oxalic, sulphuric and phosphoric acid at ambient temperatures. Subsequently, the unoxidised portion of the metal is etched away with a strong acid to leave the acid insoluble oxide film intact. Asymmetric aluminum oxide membranes, prepared by this method, have been generally found to consist of two regions, the porous layer and the barrier layer. The porous layer consists of close-packed cells of oxide, predominantly hexagonal in shape, each of which contains a single pore formed perpendicularly to the macroscopic surface of the aluminum substrate. The barrier layer is a thin compact inner region lying adjacent to the metal. The electrolyte used is an important factor in controlling the pore diameter of the membrane. Normally, further treatment such as hydrothermal treatment is necessary to improve membrane stability.

- Pyrolysis

Inorganic membranes can be prepared from organic polymers by a pyrolysis method. A thin film of the polymeric precursor supported on a porous support is firstly prepared and then pyrolysed in a furnace to transform the polymer film to a rigid inorganic framework with open pores. Silica and carbon molecular sieve membranes, for example, can be produced by pyrolysis of

silicon rubbers and certain thermosetting polymers, respectively. By varying the polymerisation and/or pyrolysis conditions, inorganic membranes with different physical properties can be obtained. The potential of using polymers as a material for producing inorganic membranes is not widely recognised due to the lack of knowledge on the changes of thermodynamic and transport characteristics that occur during pyrolysis of ceramic precursor polymers (Shelekhin *et al.*, 1991).

- Thin-Film Deposition Method

Thin-film deposition technology was widely used in the semiconductor industry for growing thin solid films and manufacturing microelectronic devices. However, it is also applicable in producing porous inorganic membranes. A porous transition metal or its alloys can form on a porous ceramic, glass, or stainless steel support by conventional deposition techniques, such as electroplating, electrodeless plating, or vapour deposition. The electrodeless plating technique is based on the controlled autocatalysed reduction of metastable metallic salt complexes on the target surfaces. For example, deposition of Pd and Ag film on porous stainless steel was done by reducing a palladium salt or a silver salt with EDTA, hydrazine and ammonia (Shu *et al.*, 1993). The vapour deposition is a versatile process that allows the exercise of fine control over the growth process and the composition and uniformity of the films. It offers attractive opportunities for the synthesis of selective inorganic membranes. Different oxide films, as well as multicomponent ceramic oxide films, can be deposited on a wide variety of porous substrates. This method has been applied in producing membranes for gas separation. For example, ultrafiltration alumina membranes were modified by chemical vapour deposition of a zirconia/yttria solid solution on the internal pore surface of the membrane top-layer in order to obtain gas separation properties of

surface diffusion or microporous diffusion (Lin *et al.*, 1991). Thin silicon dioxide films were grown on dense α-alumina wafers as well as porous α-alumina and γ-alumina substrates via oxidation of triisopropylsilane (Megiris and Glezer, 1992). This method was also used to deposit the selectively permeable SiO_2 and Al_2O_3 films on a SnO_2 conductivity sensors for the detection of organic gases in air (Althainz *et al.*, 1995).

- Track-etch Method

This method is usually used to produce porous polymer membranes such as porous polycarbonate and polyethylene teraphthalate membranes. Firstly a thin polymer film is irradiated with high-energy particles, leaving tracks on the film. Then an etching agent such as aqueous solutions of the alkalis NaOH and KOH is used to form micropores in the membrane. The track-etched membrane is uniform with capillary pores of defined size which provide for accurate separation or fractionation of solutes by size. Due to these unique characteristics, the membrane has been used as model pores in fundamental studies of membrane transport. The shape of the pores is determined by the relation between the rate of etching of the bulk membrane material and the rate of etching of the material along the high-energy charged particle track. The membrane material etching rate is determined by the concentration and temperature of the etching agent. This new type of membranes appeared in the USA in the early 1960's (Ballew, 1978) and in the USSR in the early 1970's (Flerov, 1984).

CHAPTER 2

THEORY OF GAS PERMEATION

2.1 Transport Mechanisms Through Porous Membranes

2.1.1 Viscous Bulk Flow

2.1.2 Knudsen Diffusion

2.1.3 Surface Diffusion

2.1.4 Capillary Condensation

2.1.5 Molecular Sieving

2.2 Gas Phase Flow Through Alumina Membranes

CHAPTER 2

THEORY OF GAS PERMEATION

2.1 Transport Mechanisms Through Porous Membranes

Gas permeation across porous membranes can be described by five flow mechanisms: viscous bulk flow, Knudsen flow, surface diffusion, capillary condensation and molecular sieving. Figure 2.1 shows these flow mechanisms diagramatically. In practical, however, only one or a few mechanisms predominate the total transport. The factors that determine the importance of each mechanism are, for example, membrane pore size, molecule weight of permeants, interaction between gases and membranes, and operating conditions. The following pages give more details about these mechanisms.

2.1.1 Viscous Bulk Flow

Viscous bulk flow (or Poiseuille flow) takes place when the membrane pores are larger than the mean free paths, λ, of the permeating gas molecules. Momentum is exchanged among gas molecules during the collision. As a result, all molecules pass the pores with the average velocity independent of their sizes, shape or masses. This transport mechanism is, therefore, non separative, and should be avoided in practical operation.

For a porous membrane consisting of cylindrical capillary pores of equal size, the transport rate can be described by the Hagen-Poiseuille equation (van den Berg and Smolders, 1992).

$$J_V = -\frac{\pi n d_p^4 p}{128 \tau_g \mu R T} \frac{dp}{dz} \qquad (2.1)$$

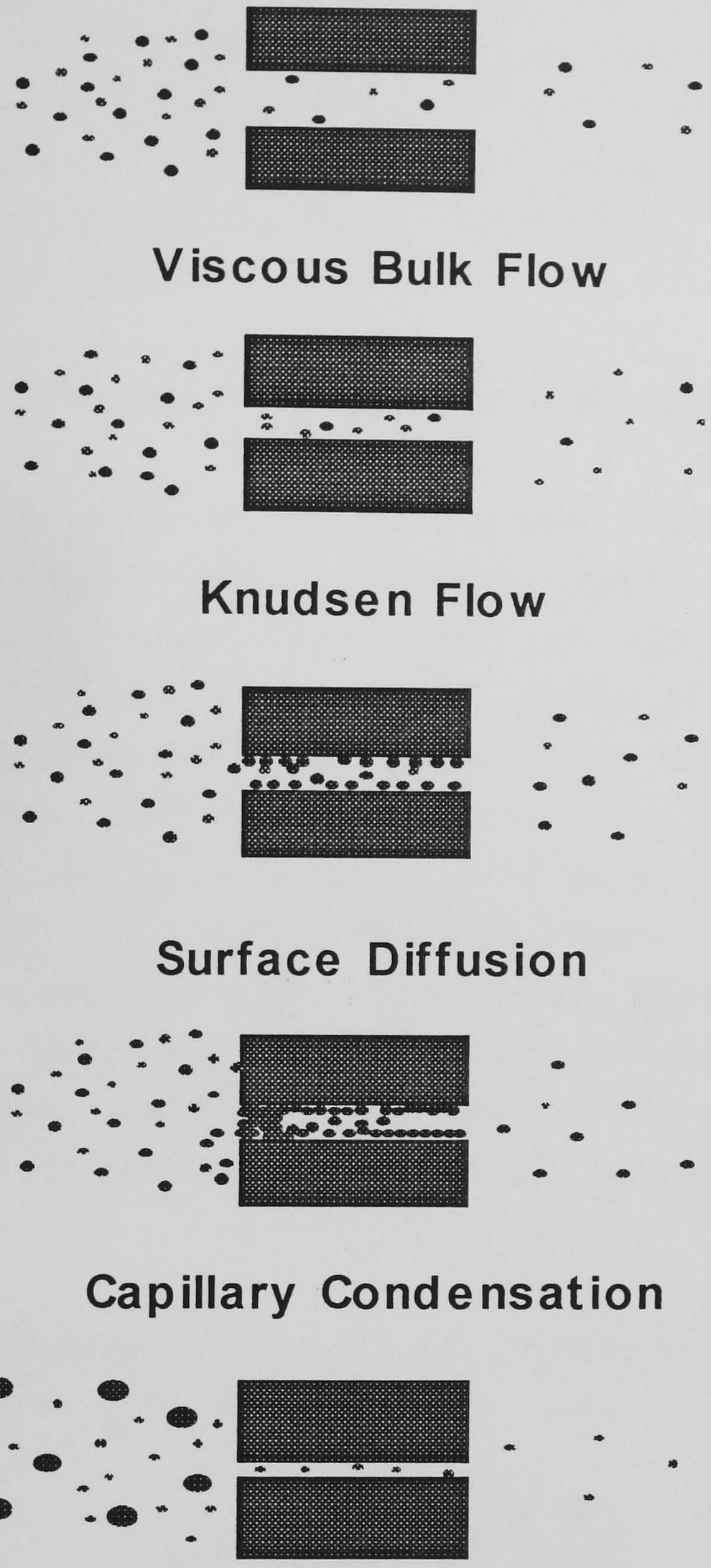


Figure 2.1 Transport mechanisms through a porous membrane

where J_v is molar flux due to the viscous flow, n is the number of pores per unit area, d_p is the pore diameter, p is the pressure, R is the gas constant, T is the operating temperature, μ is gas viscosity, τ_g is the tortuosity of the pores for gas phase flow and z is the distance across

the membrane. In reality, the pore structure in membranes are very complicated and frequently not known. Thus there are many factors introduced, for example average pore diameter, porosity, pore size distribution, tortuosity and specific surface area.

2.1.2 Knudsen Diffusion (or Free-Molecule Diffusion)

In contrast with the viscous flow, the Knudsen flow regime occurs when membrane pore diameters are smaller than the mean free path of the gases to be separated. The collision frequency among gas molecules is negligible, compared with that of the gas molecules on the pore walls. Thus, each molecule passes the pore at its own molecular speed which is roughly inversely proportional to the square root of its molecular mass. This flow is selective and can be used for some systems, such as separation of hydrogen from organic hydrocarbons in an alumina membrane. However, the selectivity of separation in this regime is not high and selectivities greater than 10 unlikely.

The Knudsen flux through microporous membrane is given by (van den Berg and Smolders, 1992)

$$J_K = -\left(\frac{\pi n d_p^3}{12RT\tau_g}\sqrt{\frac{8RT}{\pi M}}\right)\frac{dp}{dz} \qquad (2.2)$$

In this expression, J_K is the molar flux contributed by Knudsen flow and M is the molecular weight of the permeating gas.

In both Knudsen flow and Poiseuille flow, it can be seen that the fluxes in both mechanisms are dependant on maintaining a pressure difference across the membrane. Nevertheless, the Poiseuille flux is also dependent on the pressure level and gas viscosity. In a membrane with an intermediate pore size (when pore diameter is larger than

3 nm), the transport is due to the combination of both mechanisms (Huang and Chen, 1995). It should be noted that the selectivity decreases with the increase of the pressure difference across the membrane. This is because the contribution of the non-separative viscous flux is relatively higher when the pressure increases. In addition, it can be observed that the flux of Knudsen flow is proportional to d_p^3 while that of the viscous flow is proportional to d_p^4. As a result, a few large pores in a membrane consisting of very small pores can have great impact on the selectivity.

2.1.3 Surface Diffusion

In many experimental investigations, total gas flow rates were found to be much higher than that predicted from the previous two mechanisms. It may be caused by an extra flow mechanism called 'Surface Diffusion'. This phenomena occurs when there exists an interaction between gases and pore walls. The gases are adsorbed as a film on the pore surface, and the migration of this adsorbed film causes an extra flow moving parallel to the bulk gas flow. In separation of a gas mixture, some gases are preferentially adsorbed on the pore surface while the other gases are not. These effects can be very significant in some cases. Thus in the flow of an organic vapour and hydrogen through a membrane, the flux of the organic component can be higher than that of the lower molecular weight hydrogen. Propane and carbon dioxide have very similar molecular weights, so can not be separated by Knudsen diffusion. So surface flow phenomena can be used for their separation (Kammermeyer and Wyrick, 1958). The surface flow is particularly high at low temperature and high pressure. The mechanisms of the surface diffusion have been described by many workers and is discussed further in Chapter 3.

2.1.4 Capillary Condensation

Capillary condensation takes place in porous membranes when the temperature decreases and/or the pressure of the adsorbable gas increases. The adsorbed phase in both monolayer and multilayer are gradually replaced by the capillary condensed phase. In membranes with smaller pore size form condensation will take place at lower pressure. Transport in capillary condensation can be regarded as Poiseuille flow of a viscous liquid filling the pores of the porous media.

Since the saturation vapour pressure for a capillary condensation is much lower than that of an ordinary condensation process on a planar surface, the critical pore radius for the presence of capillary condensation can be estimated from the Kelvin equation

$$\frac{\rho RT}{M} \ln \frac{p_p}{p_o} = -\frac{4\sigma \cos \psi}{d_p} \tag{2.3}$$

in which p_p and p_o are the saturated vapour pressures for a capillary and for a planar interface, respectively, ρ is the density of the condensate, σ is the interfacial tension, M is the molecular weight, d_p is the diameter of cylindrical capillary, and ψ is the contact angle of the condensed liquid on the solid.

Due to the action of surface tension at the meniscus, not only is the saturation vapour pressure reduced but there is also a hydrostatic pressure difference across the meniscus, or a capillary suction pressure p_C, which can be expressed as follows.

$$p_c = -\frac{4\sigma \cos \psi}{d_p} = \frac{\rho RT}{M} \ln \frac{p}{p_o} \tag{2.4}$$

where p is the pressure outside the capillary pores. The overall hydrostatic pressure acting on the capillary condensate or capillary pressure, Δp_c is

$$\Delta p_c = \frac{\rho RT}{M} \ln \frac{p_1}{p_2} \tag{2.5}$$

where p_1 and p_2 are the pressure in the feed and the permeate sides, respectively.

The permeate flow rate of capillary condensation where the gravity and the gradient of the gas phase are neglected can be described by

$$J_c = \frac{K_d}{\mu} \frac{dp_c}{dz} \tag{2.6}$$

$$J_c = \frac{K_d}{\mu} \frac{\rho RT}{MZ} \ln\left(\frac{p_1}{p_2}\right) \tag{2.7}$$

In this expression, J_c is the molar flux of condensation phase, K_d is a constant determined by the pore structure, Z is the thickness of the membrane and μ is the viscosity of the condensate.

When capillary condensation occurs, the passage of the nonadsorbed gas is reduced or totally blocked by the condensate filling the pores. Thus the more condensible gas can be separated from the less condensible one. The separation factor in the presence of capillary condensation is usually high, and this is attractive for the recovery of condensible solvent vapours from process and plant exhausts.

2.1.5 Molecular Sieving

When the pore size of the membrane approaches the size of the molecule that is passing through it, a sieving mechanism can occur for gas separation. Under these conditions the pore is extremely small in the range of 2-15 Å or 0.2-1.5 nm. These are almost five times smaller the mean free path of a perfect gas molecule. Selectivity based on this mechanism is very high because the separation is caused by size selection. The smaller molecules in a gas mixture are allowed to pass through the membrane while the larger molecules are obstructed.

Membranes made from polymers or zeolites can use this mechanism for gas separation as they have these extremely small pore size. A molecular sieve carbon membrane is another example of molecular sieve membranes. The technique to make the membrane containing pores no greater than those of molecular dimensions is by pyrolysis of organic compounds. The pore dimensions of the same starting carbon membrane may be adjusted by simple thermochemical treatments to achieve optimised separation power for any gas mixture composition.

There are two important points that should be compared between the molecular sieving and Knudsen diffusion mechanisms. Firstly the molecular sieving mechanism is an activated process. The gas permeability increases when the temperature increases while it decreases with temperature in accordance with the Knudsen diffusion mechanism. The other fact is that the permeability coefficient in the molecular sieving mechanism is found to be strongly dependent on the diameter of the diffusing gas molecule rather than on the molecular weight in the Knudsen diffusion mechanism.

2.2 Gas Phase Flow Through Alumina Membranes

Gases can permeate through a membrane as both a gas phase and an adsorbed phase. When the gas molecules are not adsorbed on the membrane pore surface and when the operating condition is far from its saturation point, only permeation through gas phase occurs. The membranes used in this study have pore size of 4 and 10 nm. As a result, gas phase flow is the combination of Knudsen diffusion and viscous bulk flow and the flux can be described by the combination of the expressions given before in Equations (2.1) and (2.2) as follows

$$J = -\left(\frac{\pi n d_p^3}{12RT\tau_g}\sqrt{\frac{8RT}{\pi M}} + \frac{\pi n d_p^4 p}{128\tau_g \mu RT}\right)\frac{dp}{dr} \qquad (2.8)$$

where r is radial distance along the membrane.

To simplify the equation the following parameters are defined.

$$R_K = \frac{\pi n d_p^3}{12RT\tau_g}\sqrt{\frac{8RT}{\pi M}} \quad \text{and} \quad R_V = \frac{\pi n d_p^4}{128\tau_g \mu RT} \qquad (2.9)$$

so, the total gas flux is

$$J = -(R_K + R_V p)\frac{dp}{dr} \qquad (2.10)$$

Since the membrane is cylindrical in shape, the total molar flow rate across the membrane per unit length of membrane (F/L) can be expressed by

$$\frac{F}{L} = -2\pi r(R_K + R_V p)\frac{dp}{dr} \qquad (2.11)$$

where F is total molar flow rate through the membrane of the length of L.

Equation (2.11) can be integrated with respect to the boundary condition where the pressure inside the tube at radius r_1 is p_1 and the one outside the tube at radius r_2 is p_2, giving

$$\int_{r_1}^{r_2} -\frac{F}{2\pi r L} dr = \int_{p_1}^{p_2} (R_K + R_V p) dp \tag{2.12}$$

which becomes

$$\frac{F}{2\pi L} \ln\left(\frac{r_2}{r_1}\right) = R_K(p_1 - p_2) + \frac{R_V}{2}(p_1^2 - p_2^2) \tag{2.13}$$

Rearranging (2.13) gives

$$\frac{F}{(p_1 - p_2)L} = \frac{2\pi R_K}{\ln(r_2 / r_1)} + \frac{2\pi R_V}{\ln(r_2 / r_1)} \frac{(p_1 + p_2)}{2} \tag{2.14}$$

The equation (2.14) can be simplified to

$$P = \frac{F}{(p_1 - p_2)L} = \frac{a}{\sqrt{MT}} + \frac{b}{\mu T} \bar{p} \tag{2.15}$$

where the permeability (P) is defined as $F/(p_1-p_2).L$, the Knudsen parameter (a) is $2\pi R_K \sqrt{MT} / \ln(r_2 / r_1)$, the viscous parameter (b) is $2\pi R_v \mu T / \ln(r_2 / r_1)$ and $\bar{p}$ denotes mean pressure over the membrane or $(p_1+p_2)/2$.

Equation (2.15) can be used to interpret permeation of nonadsorbed gases. The permeability is plotted against the mean pressure across the membrane. The intersection at mean pressure of zero gives the contribution of Knudsen diffusion while the slope shows the contribution of viscous flow. The equation, in addition, allows the permeability of other gas to be predicted.

For a gas mixture, the gas flow rate per unit membrane length of component i can be expressed as

$$\left(\frac{F}{L}\right)_i = \frac{a(p_1 x_i - p_2 y_i)}{\sqrt{M_i T}} + \frac{b x_i (p_1^2 - p_2^2)}{2\mu T} \qquad (2.16)$$

x_i and y_i are mole fraction of species i in feed side and permeate side respectively.

CHAPTER 3

LITERATURE REVIEWS

3.1 Surface Diffusion

3.2 Membrane Reactors

CHAPTER 3

Literature Reviews

3.1 Surface Diffusion

Surface diffusion is an important phenomena occurring in many chemical engineering processes; for example, in heterogeneous catalysis, in adsorption operations and in gas separation process. The last one is the subject of this study. It was first suggested by Wicke and Kallenback (1941) and Tomlinson and Flood (1948) that surface diffusion contributes to the total transport in a porous membrane in the direction of decreasing surface concentration. Surface diffusion can not be significant unless appreciable adsorption occurs. However, if adsorbed molecules are held so strongly as to be essential immobile, surface diffusion will not be significant. Compared to surface diffusion in the liquid phase, surface diffusion in gas phase is well documented and reviewed by Ruthven (1984) and Suzuki (1990).

Surface diffusion is a process that can be measured by direct and indirect methods. The direct methods are rather complicated and require sophisticated instruments such as a field ion microscope. The indirect methods can be performed by measuring gas flow rate through a porous solid. However, diffusion through the gas phase is always present in parallel with surface diffusion. Therefore, it is necessary to subtract the contribution of gas phase diffusion from the total flow rate. The gas phase diffusion can be determined by either performing experiments at high temperature where adsorption is negligible, or by calculation from permeation data of nonadsorbed gas. Permeation studies can be carried out by several types of operation. In steady-state counterdiffusion two gases are allowed to

diffuse across a porous solid from different sides. One gas such as helium acts as an indicator for the other gas. If mass transfer only takes place by gas phase diffusion, the flux ratio should be inversely proportional to the square root of the molecular weight of the gas. Any excess from the values calculated from the relationship can be attributed to surface diffusion.

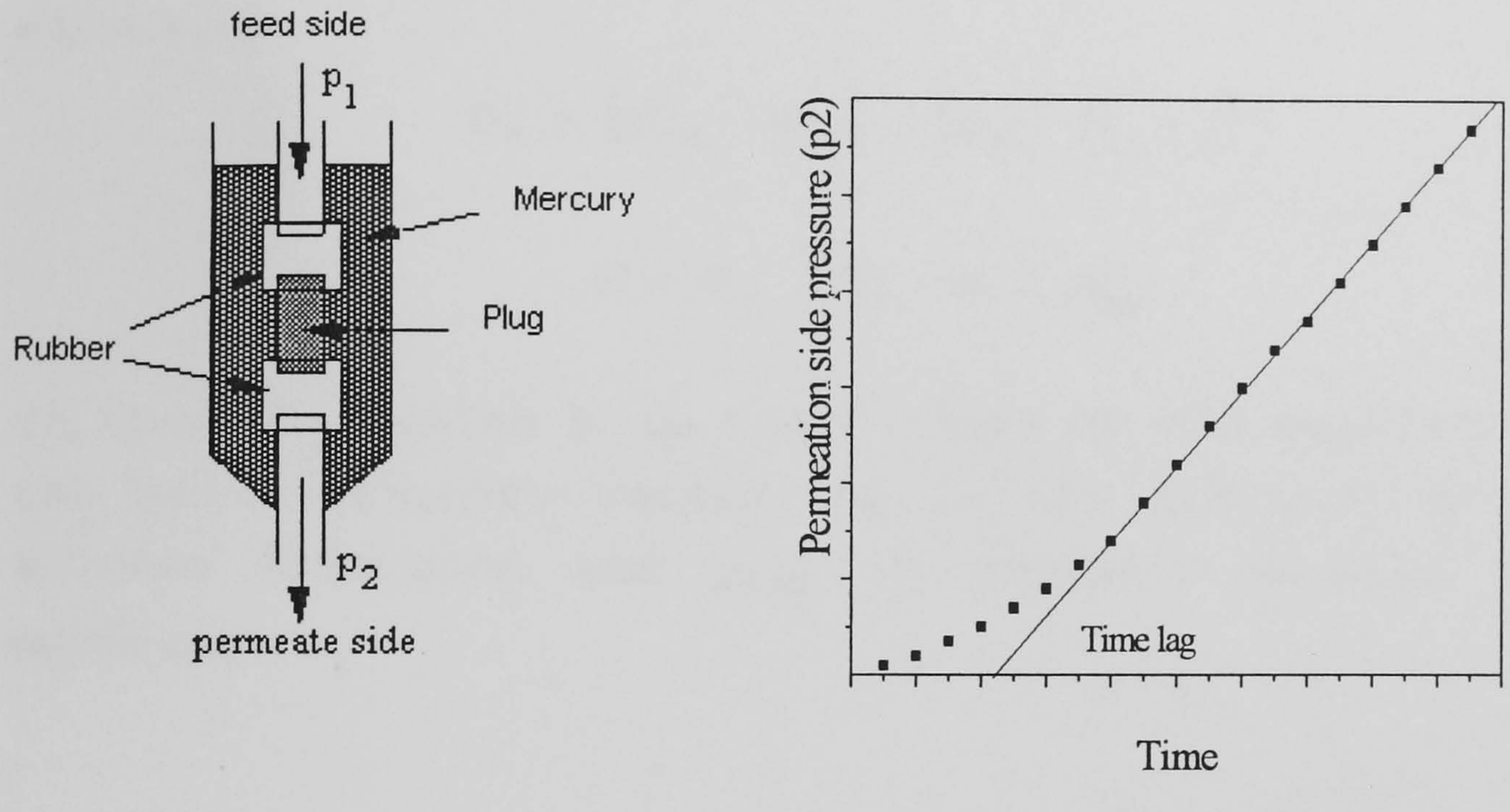


Figure 3.1 The apparatus for transient studies and an experimental result (Barrer, 1948)

It is not necessary to study surface diffusion in the steady-state mode. Barrer (1948) proposed a 'time-lag' method to study surface diffusion. Figure 3.1 demonstrates the experimental apparatus and gives an example of the result used to find a time lag. Before the experiment is performed, the pressure at the permeate side (p_2) is kept at very low level. Then the feed gas is introduced to the feed side with pressure p_1 and the pressure p_2 is measured as a function of time to obtain the graph. This method allows transient and steady-state transport studies to be combined in one experiment.

A new method to study the surface diffusion was proposed by Okubo and Inoue (1987). The method is based on measuring the response of concentration in the

permeate side after introducing a 'square pulse' input in the feed side. Their experimental hardware is illustrated in Figure 3.2. An apparent diffusivity (D_a) can be obtained from the 'square pulse' response measurement while an effective diffusivity (D_e) is determined from the 'quasi-steady state' measurement. Then surface diffusivity (D_S) and the Henry's law constant of adsorption (K') can be calculated by the following equations.

$$D_s = \left(\tau D_e - \varepsilon D_K\right) / \left(D_e / D_a - \varepsilon\right) \qquad (3.1)$$

$$K' = \left(D_e / D_a - \varepsilon\right) / \rho_{app} \qquad (3.2)$$

In this expression ε is the voidage of the membrane, τ is the bed tortuosity factor, D_K is the diffusivity due to Knudsen diffusion and ρ_{app} is apparent density of the membrane.

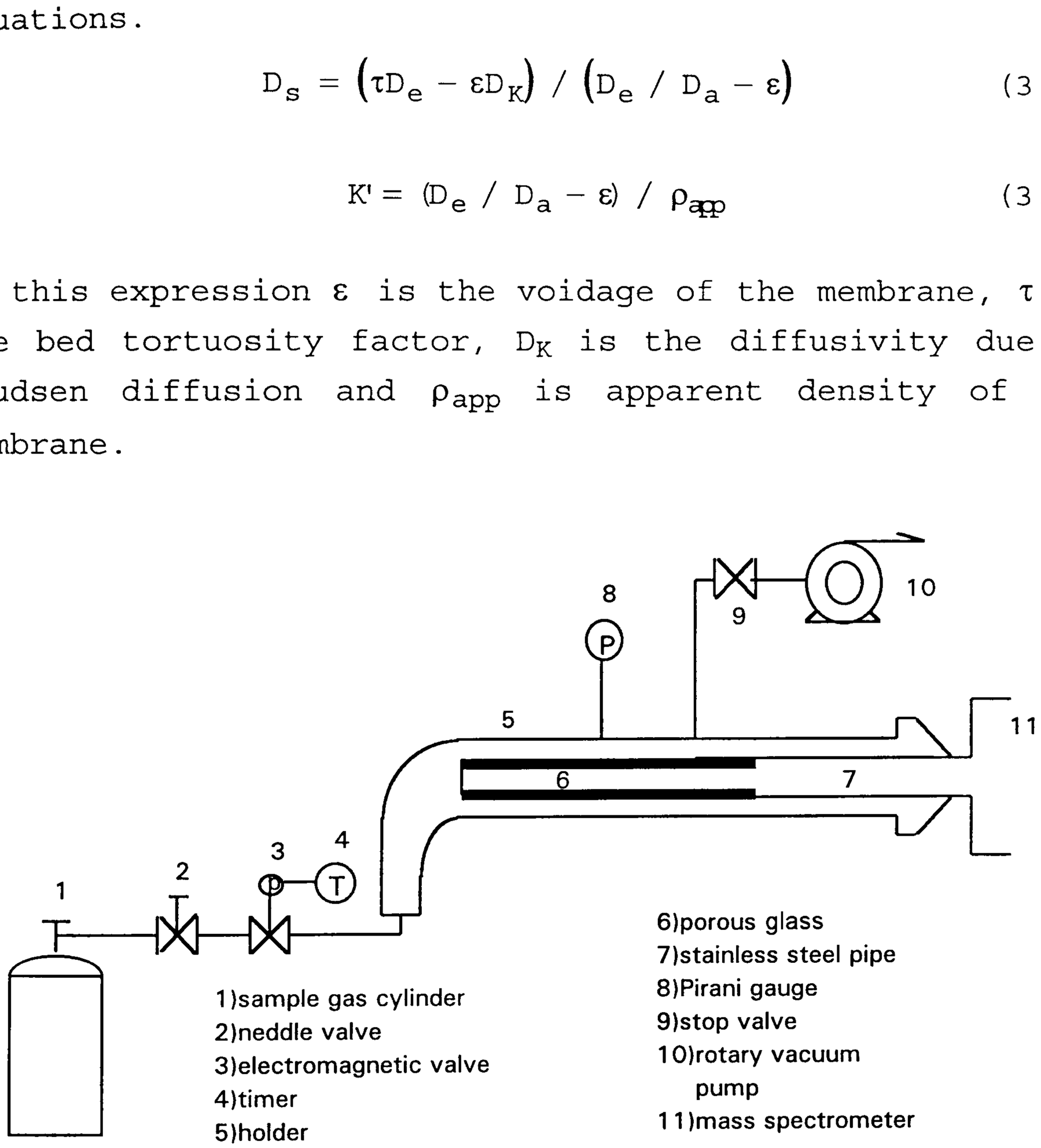


Figure 3.2 Experimental setup of 'square-pulse' method

The relative contribution of surface diffusion to the total flow across a porous material is determined by two major factors: surface diffusivity (D_s) and the degree of adsorption. Both factors relate to the

interaction between an adsorbate and the pore surface. In general, the relative contribution of surface diffusion decreases with increasing temperature because the activation energy of surface diffusion is usually smaller than a heat of adsorption. Several models have been proposed to describe surface diffusion. The first and most frequently used model is based on Fick's first law in which the flux of surface diffusion is proportional to the gradient of the concentration of adsorbed gas on a surface, and can be shown as follows

$$J_s = -\frac{D_s \rho_{app}}{\tau_s} \frac{d}{dz} q \qquad (3.3)$$

$$D_s = D_s^{\circ} \exp\left(-E_s / RT\right) \qquad (3.4)$$

where J_s is surface diffusion flux, q is surface concentration of the adsorbed species, τ_s is the tortuosity of the pores for surface flow, D_s is surface diffusivity, D_s° is constant and E_s is activation energy for surface diffusion. R is the universal gas constant and T is the absolute temperature.

The second model is a hydrodynamic one which treats the phase of the adsorbed gas on the solid surface as a laminar-flowing film of a viscous fluid. Gilland *et al.* (1958), one of the leading proponents of the hydrodynamic model, derived an equation describing adsorbed layer movement by utilising a force balance together with thermodynamic principles. The resulting equation shown below has one empirical constant and its use requires adsorption isotherm data.

$$J_s = \frac{RT\rho_{app}}{1000\tau_s C_R S_t Z} \int_{p_2}^{p_1} \frac{q^2}{p} dp \qquad (3.5)$$

In this expression C_R is the coefficient of resistance, Z is the plug length, S_t is the specific surface area of the porous media, p is the pressure at any point in the membrane, p_1 is the pressure in the feed side and p_2 is the pressure in the permeate side. The model can describe the results well in a range of 1/10 of monolayer coverage up to the condensation regime. The last model is a molecular hopping one which can be subdivided into two groups. One is a random hopping model, which pictures the adsorbed gas molecules randomly hopping and migrating from site to site on the surface. The other one is a mechanistic hopping model, which is based on calculation of the trajectories of hopping molecules along the solid surface.

Interpretation of surface flow results is usually based on the same assumption of local thermodynamic equilibrium between the gas and adsorbed phases within the porous solid. Carman and Malhere (1950) studied the steady-state surface diffusion of SO_2 and CCl_2F_2 through plugs of 'Linde' porous silica 'blacks' and carbon black under constant pressure difference and at low temperatures such that the surface flow was comparable in magnitude with the gas phase flow. Helium and air were used as calibrating gases to find gas permeability. It was assumed that surface flow and gas phase flow occurred independently. So the surface permeability was the difference between the total permeability and the gas permeability. The results were interpreted using the Fick's law model. They found that the surface diffusivity increased and the activation energy (E_s) decreased with the increase of surface coverage (θ). Carman and Raal (1951) continued this study and found that the surface flow and bulk gas flow could not be treated independently because the gas phase was hindered by the adsorbed molecules. Within a range of monolayer coverage the results indicated the rapid

decrease of surface diffusion coefficient as surface coverage (θ) decreased.

Barrer and Barrier (1952) used a 'time-lag' method to study surface diffusion of O_2, N_2, Ar, SO_2 and NH_3 through porous 'Vycor' glass at very low dilution. It was found that in the transient state, surface diffusion made a substantial contribution to flow while in the steady state there was less evidence of surface diffusion. Hence, the surface diffusion in the transient state was not necessarily the same as the steady state. This was later confirmed by Ash *et al.* (1962a) from the results of the surface diffusion measurements of SO_2, CO_2, N_2, Ar and He through 'Carbolac', a high density activated carbon. They also suggested that causes for the discrepancy may arise from the invalidity of the assumption of isothermal conditions, which was usually assumed in the steady state condition. Ash *et al.* (1962b) extended their studies to the case of binary mixtures of four systems; namely H_2-SO_2, N_2-CO_2, Ne-CO_2 and Ar-N_2. The nonadsorbed gas in each system was used as an indicator to investigate the pore blockage caused by an adsorbed phase. In some cases the blockage can be so marked that the porous solid becomes impermeable to a nonadsorbed component while being freely permeable to a strongly sorbed one.

A main complication of surface diffusion arises from its strong concentration dependency on surface diffusivity. However, this is exceptional within the Henry's law region (Ruthven, 1984). Some evidence was provided by Okubo and Inoue (1989) who studied the permeation of CO_2, N_2O, ethane, ethylene, propane, propylene, 1-butene and refrigerants, R-12, R-22 and R-114, through a porous glass at low dilution. The concentration dependency of surface diffusivity is due to many factors such as the heterogeneity of the solid surface. Some efforts have been made to improve the

BIBL. LOUVAIN. UNIV.

representation of the results. Higashi *et al.* (1963) proposed a H.I.O. model by assuming that as the coverage increases there is an increase in the distance travelled in one hop of a migrating molecule. Then the surface diffusivity becomes a function of surface coverage (θ) as

$$D_s = \frac{D_s^\circ}{(1-\theta)} \exp\left(-E_s/RT\right) \qquad (3.6)$$

This model correlated experimental results well at surface coverage up to θ = 60 %. Gilland *et al.* (1974) tried to consider the effect of surface heterogeneity by proposing that the change of surface diffusivity with surface concentration was attributed to a change in the strength of adsorption. They assumed that the activation energy of surface diffusion was proportional to the heat of adsorption. The results of new data on the flow of physically adsorbed molecules CO_2, SO_2 and NH_3 in a porous glass were correlated successfully together with literature data for five other systems using a dimensionless heat of adsorption (Q_{st}/RT). This concept was successfully extended to the case of chemisorption by Sladek *et al.* (1974).

A random hopping model, based on the hypothesis of nearly complete desorption of the mobile molecules on the solid surface, followed by random 'jumps' to nearly viable surface sites, was developed by Smith and Metzner (1964). Their equations are shown below.

$$P_s = D_s \left[1.637 q\rho \frac{\partial q}{\partial p} + q^2\right] \qquad (3.7)$$

$$D_s = \left(\frac{S_t \rho_{app} M}{4\tau_s}\right) \frac{W^2 T}{p} \qquad (3.8)$$

in which

(the symbols P_s and W denote the surface permeability and a constant respectively.) This model could correlate the results of the surface diffusion of C_3H_8, C_4H_{10}, C_3H_6, and CBr_2F_2 on an alumina catalyst support surface well with less than monolayer coverage.

Weaver and Metzner (1966) derived an expression that related the rate of surface diffusion to the pressure gradient within a cylindrical porous pellet. Their expression was

$$P_s = \frac{\rho_{app} S_t}{2\pi\tau_s}\left(r_h \frac{\partial\overline{\lambda^2}}{\partial p} + \frac{\pi}{2}\overline{\lambda^2}\frac{\partial r_h}{\partial p}\right) \qquad (3.9)$$

where r_h is the rate of migration and $\overline{\lambda^2}$ is the average value of the square of the migration distance. The migration distance transversed in a single jump for the case of a gas adsorbed on a homogeneous surface was assumed to occur as a result of a random hopping of the partially desorbed species. To calculate the migration distance a molecule escaping from the surface with a velocity v^o at an angle φ with respect to the surface was further assumed to follow a quasi-ballistic trajectory as indicated in Figure 3.3.

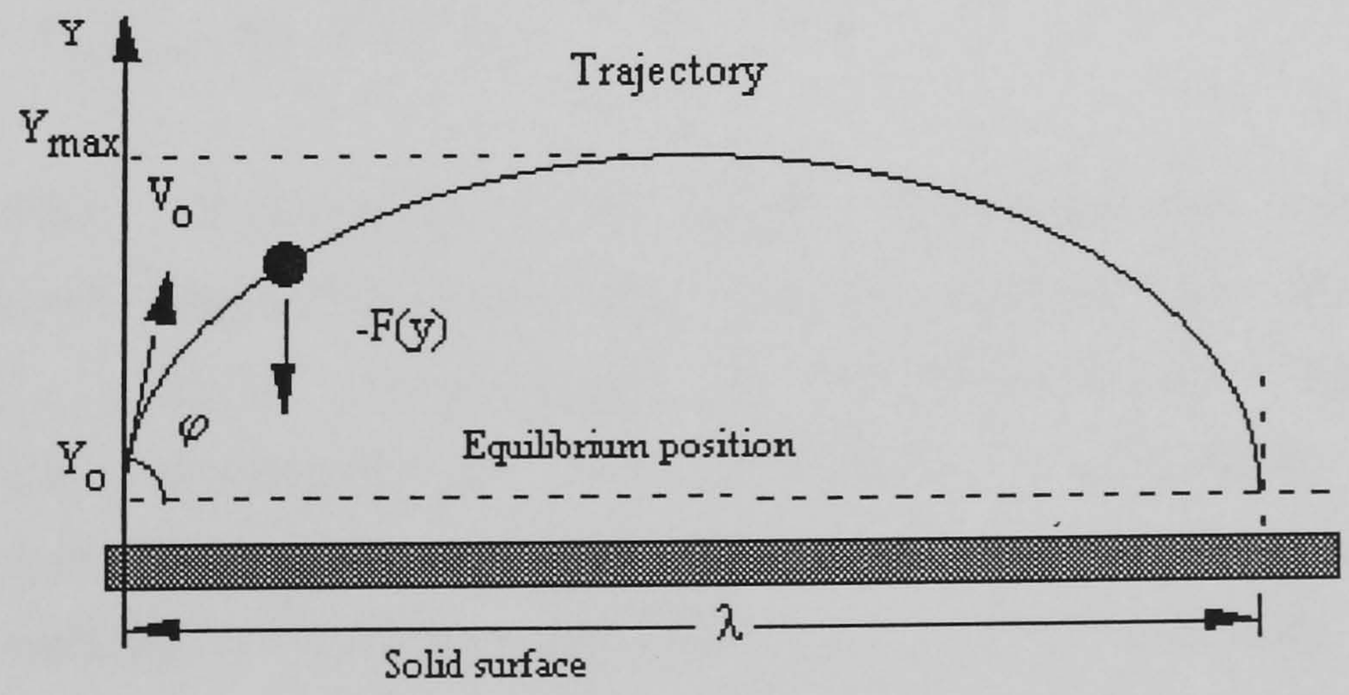


Figure 3.3 Trajectory of a molecule on a solid surface

A model based on the hopping mechanism of surface diffusing molecules was developed by Ponzi *et al.*

(1977) for an energetically heterogeneous surface. The probability of an activated molecule being captured when it passes over an empty site is an important parameter in the model. Okazaki *et al.* (1981) developed a random walk model based on the concept of the average holding time of molecules adsorbed in the monolayer and multilayers to hop to a neighbouring site. The model was correlated with steady flow data for mixtures of the adsorbed gases; C_2H_4, C_3H_6, i-C_4H_{10} and SO_2, and the nonadsorbed gases; N_2 and He, through porous glass in constant pressure countercurrent diffusion.

Attempts to study the effect of a porous surface on surface diffusion was carried out by Ash *et al.* (1966). They chose 'Graphon' and 'Black Pearl' activated carbons as examples of sorbing surfaces. From the permeation study of sulphur hexafluoride through plugs of the two carbons, they found that the effect of surface flow were considerably greater than those of other sorbents having much larger surface area such as an alumina-silica cracking catalyst. They concluded that this behaviour was a result of the smoother, more homogeneous and less porous nature of these carbon particles. The results were subsequently verified by Horiguchi *et al.* (1971) using 'Vycor' glass and 'Graphon' plugs with C_2H_6, N_2 and He.

The validity of the assumption of local thermodynamic equilibrium was investigated by Sircar and Rao (1990). They developed a mathematical model for steady-state nonequilibrium surface diffusion of an adsorbing gas through an energetically homogeneous porous medium assuming a linear adsorption isotherm and a linear driving force model. They found that conventional assumption of local thermodynamic equilibrium between the gas and solid phases within the porous medium can seriously underestimate the surface diffusion coefficient when the mass transfer rate is finite.

There are only a few studies that have investigated multicomponent surface diffusion, even though this topic is more important in real operation. Yamasaki and Inoue (1991) developed an equation to describe surface diffusion of binary system by extending the BET equation by introducing interaction terms among different compounds and the hopping model. They studied the permeation of four mixtures benzene-hexane, benzene-cyclohexane, benzene-acetone and benzene-methanol through porous glass at 35 ^{o}C. In all cases the surface flux was changed by the presence of the accompanying component. Chen and Yang (1992) predicted binary Fickian diffusivities from pure component Fickian data.

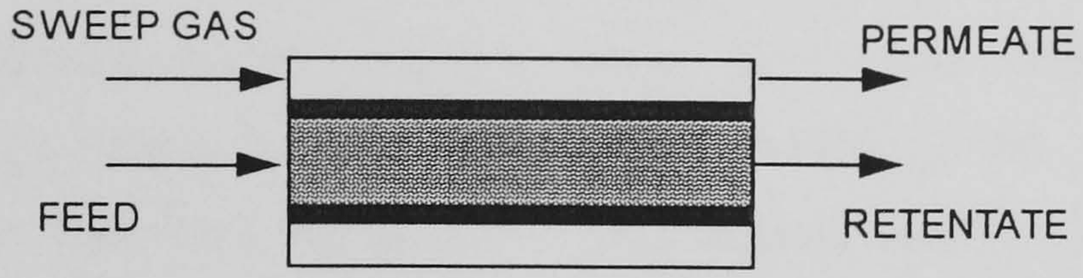
Recent work is more pragmatic in nature and is more suitable for process engineering studies. Okubo and Inoue (1987) investigated the effect of surface modification of 'Vycor' glass using methanol, ethanol and 1-propanol for improving the surface diffusion of CO_2, C_3H_8 and refrigerants, R-22 and R-114 at low surface coverage. Their experimental apparatus was based on the 'square pulse' method. The diffusivities were correlated with the dimensionless heat of adsorption. An alumina based membrane was modified with silver to enhance the surface diffusion of H_2 and O_2, and with magnesia for CO_2 diffusion (Uhlhorn *et al.* 1989). The experiment was carried out in the countercurrent diffusion mode and the model was described by Fick's law. Qiu and Hwang (1991) applied the idea of surface diffusion to encourage the recovery of solvent ethanol and acetone vapours from their mixtures with nitrogen gas in a continuous vapour-gas separation with a porous membrane permeation system using 'Vycor' glass. Sloot *et al.* (1992a) studied the surface diffusion of H_2S and SO_2 through alumina membranes with a flat-sheet geometry in a continuum regime and in the absence of a pressure difference. The effect of mass transfer resistances in the gas phase from both sides of

the membrane was considered. They found that the resistances are very small and did not affect their model. Rao and Sircar (1993) applied the concept of surface diffusion to recover hydrogen gas from refinery waste gases by selectively removing hydrocarbon gases through a carbon membrane. Jia *et al.* (1994) prepared ceramic-zeolite composite membranes by depositing a thin polycrystalline silicalite layer on the inner surface of an alumina membrane. Owing to the surface diffusion of n-C_4H_{10}, the permeation rate ratio of n-C_4H_{10} and i-C_4H_{10} was considerable different.

3.2 Membrane Reactors

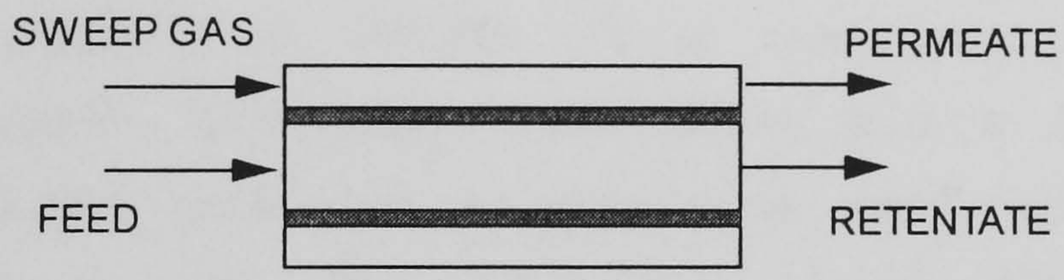
Active consideration of membrane reactors started in the 1950's. A membrane reactor combines reaction and separation in a single unit operation. The membrane selectively removes one or more of the reactant or product species. Early applications were found in the field of biotechnology using polymer membranes at low operating temperature. With the advance in development of new membranes, the concept was extended to the application of high temperature catalytic reactions. The early applications included the use of thin metallic palladium or palladium alloy membranes. A palladium membrane is known as a highly selective membrane for hydrogen. Many hydrogenation and dehydrogenation reactions were studied using these membrane reactors. A review of catalytic palladium-based membrane reactors was given by Shu *et al.* (1991). However, the use of the membranes is limited because they have many disadvantages, for example, their brittleness, very low permeability and high cost. Another class of membrane reactors had porous glass membranes. They were applied in reactions such as the dehydrogenation of cyclohexane, methanol and isobutane, and the decomposition of H_2S and HI. However, the membranes are brittle and do not have desirable resistance to thermal and mechanical stresses.

High temperature catalytic membrane reactors using ceramic membranes such as 'sol-gel' alumina, zirconia and titania membranes, are a more recent development. The concept of inorganic membrane reactors was reviewed by a number of workers (Armor, 1988, Hsieh, 1989 and Zaman and Chakma, 1994).



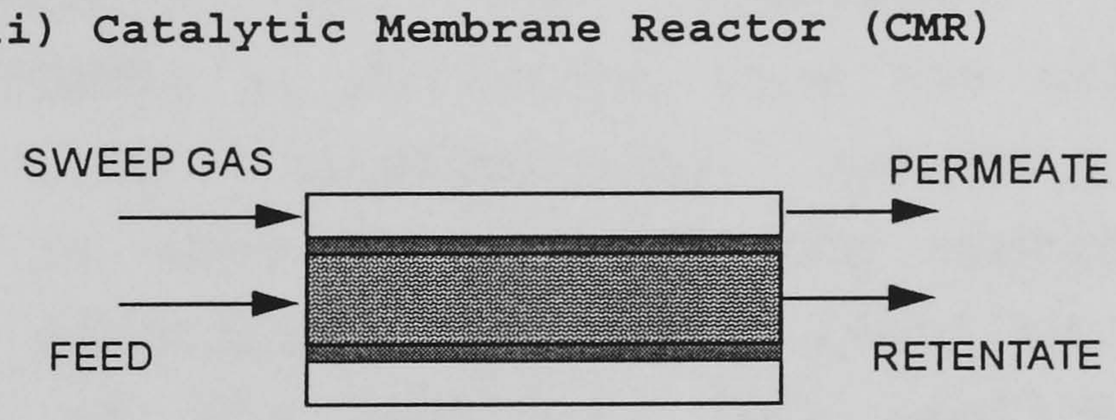
Permselective Membrane

i) Packed/Fluidised Bed Membrane Reactor (PBMR,FBMR)



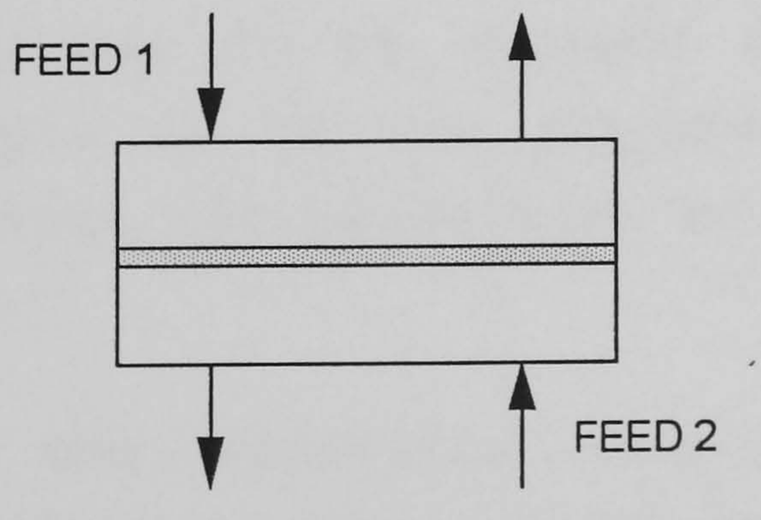
Permselective and Catalytically Active Membrane

ii) Catalytic Membrane Reactor (CMR)



Permselective and Catalytically Active Membrane

iii) Packed/Fluidised Bed Catalytic Membrane Reactor (PBCMR,FBCMR)



Nonpermselective and Catalytically Active Membrane

iv) Catalytic Nonpermselective Membrane Reactor (CNMR)

Figure 3.4 Membrane reactor configurations

The membrane reactor configurations can be categorised into four types; namely (1) packed or fluidised bed membrane reactor (PBMR or FBMR), (2) catalytic membrane reactor (CMR), (3) packed or fluidised bed catalytic membrane reactor (PBCMR or FBCMR) and (4) catalytic nonpermselective membrane reactor (CNMR). The first case is the simplest configuration. The membrane acts as a permselective layer for one (or more) of the reactants or products while the catalytic action is provided by the packed bed or fluidised bed. In the CMR, on the other hand, the membrane is catalytically active either by itself or by deposition of a catalyst on the membrane surface where the high specific surface area is exploited. The PBCMR or FBCMR is a combination between the first two cases. The reaction takes place in both the packed or fluidised bed and within the membrane. In this operation the loss of the reactant from the reaction chamber through the membrane can be reduced by the catalytic activity of the membrane. The last configuration (CNMR) is different from the other three. The membrane is catalytically active but not permselective. It acts as a media for controlling the supply of two reactants entering a reaction zone from opposite sides of the membrane. Its applications are particularly useful for a process in which severe constriction on the stoichiometry of the reactant feeds is required, or the cases where the direct contact between two streams has to be avoided to prevent over-oxidation. An example is in the production of methanol from methane to prevent the production of formaldehyde.

Most of the reactions studied in membrane reactors are dehydrogenation reactions because they produce low molecular weight hydrogen gas which can be preferably removed by a membrane. However, the concept is potentially applicable on a number of other reactions. Table 3.1 gives some examples of the membrane reactor systems.

Table 3.1 Some reactions using membrane reactors

Reaction	Membrane	Catal-yst	T (^oC)	Configu-ration	Reference
Dehydrogenation of ethane to ethylene	Pd-Ag impregnated Vycor glass membrane	Pd/Al_2O_3	400	PBCMR	Gobina and Hughes (1994)
Dehydrogenation of propane	γ-Al_2O_3 membrane	Pt/Al_2O_3	480 - 625	PBMR	Ziaka *et al.* (1993)
Dehydrogenation of cyclohexane to benzene	Pd impregnated Vycor glass membrane	Pd/Al_2O_3	185	PBCMR	Cannon and Hacskaylo (1992)
Dehydrogenation of ethylbenzene to styrene	γ-Al_2O_3 membrane	iron oxide catalyst	600 - 640	PBMR	Wu *et al.* (1990)
Methane steam reforming	ruthenium-dispersed alumina membrane	Ru/Al_2O_3	300 - 500	PBCMR	Chai *et al.* (1993)
Decomposition of ammonia	Pd-alumina membrane	Ni/Al_2O_3	550 - 600	PBMR	Collin and Way (1994)
Dehydrogenation of methanol	γ-Al_2O_3 modified with Ag		200 - 500	CMR	Zaspalis *et al.* (1991a)
Oxidative coupling of methane	MgO/PbO impregnated alumina membrane		750	CMR	Omata *et al.* (1989)
Methanol synthesis	perfluori-nated cation exchange material	Cu/Zn	200	PBMR	Struis *et al.* (1996)
Reduction of nitrogen oxide with ammonia	vanadia modified titania and alumina membranes		300 - 350	CNMR	Zaspalis *et al.* (1991b)
Claus reaction	α-Al_2O_3		200 - 300	CNMR	Sloot *et al.* (1992b)

There are many benefits from applying the concepts of membrane reactors to catalytic chemical reactions. Since reaction and separation are integrated into a single unit, separation cost and recycle feed requirement are reduced. For reactions subject to thermodynamic limitation, conversion can be improved by the use of a membrane to selectively separate some products from the reaction side to the permeate side. For example, Champagnie *et al.* (1990) showed that the

dehydrogenation of ethane in a Pt-impregnated alumina membrane reactor gave a conversion six times higher than the corresponding equilibrium conversion. Shinji *et al.* (1982) studied the dehydrogenation of cyclohexane using a porous-glass reactor. Nitrogen was used as a carrier gas for cyclohexane in the reaction side and as a sweep gas in the permeate side. The conversion achieved was more than twice the equilibrium conversion.

The enhancement of conversion from the separation of a product from the reaction chamber, in addition, allows the reactor to operate at lower operating temperature. For example the dehydrogenation of cyclohexane to benzene can be carried out at as low as 185 ^{o}C (Cannon and Hacskaylo, 1992). The yield of the conversion of propane to aromatics was improved by selective removal of hydrogen gas through a Pd-impregnated alumina membrane (Uemiya *et al.* 1991b).

Even though air can be used directly as the oxidant for methane, it is difficult to separate the nitrogen gas left from methane and hydrocarbon products. A membrane reactor to solve this problem used a membrane for separating oxygen from air in one side of the membrane to supply it to the reaction side on the other side of the membrane (Nozaki *et al.* 1992 and Tonkovich *et al.* 1996). Membrane reactors can be used to improve yield of intermediate products of heterogeneous catalytic reactions. Thus Bernstenin and Lund (1993) showed that the most critical parameters for improving the yield were 1) the relative rate of reaction to the rate of membrane permeation, and 2) the relative permeability of the intermediate product to the permeability of the reactant.

Itoh *et al.* (1985) showed that there was an optimum thickness of 'Vycor' glass membrane where the conversion of cyclohexane was maximised. Theoretical studies of a catalytic membrane reactor and a packed bed

membrane reactor indicated that the performance of the catalytic membrane reactor was superior to the packed bed membrane reactor for operation with high residence time while there was no significant difference at low residence time (Sun and Khang, 1988).

Uemiya *et al.* (1991a) showed that even though steam reforming of methane was favourable at low operating pressure, the increase of the reaction side pressure in a hydrogen-permeable membrane reactor could improve the conversion. This was due to the effective removal of hydrogen gas to the permeation side. Sun and Khang (1990) showed that the performance of membrane reactors was significantly dependant on the nature of volume change of reaction. Mohan and Govind (1988) investigated the effect of cocurrent or countercurrent operation on the performance of catalytic membrane reactors in reversible reactions. They found that the physical properties and operating conditions were important factors for selecting the mode of operation.

For a membrane that is permeable to both products and reactants, the maximum equilibrium shift was limited by the loss of reactant from the reaction zone (Mohan and Govind, 1986). The conversion can be improved by using a recycle membrane reactor where part of the feed or permeate exit streams are recycled to the feed stream. The use of hybrid reactor system consisting of a conventional packed bed reactor followed by a membrane reactor was proposed to increase the overall conversion. The initial packed bed section reduces the leakage of reactant to the permeation side in the membrane reactor. However, the improvement is still subject to the constraint of equilibrium conversion in the first section (Assabumrungrat and White, 1996).

Tekic *et al.* (1994) proposed the use of two membranes for improving performance of a membrane

reactor. This concept was applicable when the reactant was the slowest of the permeating components. Enhancing the separation of a product from the reaction side by performing another reaction using the permeating species as a reactant on the other side of the membrane is another approach to improve the performance of the membrane reactor. The reaction on the other side the membrane, in addition, can provide heat for endothermic dehydrogenation (Itoh, 1990). Gobina *et al.* (1995) developed a model to compare the experimental results of the dehydrogenation of ethane to ethylene in a catalytic membrane reactor, with and without reaction on the permeation side. The studies were extended to the dehydrogenation of n-butane. Increases of conversion of 5 to 8 fold above the equilibrium value were observed when using carbon monoxide and oxygen (Gobina and Hughes, 1996).

The majority of current development on membrane reactors is still based on the motivation for the use of membrane reactor to increase the conversion and selectivity of catalytic reactions. Catalytic performance of different reactor configurations is compared. For example, Capannelli *et al.* (1996) studied the oxidative dehydrogenation of propane to propylene in a packed bed, monolith-like reactor and a catalytic membrane reactor. Development of new membranes or modification of membrane surface to improve catalytic activity or membrane selectivity particularly for a certain reaction is still an active research area. Even though much work has been carried out on the topic of membrane reactors in high temperature catalytic reactions, they have not yet been used in an industrial context. There are still a number of problems to be overcome before implementing the membrane reactor to industrial use. These include the long-term stability and mechanical integrity of the membrane, the effect of fouling and deactivation and the durability of the reactor module.

CHAPTER 4

EXPERIMENTAL STUDIES OF PURE GAS PERMEATION

4.1 Introduction

4.2 Description of Experimental System

4.3 Results and Discussion

4.4 Prediction of Permeability of Other Gases

4.5 Conclusion

CHAPTER 4

EXPERIMENTAL STUDIES OF PURE GAS PERMEATION

4.1 Introduction

There are a number of methods for investigating gas permeation through a membrane such as the 'square pulse' method, the countercurrent flow method, the cross flow method and the forced flow method. The last method is to be applied in this study. One end of the membrane is closed and gas is introduced into the inner tube and the permeate flows to the outer part which is open to atmosphere. In this chapter permeation of nitrogen and hydrogen through commercially available multilayer alumina membranes with pore diameters of 4 nm and 10 nm were investigated at six temperature levels ranging from room temperature to 200 ^{o}C. Permeability data of nitrogen gas was used to predict the permeability of hydrogen. In both cases Knudsen diffusion and viscous bulk flow are found to be the predominant flow mechanisms.

4.2 Description of Experimental System

Figure 4.1 shows the schematic diagram of the experimental apparatus. Nitrogen or hydrogen gas from a gas cylinder was first heated up by passing it through a heat exchanger made of a stainless steel tube with 1/8" diameter, 0.012" wall thickness and 4 m in length. It was then fed into the membrane. The membranes used in this study are tubular ceramic alumina membranes (Membralox) made by Societe des Ceramiques Techniques Company (SCT) in France. They are four-layered composite membranes

consisting of three thin γ-alumina membrane layers supported on a microporous α-alumina support. These membranes have an inner diameter of 7 mm and an outer diameter of 10 mm, and a length of 25 cm. The commercial available pore diameters of the separative layer are 4 and 10 nm.

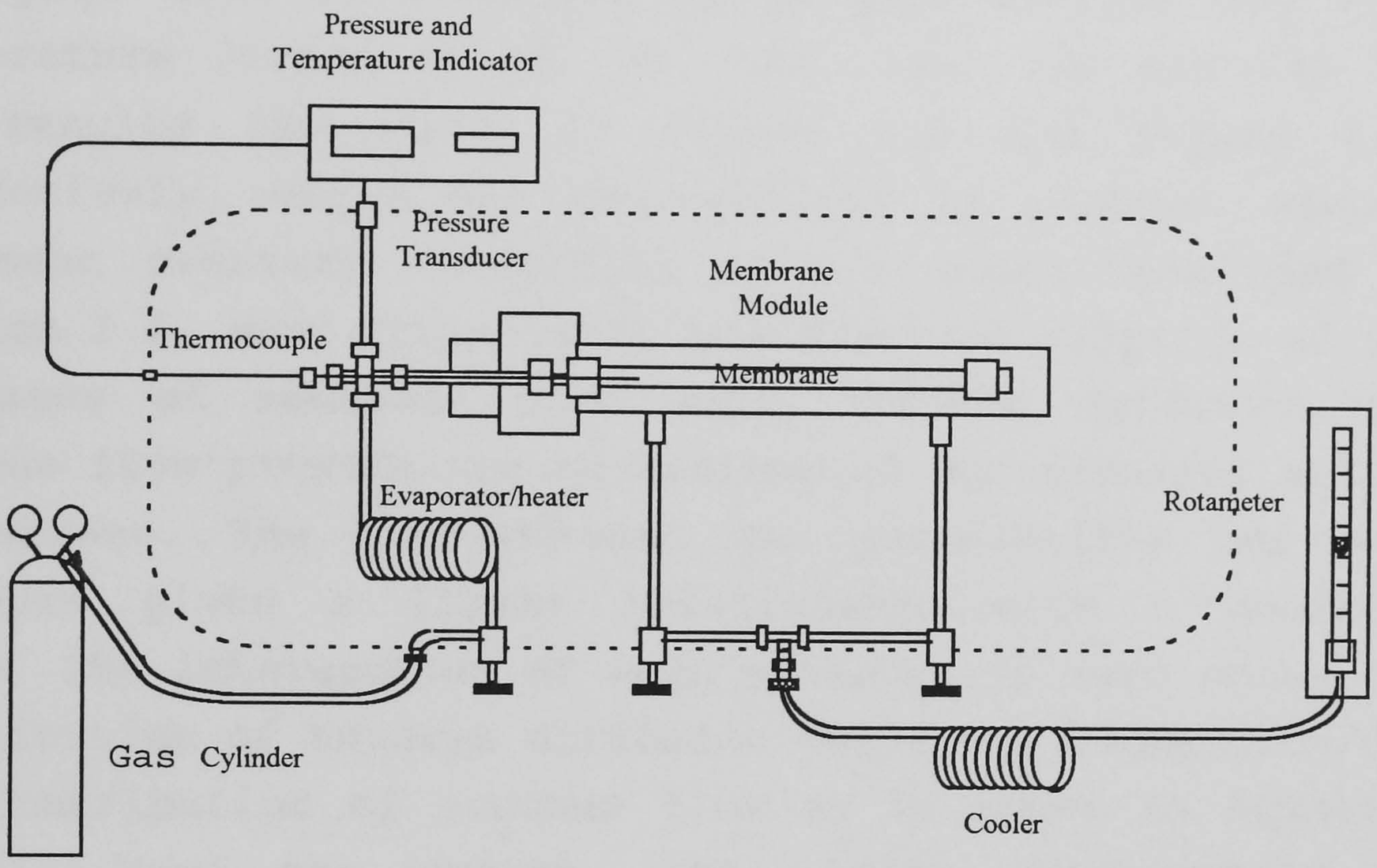


Figure 4.1 The schematic diagram of experimental setup for gas permeation measurement

The membrane module consisted of a stainless steel casing, inside of which the ceramic tube was placed and sealed to the stainless steel body using 'Swagelok' fittings and 'Teflon' tape wrapped around the membrane. Tightness at the joint between the fitting and the membrane was very important to make a good seal. One end of the membrane was closed using the fitting and teflon tape. The shell side inlet and outlet openings were situated 17.5 cm apart. Both the heating system and the membrane module were placed in an oven, so that, the system was operated under isothermal condition. The temperature in the membrane module was measured by a type-K thermocouple and the pressure of the tube side was measured by a pressure transducer placed at the gas inlet.

The output of permeate stream from the membrane module was measured by a rotameter calibrated for a specific gas.

4.3 Results and Discussion

Permeation of nitrogen gas through the membranes with pore size of 4 nm and 10 nm were carried out at 6 temperature levels of 20, 90, 120, 150, 180 and 200 ^{o}C. The results are shown in Figure 4.2 and Figure 4.3, respectively, where gas permeability is plotted against the mean pressure. According to the model developed in section 2.2, when there is no preferential sorption of any of gases on membrane pore wall, Knudsen diffusion and viscous flow provide the mechanisms of gas transfer across a membrane. The plot between gas permeability and mean pressure gives a linear relationship with a positive slope. The intersection at mean pressure of zero shows the contribution of Knudsen diffusion while the slope provides the contribution of viscous flow as is shown in Equation (2.15). From the graphs, the linear relationship is obtained in all cases with goodness of fit (R^2) of at least 95 %. This confirms that the permeation of nitrogen through the porous γ-Al_2O_3 membrane is due to Knudsen diffusion and viscous flow which also agrees with the previous work done with the permeation of helium, argon and nitrogen through similar membranes (White, *et al.*, 1992).

The graphs also show that the total permeability decreases with the increase of the operating temperature and that the contribution of viscous flow becomes smaller at higher temperature as is seen from the decrease of the slope of the lines. For the membrane with pore diameter of 4 nm, the main transport mechanism at high temperature is Knudsen diffusion since the curves are almost parallel to the horizontal axis. However, the contribution of viscous flow is more pronounced for the membrane with pore diameter of 10 nm.

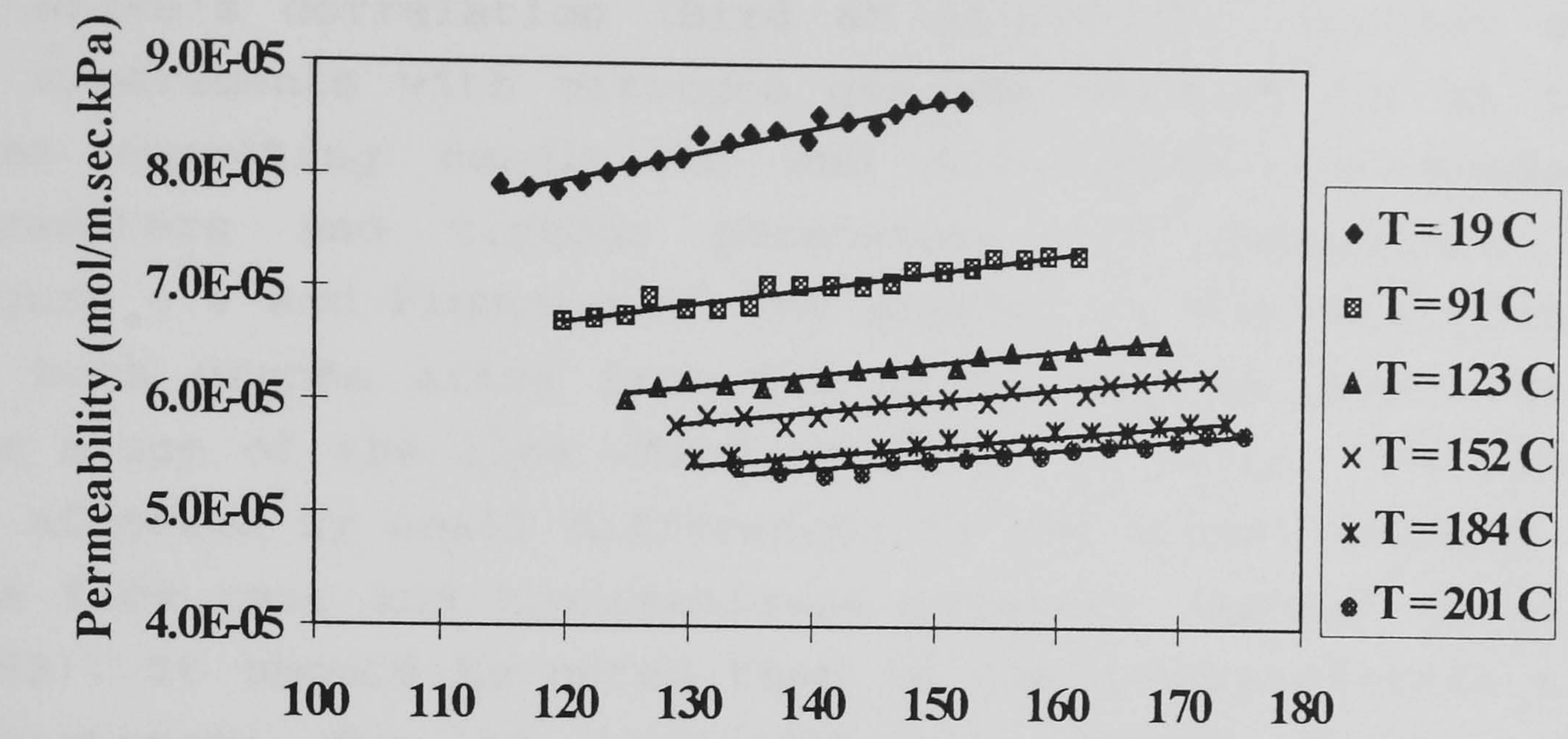


Figure 4.2 Nitrogen gas permeability through the membrane with 4 nm membrane pore size

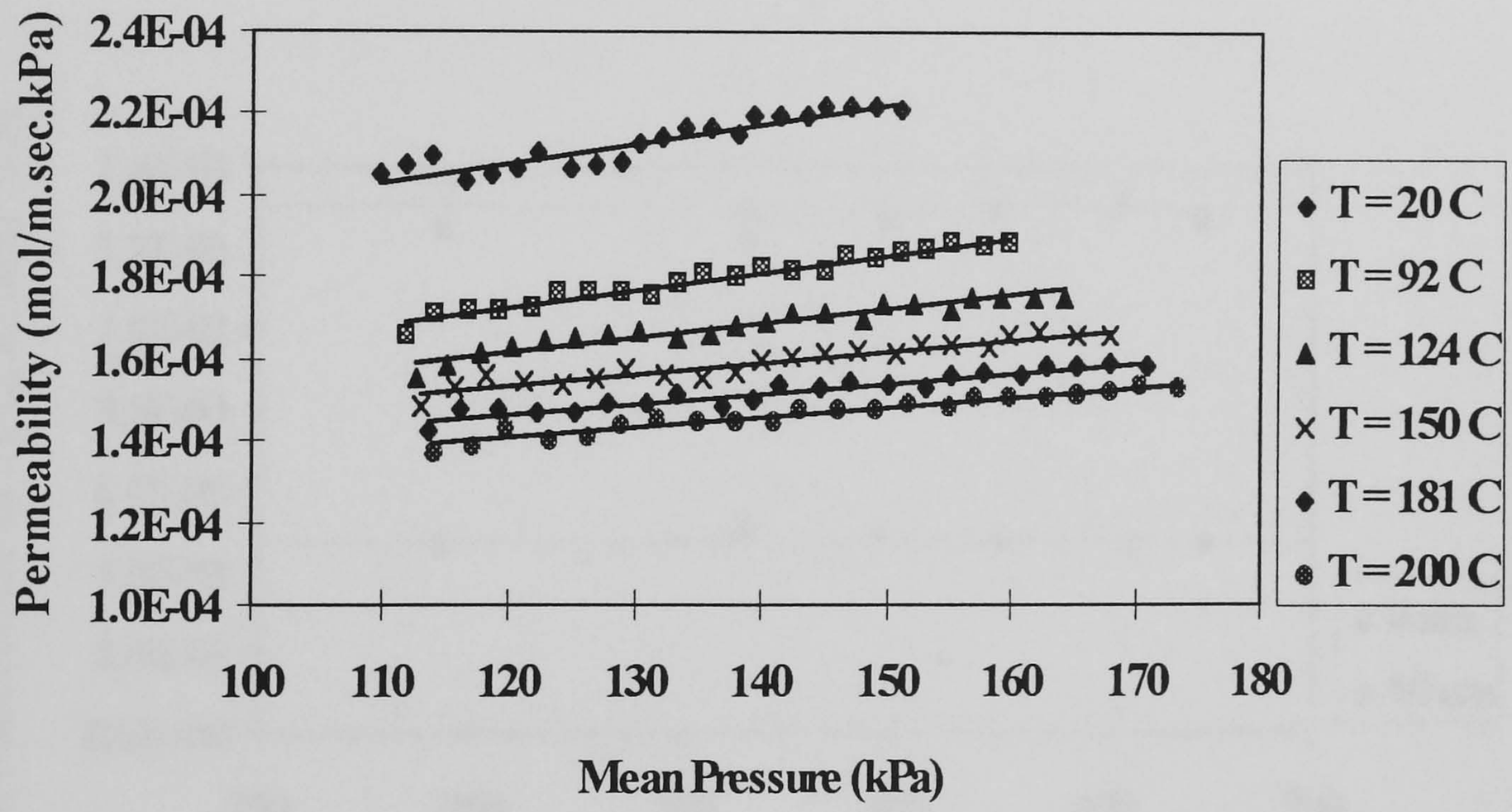


Figure 4.3 Nitrogen gas permeability through the membrane with 10 nm membrane pore size

Because an intersection at mean pressure of zero and a slope of the curve gives the values $a/\sqrt{MT}$ and $b/\mu T$, respectively, the Knudsen parameter (a) and the viscous parameter (b) can be calculated when the operating temperature, gas molecular weight and gas viscosity are known. The gas viscosity can be estimated

by Wilke's correlation (Bird *et al.*, 1960). Another set of experiments with nitrogen gas was carried out at the same operating conditions and the values of Knudsen parameters and viscous parameters are summarised in Figure 4.4 and Figure 4.5. The scatter of the data points in both graphs arise from the difficulty in determining the slope of the line which is small in value. The slope is affected by small differences in the actual reading of the flow rate and transmembrane pressure (Altena *et al.*, 1983). It should be noted that in the interpretation the resistances due to the membrane support layers are assumed to be small compared to that of the separative top layer. Appendix 1 provides the characteristics of each layer of the membrane with a pore size of 4 nm. It also shows that the resistance of the separative layer is around ten times as high as that of the next layer.

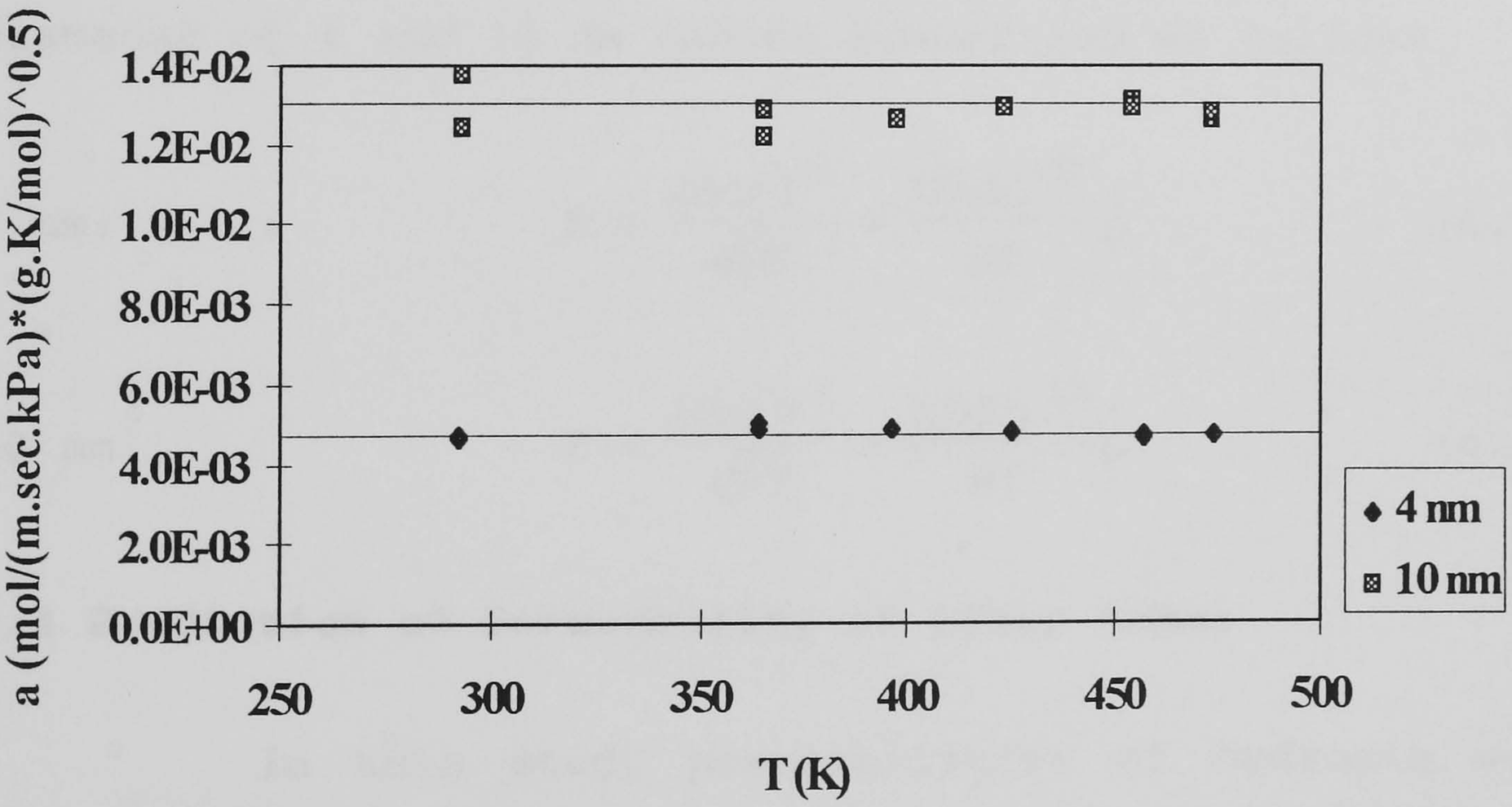


Figure 4.4 Knudsen parameters from N_2 experiments

It should be noted that in Figure 4.4 and Figure 4.5 the continuous lines show the average values of the a parameters and b parameters.

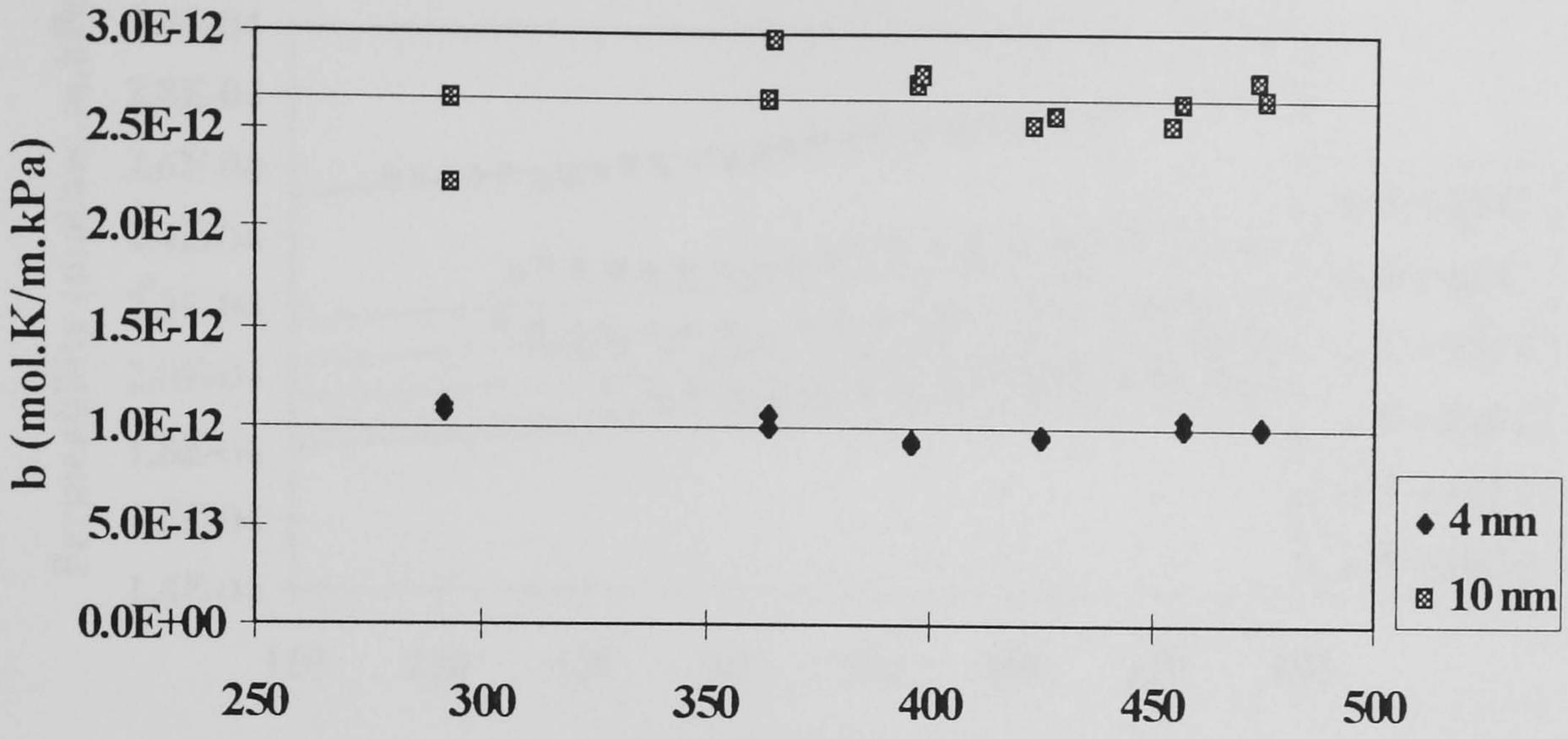


Figure 4.5 Viscous flow parameters from N_2 experiments

From the experiment of nitrogen permeation, the gas phase flow through the γ-Al_2O_3 membranes with pore diameter of 4 and 10 nm can be summarised as follows

4 nm:
$$P = \frac{4.8\times10^{-3}}{\sqrt{MT}} + \frac{1.0\times10^{-12}}{\mu T}\bar{p} \qquad (4.1)$$

10 nm:
$$P = \frac{1.3\times10^{-2}}{\sqrt{MT}} + \frac{2.7\times10^{-12}}{\mu T}\bar{p} \qquad (4.2)$$

4.4 Prediction of Permeability of Other Gases

In this study permeabilities of hydrogen were measured at the same temperature levels as performed in the nitrogen experiments. It was found earlier that the permeation of hydrogen through an alumina membrane took place only in the gas phase (Okubo *et al.*, 1991). The results are shown in Figure 4.6 and Figure 4.7. The continuous lines show the hydrogen permeabilities predicted from nitrogen permeation studies.

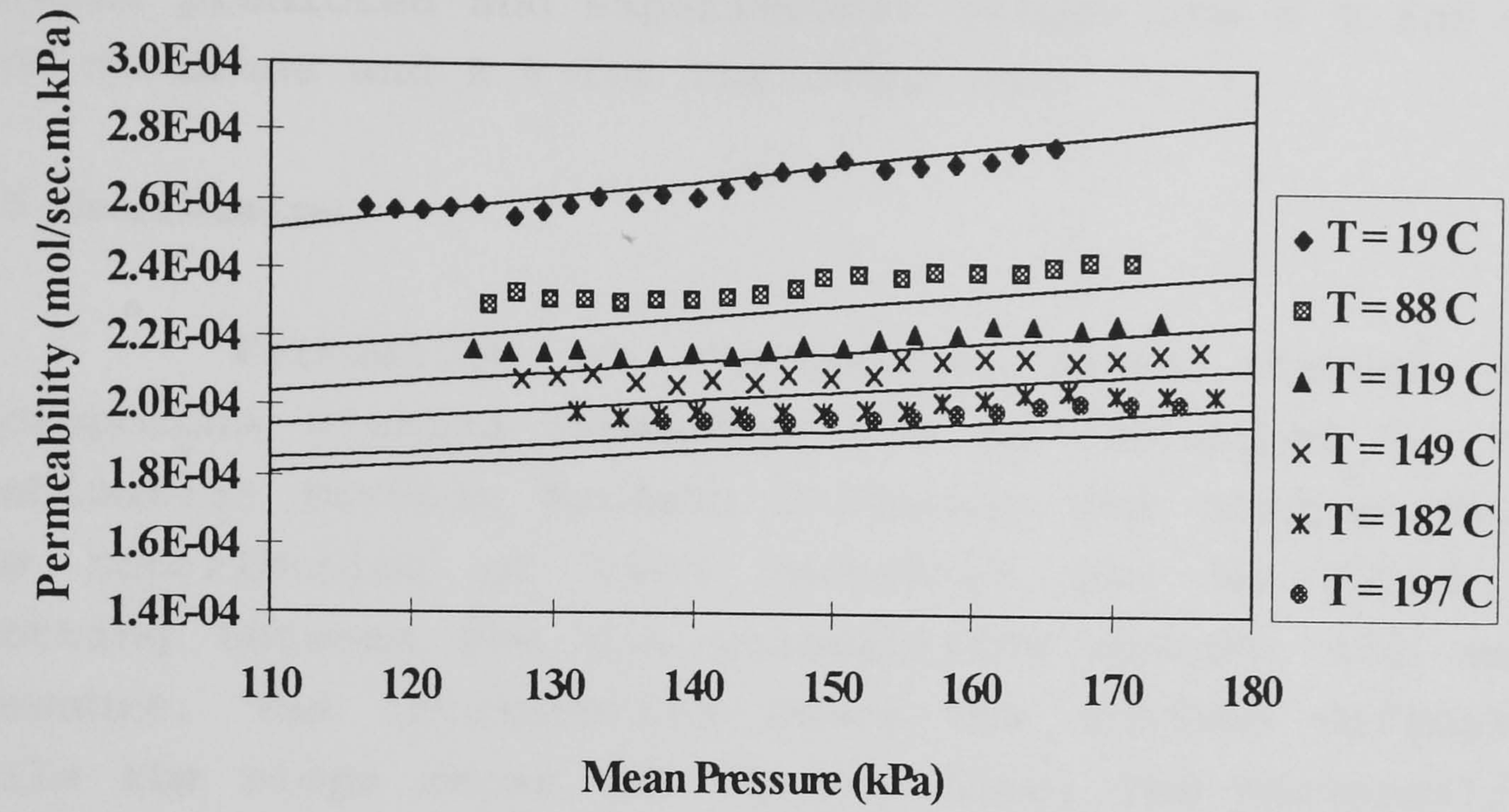


Figure 4.6 Hydrogen gas permeability through the membrane with 4 nm membrane pore size

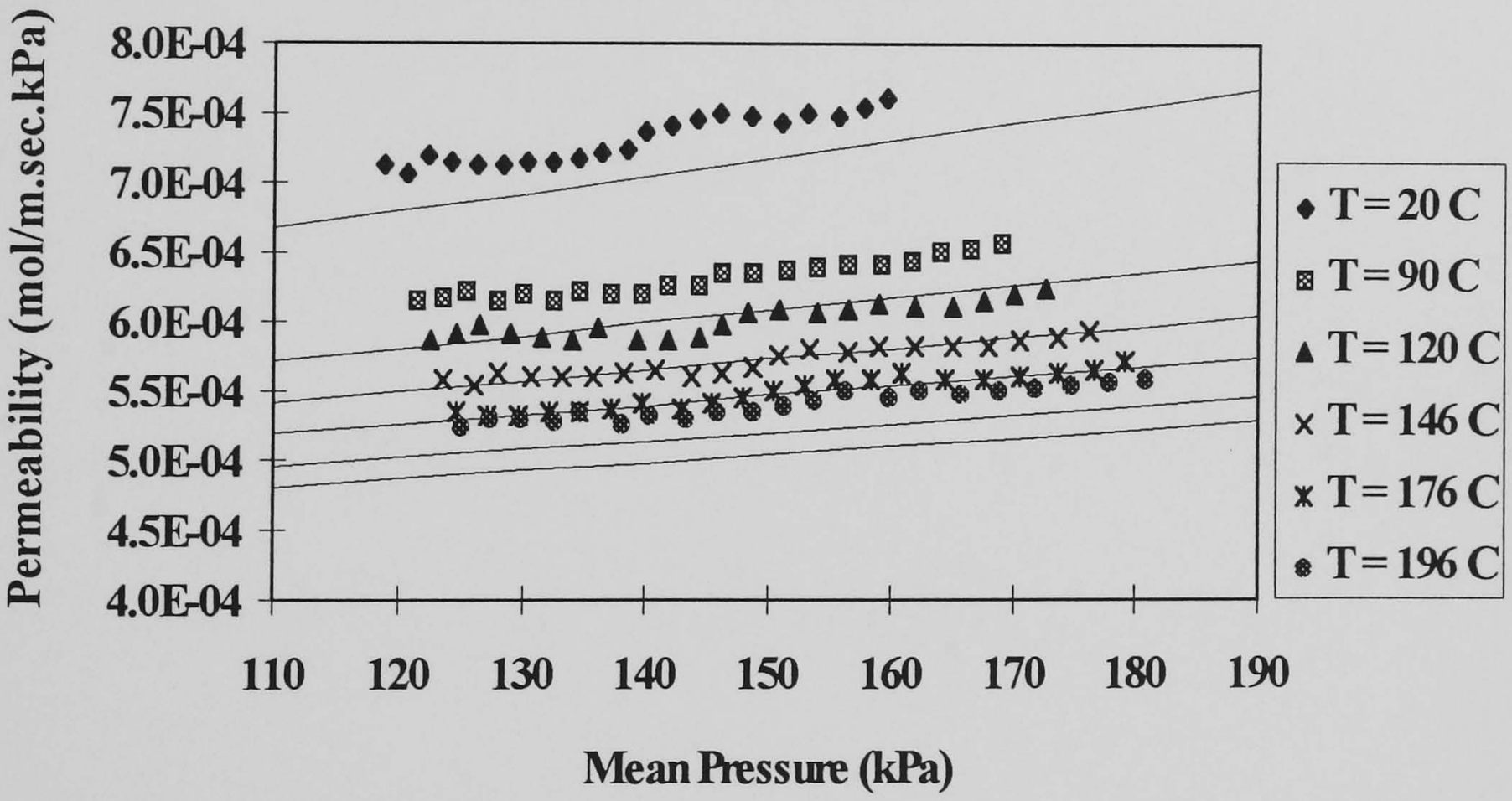


Figure 4.7 Hydrogen gas permeability through the membrane with 10 nm membrane pore size

It can be seen that there is a discrepancy between the experimental results and the predicted values and it is larger for the membrane with pore diameter of 10 nm. The cause of this discrepancy is probably due to the effect of the supporting layers. However, the average deviation

between predicted and experimental values are 4 % for the 4 nm membrane and 8 % for the other one.

4.5 Conclusion

Permeation of nonadsorbed gases through the microporous alumina membranes can be described by the combination between Knudsen diffusion and viscous flow. The contribution of each mechanism can be found by plotting between the gas permeability against the mean pressure. The intersection shows the Knudsen diffusion while the slope shows the viscous flow. The permeability of a nonadsorbed gas such as N_2 can be used to predict the permeability of another gas such as H_2. The alumina membranes are composite in nature; however, the resistance of the support has small effect on the permeation of the separative layer.

CHAPTER 5

EXPERIMENTAL STUDIES OF ETHANOL AND METHANOL VAPOUR PERMEATION

5.1 Introduction

5.2 Description of Experimental System

5.3 Model Development

5.4 Results and Discussion

5.5 Conclusion

CHAPTER 5

EXPERIMENTAL STUDIES OF ETHANOL AND METHANOL VAPOUR PERMEATION

5.1 Introduction

In this chapter, experimental studies of the permeation of ethanol and methanol vapours through alumina membranes with pore diameter of 4 and 10 nm were performed. These were carried out at three temperature levels between 150 to 200 ^{o}C. The permeability of ethanol and methanol vapours was found to be less than that predicted from a model which combines bulk viscous and Knudsen flow. A new mathematical model based on the assumption that the contribution of the adsorbed phase of ethanol and methanol on the membrane pore wall is small compared to that in the gas phase was proposed to describe the results. Experiments with nitrogen - ethanol and nitrogen - methanol mixtures were conducted to verify this assumption.

5.2 Description of Experimental System

- **Alcohol Vapour Permeation Studies**

Figure 5.1 shows the modified experimental system for the permeation study with ethanol and methanol. The main modifications from the experimental system described in Chapter 4 are at the feed and the product collection systems. A 'Watson Marlow' peristaltic pump was used to transport pure alcohol from its container to the system. The liquid alcohol firstly passed a preheater made of a stainless steel tube with 1/8" diameter and 1.5 meter length. An electric bulb (100 watts) was used as a heat source for the preheater where

most of the liquid alcohol was vaporised. Then the vapour and the rest of liquid alcohol was superheated in another heat exchanger inside the oven to the desired temperature level. The flow rate of alcohol was obtained by weighing the alcohol feed container. The system was allowed to reach steady state which took around 30 to 40 minutes, and then the pressure inside the membrane was recorded. The experiment was repeated at different feed flow rates. It should be noted that before each experiment with the pure alcohol, a nitrogen gas permeation was performed so that predicted gas permeability of alcohol vapour can be estimated. This was done to check if any fouling of the membrane had occurred.

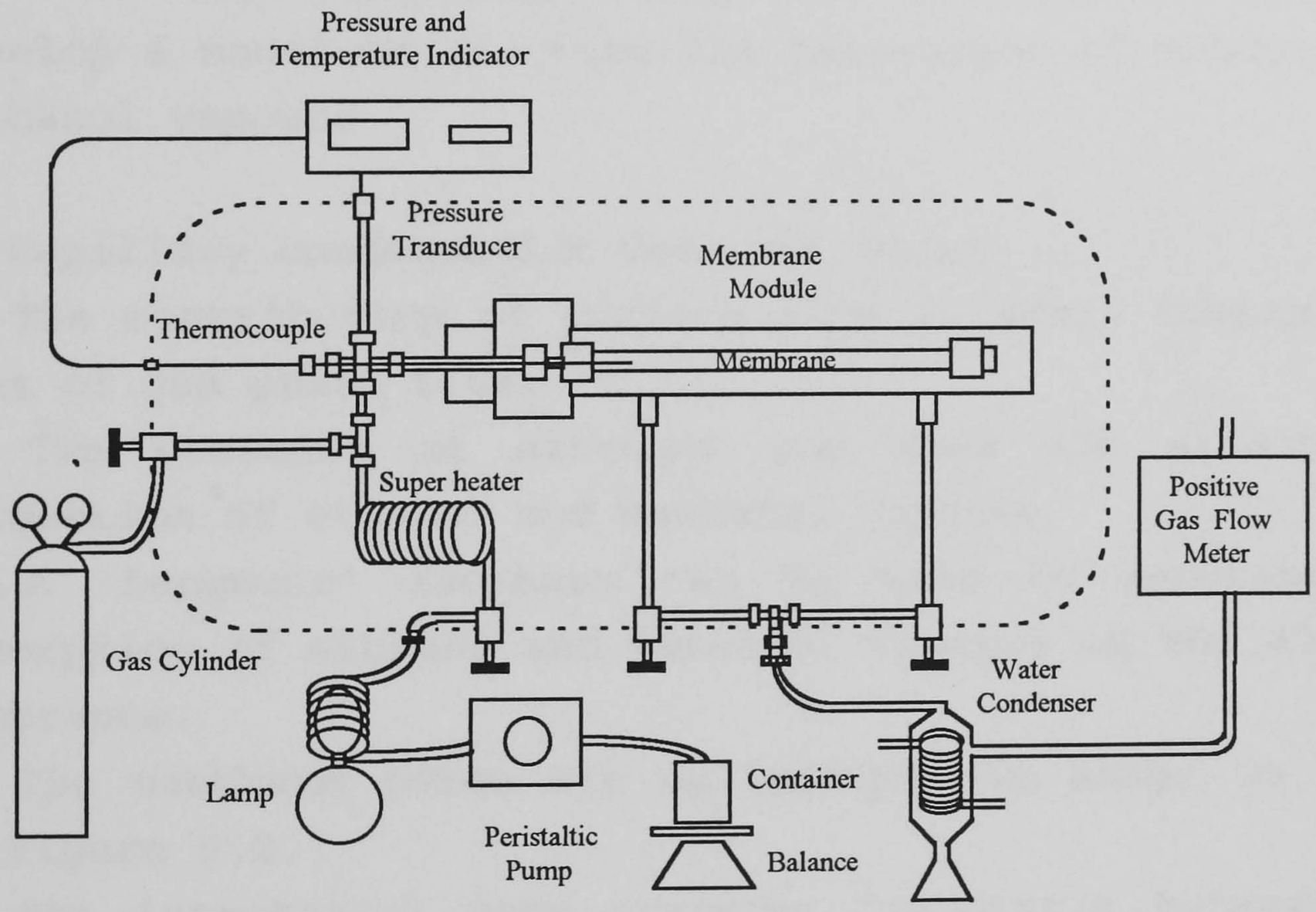


Figure 5.1 The schematic diagram of experimental setup for vapour permeation measurement

- **Mixture Permeation Studies**

The permeation studies of mixtures of nitrogen gas and alcohol vapour were performed as follows. Firstly the system was filled with nitrogen gas at a given pressure. The nitrogen flow rate was measured, and then

alcohol was fed into the system as described before. The system was then allowed to achieve steady state. The feed rate of alcohol was measured from the weight loss read from the balance. Because the outlet stream consisted of nitrogen and alcohol, alcohol was separated from nitrogen gas by passing the outlet to a water condenser before it was further trapped in a test tube immersed in liquid nitrogen. A positive displacement gas flow meter was used to measure the flow of non condensible gas leaving the cooling system.

5.3 Model Development

The following assumptions are made in order to develop a model to describe the permeation of ethanol and methanol vapours

1) Capillary condensation does not occur.
2) The contribution of surface flow is small compared to that of gas phase flow.
3) The presence of nitrogen gas does not affect the permeation of ethanol and methanol vapours.
4) A 'Langmuir' isotherm can be used to describe the adsorption of ethanol and methanol vapours on the alumina membranes.
5) The membrane pores are cylindrical in shape as shown in Figure 5.2.
6) The interfacial mass transfer resistance between the gas and the surface of membrane is small compared with the internal mass transfer resistance in the membrane.

The validity of assumption 1 can be checked by calculation of saturation pressure of gas or vapour in membrane pores using the Kelvin equation. It has been known from the literature (Ciordano *et al.*, 1981) that methanol and ethanol are usually strongly chemisorbed on an alumina. As a result, the contribution of surface flow of methanol and ethanol through the alumina membrane is

likely to be small, compared to the gas phase flow. Assumption 4 is based on the fact that the Langmuir isotherm is a suitable model to describe a system of chemisorption (Brunauar, 1944). The validity of assumption 3 is not so obvious. However, there is evidence from other systems for this. For example, the permeation of ethylbenzene is not strongly affected by the presence of hydrogen gas (Liu *et al.*, 1990). Assumption 6 arises from the fact that gas phase diffusivity is usually high. In a study by Sloot *et al.* (1992) for the permeation of hydrogen sulphide and sulphur dioxide through an alumina membrane, they found that when the mass transfer resistance in the gas phase outside the membrane was increased by 50 %, the parameters in their model deviated only 4 to 8 %.

The adsorbed vapour phase on the membrane pore wall can hinder the gas phase flow through the membrane. This effect is significant especially when the membrane pore diameter is small. The diameter of an ethanol molecule is 4.6 Å (0.46 nm) and that of a methanol one is 4.1 Å (0.41 nm) or 10 - 20 times smaller than the pores of the membrane used in this study (see Table A2.1 in Appendix 2). The model of the sorption of alcohol molecules is shown in Figure 5.2. These sorb on to the membrane wall as shown reducing the effective diameter of the pores from d_o to d_n.

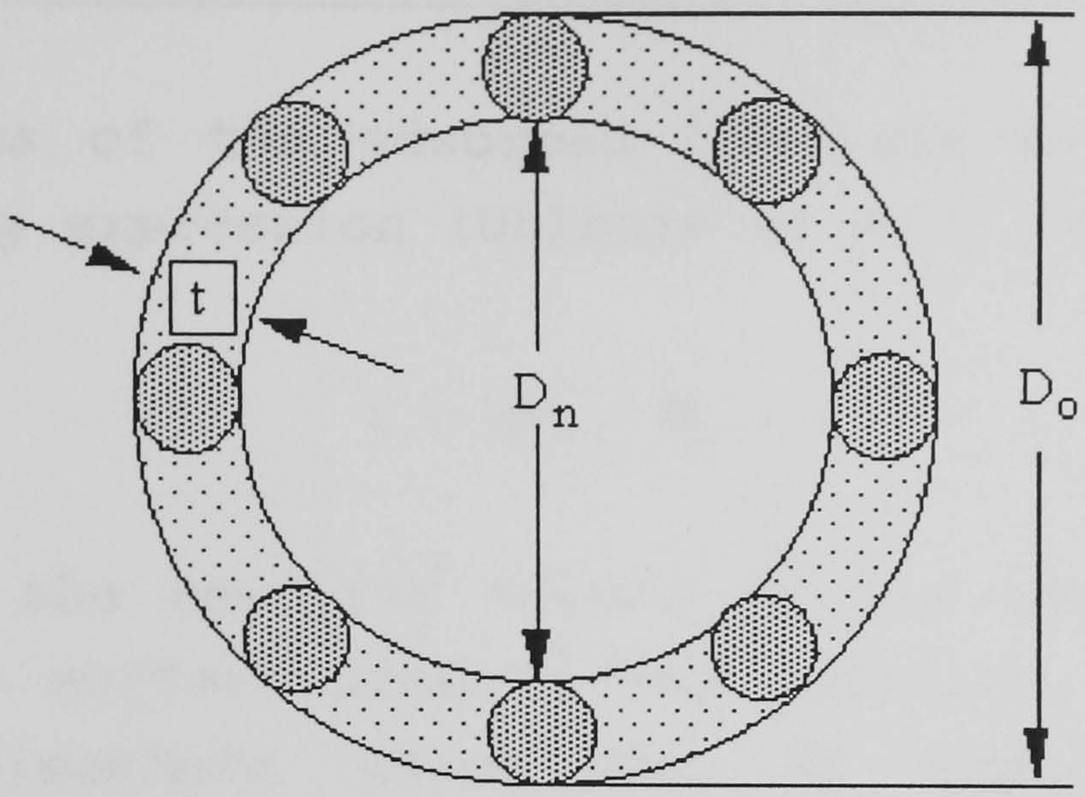


Figure 5.2 Cross sectional of a membrane pore

Let ϕ be the fraction of the membrane area blocked by the adsorption of alcohols on the membrane. Now the available area for gas permeation is

$$\frac{\pi}{4} d_n^2 = (1 - \phi) \frac{\pi}{4} d_o^2 \qquad (5.1)$$

So the ratio of new membrane pore diameter and the original diameter is

$$\frac{d_n}{d_o} = \sqrt{1 - \phi} \qquad (5.2)$$

Since the Knudsen parameter is proportional to d_p^3 and the viscous flow parameter is proportional d_p^4 as shown in Equation (2.1) and (2.2), the new expression for molar flow rate of pure component i (F_i) is

$$\frac{F_i}{L} = \frac{a(1 - \phi)^{3/2}}{\sqrt{M_i T}} (p_1 - p_2) + \frac{b(1 - \phi)^2}{2\mu T} (p_1^2 - p_2^2) \qquad (5.3)$$

The membrane blockage (ϕ) can be related to an adsorption of alcohol on the alumina membranes by the following consideration.

The thickness of the adsorbed film can be described by the following expression (Uhlhorn *et al.*, 1992).

$$t = qV_t / S_t \qquad (5.4)$$

where V_t is the specific volume of the adsorbate, S_t is the specific surface area of the membrane, and q is the adsorption isotherm which can be expressed by the following expression. This is of the 'Langmuir' type where,

$$q = K'p/(1+Kp) \qquad (5.5)$$

K' and K are parameters in this equation with units mol/kg.kPa and kPa^{-1} respectively.

Since the relation between d_o and d_n is related by

$$d_o = d_n + 2t \qquad (5.6)$$

or

$$\frac{d_n}{d_o} = 1 - \frac{2t}{d_o} \qquad (5.7)$$

Substitution of (5.2), (5.4) and (5.5) in (5.7) and rearranging it gives

$$1 - \omega = \sqrt{1 - \phi} \qquad (5.8)$$

where

$$\omega = \frac{\chi p}{(1 + Kp)} \qquad (5.9)$$

and

$$\chi = \frac{2K' V_t}{S_t d_o} \qquad (5.10)$$

With equation (5.8), the molar flow rate of pure component i can be shown as a function of the parameter ω as

$$\frac{F_i}{L} = \frac{a(1-\omega)^3}{\sqrt{M_i T}}(p_1 - p_2) + \frac{b(1-\omega)^4}{2\mu T}(p_1^2 - p_2^2) \qquad (5.11)$$

This expression is used to interpret the results from the permeation studies of pure alcohol. With the known parameters; a and b, and experimental data, the parameter ω can be calculated. The obtained values can be further correlated to the operating pressure by Equation (5.9).

5.4 Results and Discussion

Permeability of ethanol and methanol vapours through the membranes with pore diameter of 4 and 10 nm were measured and the results are shown in Figure 5.3 - 5.6. Permeation studies of ethanol vapour were carried out at 160 and 200 °C while those of methanol vapour were performed at 150, 175 and 200 °C. Since some of the alcohol may be converted to other species on the alumina membranes, the composition of the liquid outlet condensed by liquid nitrogen was checked by using a gas chromatograph with an FID (Flame Ionisation Detector) detector and the conversion of alcohol was found less than 4 % in all experiments. There was also an evidence that the conversion of methanol on γ-Al_2O_3 was only a few percent at 200 °C (Zaspalis *et al.*, 1991a). In all cases, the permeation results were less than the gas phase permeabilities which were predicted from the results of experiments with nitrogen*. This behaviour of ethanol vapour permeation was noted earlier in the literature (Berg *et al.*, 1987) which also suggested that the interaction between ethanol and an alumina membrane may be the cause of the discrepancy. It should be pointed out that the difference between the predicted values and

* see Equation 2.15 for the predicted values

those from experiment is more pronounced when the operating temperature is lower.

In order to check for the presence of capillary condensation, the Kelvin equation was used to calculate the saturation pressure of ethanol and methanol vapours in the membrane pores and the results are shown in Table A3.1 and Table A3.2 in Appendix 3. Since the operating pressure in this study was less than 200 kPa, it is clear that the operating condition was far below the saturation pressure at every temperature level. Hence, it is unlikely that the capillary condensation took place in this study.

Apart from the gas phase permeation of alcohol vapours through the alumina membranes, surface diffusion is another possible mechanism. In general, in the presence of the surface diffusion, the total permeation rate is usually higher than the predicted values from the nonadsorbed gas permeation. However, in this study, both the permeation of methanol and ethanol were found less than the predicted values. This may be because the adsorbed molecules do not make a significant contribution on the total transport but block the membrane pores, lowering the gas phase flow rate. Work on the adsorption of ethanol and methanol on γ-Al_2O_3 was done by Russian workers (Litinskii *et al.*, 1981). They found that both alcohols are strongly and irreversibly chemisorbed on alumina. As a result, the surface diffusion of alcohols should be small.

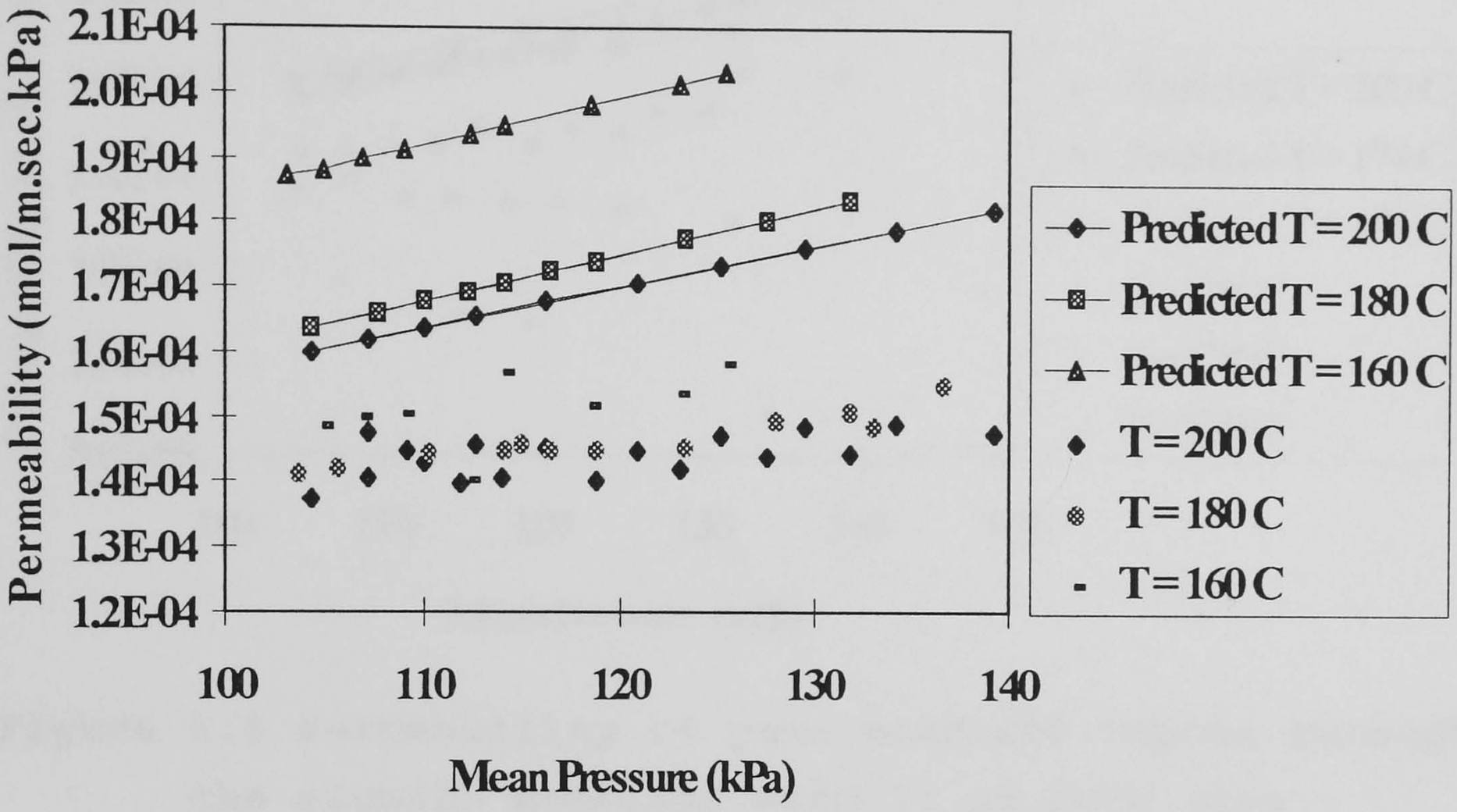


Figure 5.3 Permeability of pure ethanol vapour through the alumina membrane with 10 nm pore size

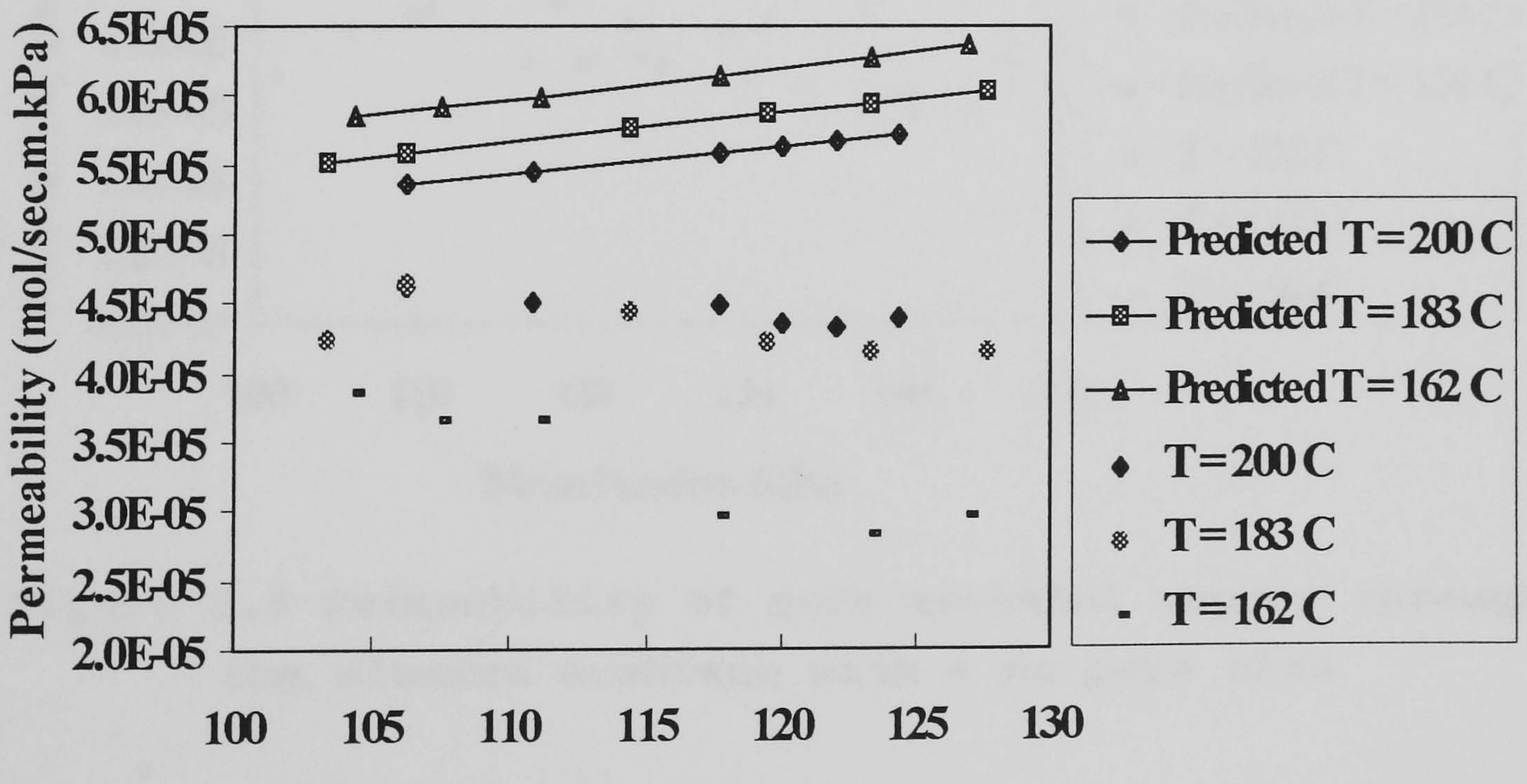


Figure 5.4 Permeability of pure ethanol vapour through the alumina membrane with 4 nm pore size

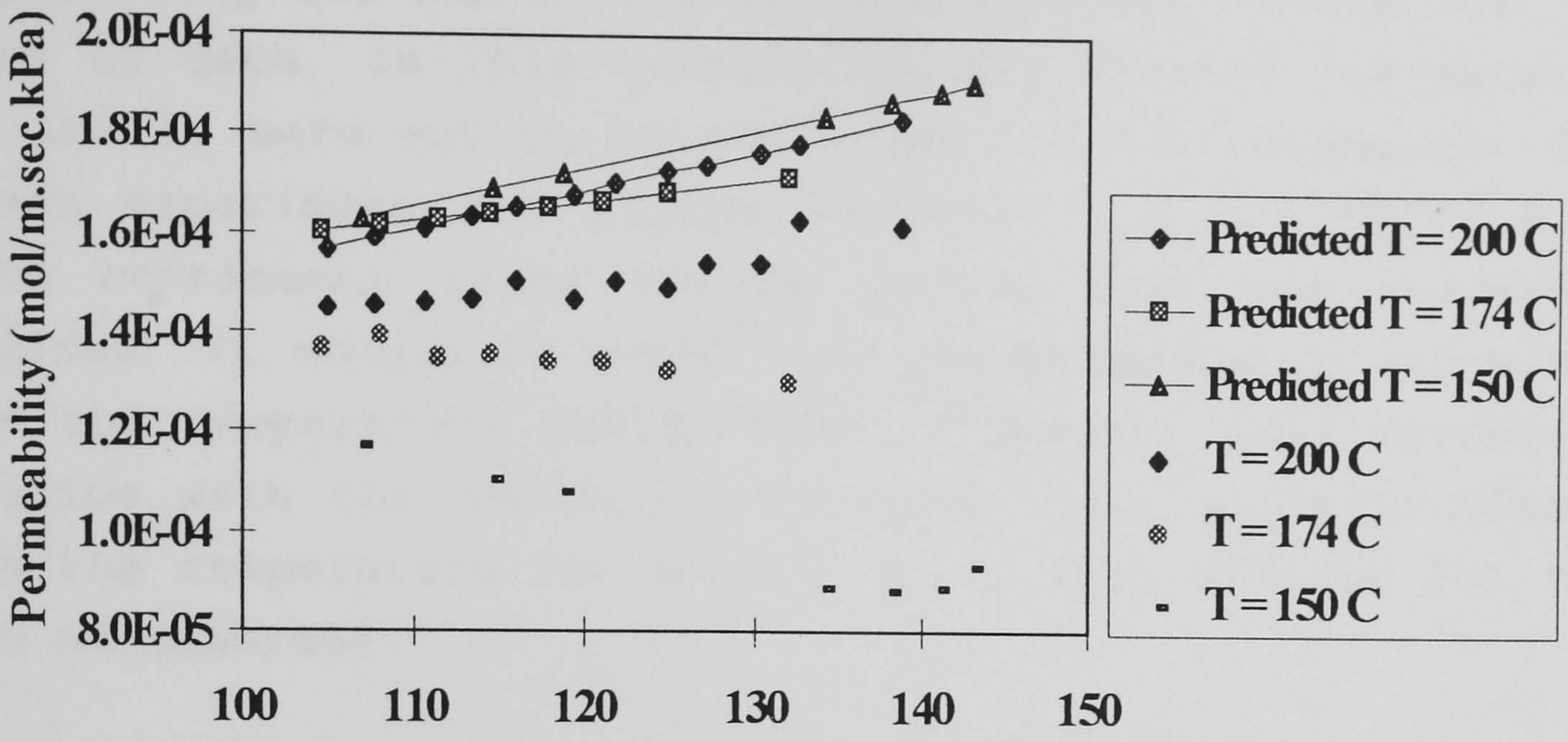


Figure 5.5 Permeability of pure methanol vapour through the alumina membrane with 10 nm pore size

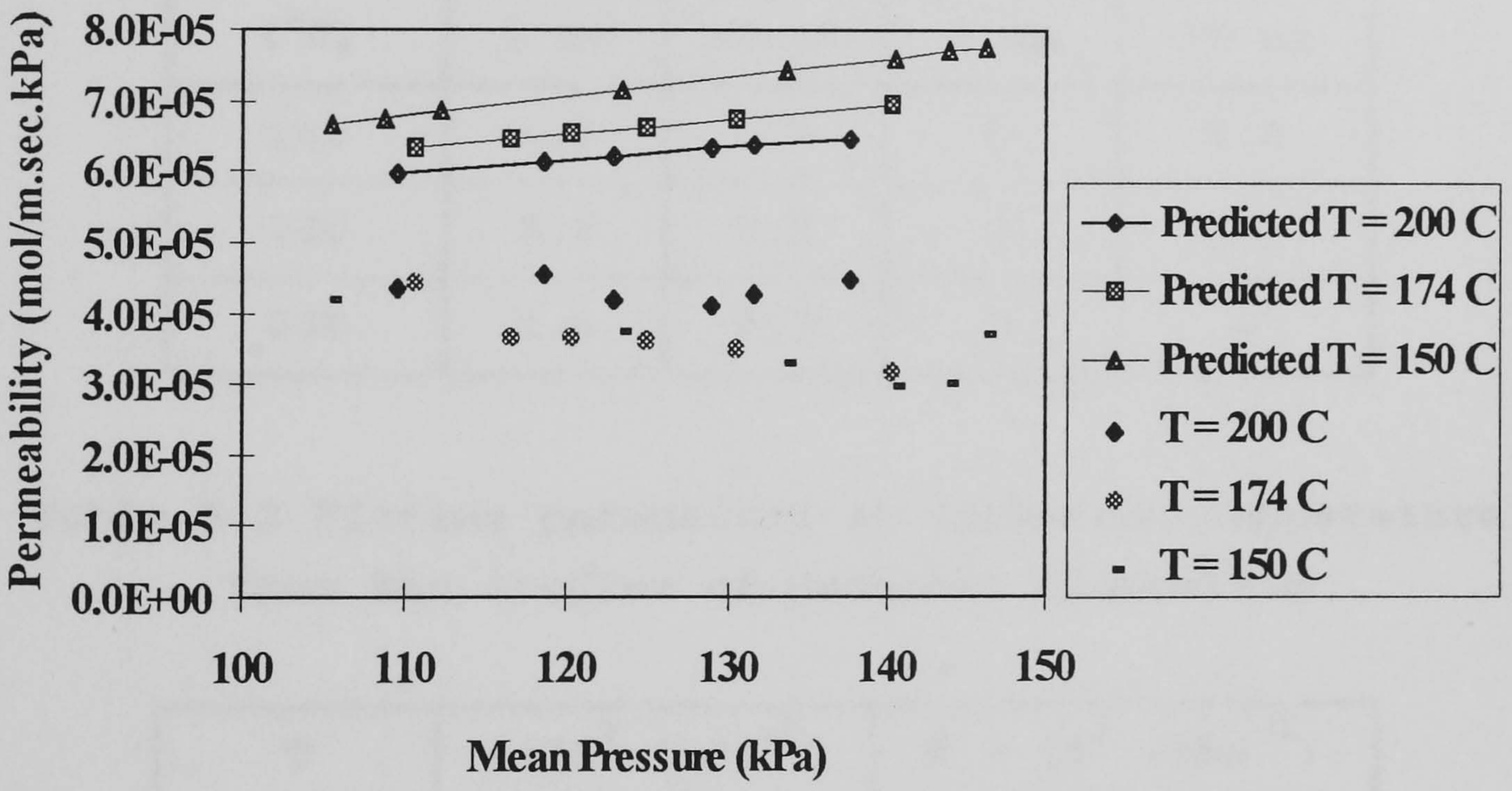


Figure 5.6 Permeability of pure methanol vapour through the alumina membrane with 4 nm pore size

From the experimental results, the parameter ω in the equation (5.11) can be solved using Newton's method for the nonlinear equations. The parameter is plotted against the pressure in the feed side as shown in Figure 5.7 - Figure 5.10. This relationship was correlated to Equation (5.9) by using the software 'ORIGIN' where fitting parameters are determined by

minimising the sum of the squared residual values for the set of data. In this calculation the fitting parameters; χ and K, were set to be non-negative. The parameters for each experiment are listed in Table 5.1 and Table 5.2. The continuous lines in the graphs show the regressed values. It should be noted that the parameter χ increases as the temperature falls. This is because this parameter varies with the amount of adsorbed phase which increases as the temperature is lowered. χ is also smaller for the 10 nm membrane.

Table 5.1 Fitting parameters at different temperature from the studies of ethanol permeation

T (^{o}C)	$\chi*10^{3}$ (kPa^{-1})		K * 10^{3} (kPa^{-1})	
	4 nm	10 nm	4 nm	10 nm
160	1.3	0.8	0	3.8
180	0.7	0.5	0	2.1
200	0.5	0.3	0	0

Table 5.2 Fitting parameters at different temperature from the studies of methanol permeation

T (^{o}C)	$\chi*10^{3}$ (kPa^{-1})		K * 10^{3} (kPa^{-1})	
	4 nm	10 nm	4 nm	10 nm
150	1.5	1.0	1.3	0
173	1.1	0.5	0	0
200	0.6	0.4	0	1.8

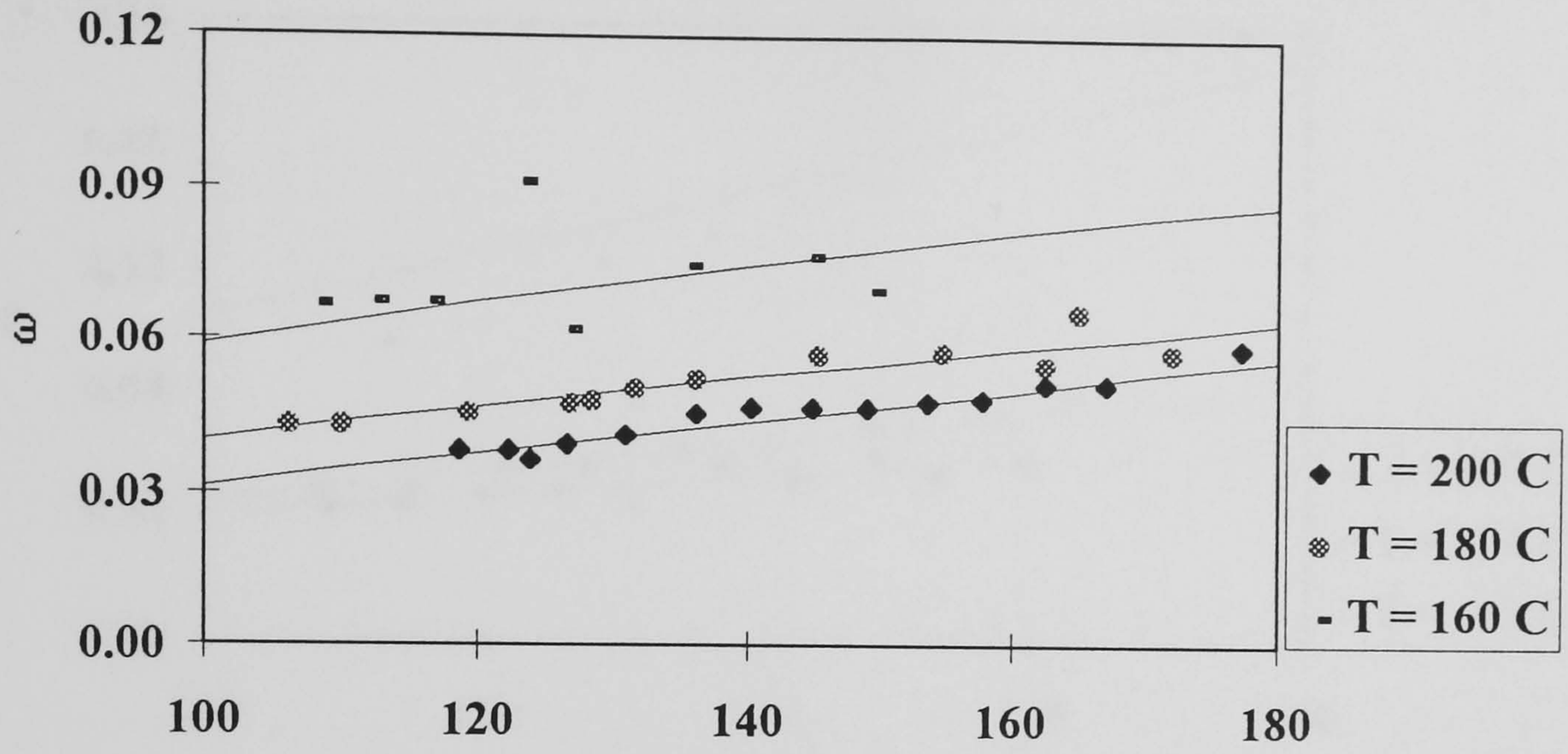


Figure 5.7 The relation between ω and feed pressure (From pure ethanol vapour permeation through the membrane with 10 nm pore size)

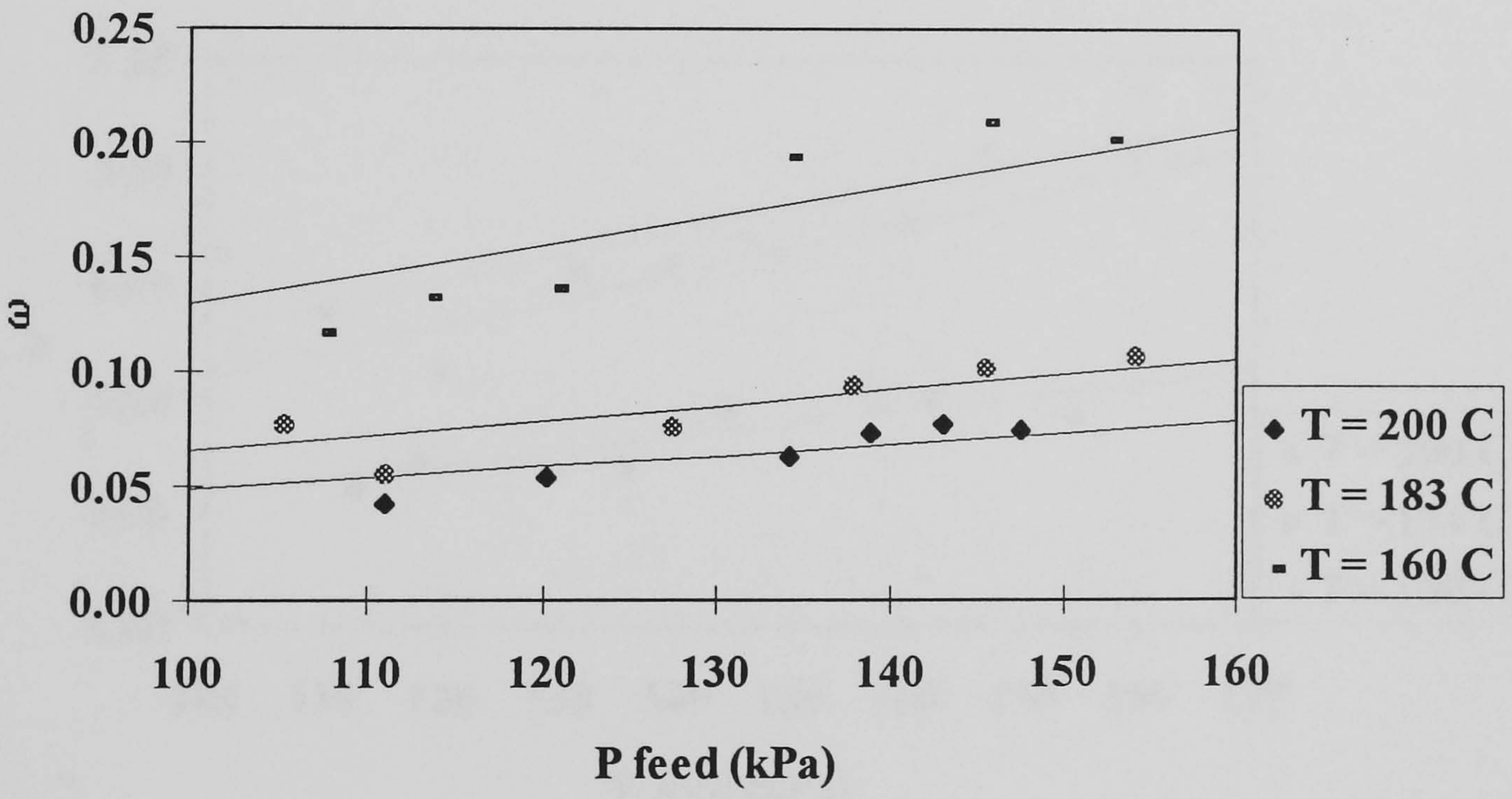


Figure 5.8 The relation between ω and feed pressure (From pure ethanol vapour permeation through the membrane with 4 nm pore size)

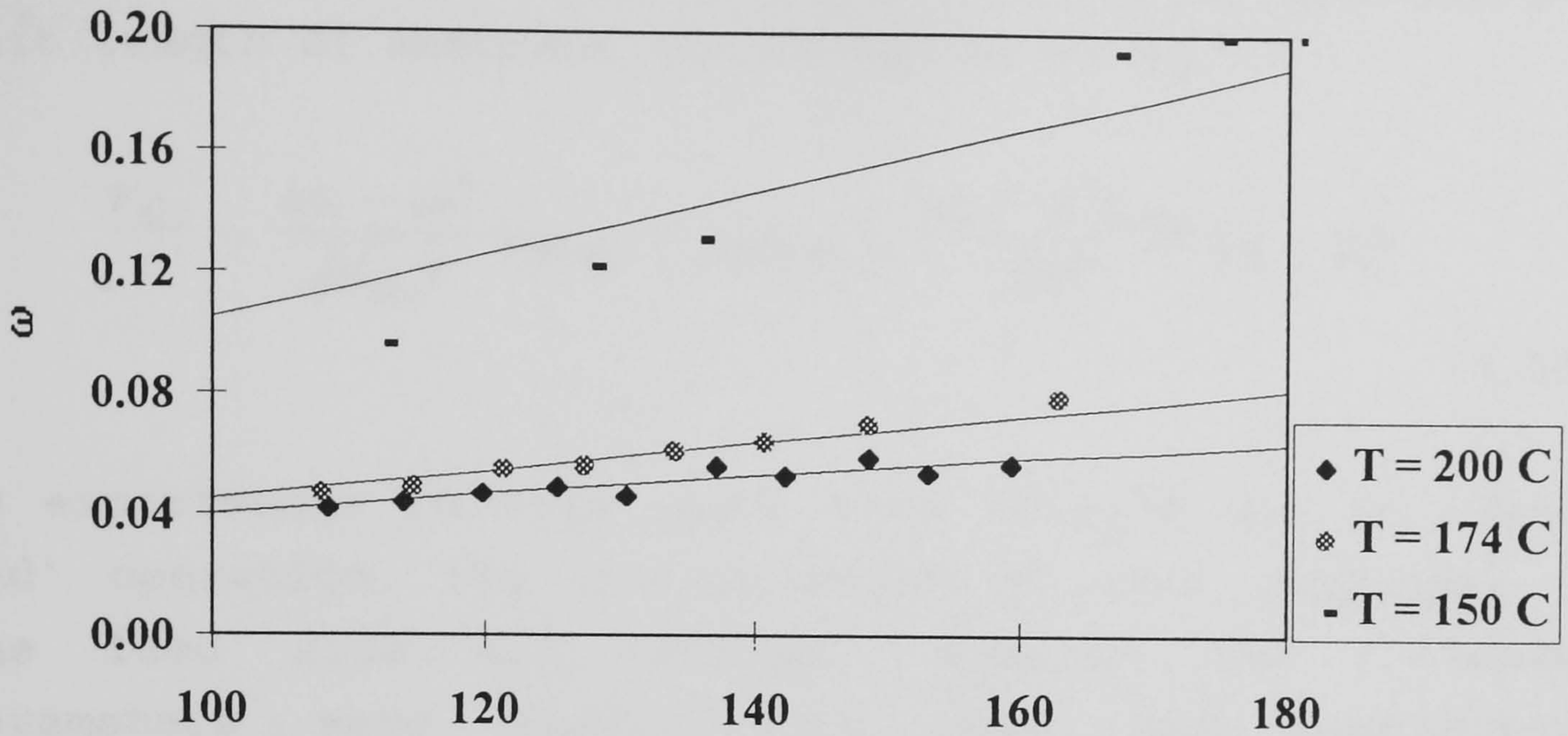


Figure 5.9 The relation between ω and feed pressure (From pure methanol vapour permeation through the membrane with 10 nm pore size)

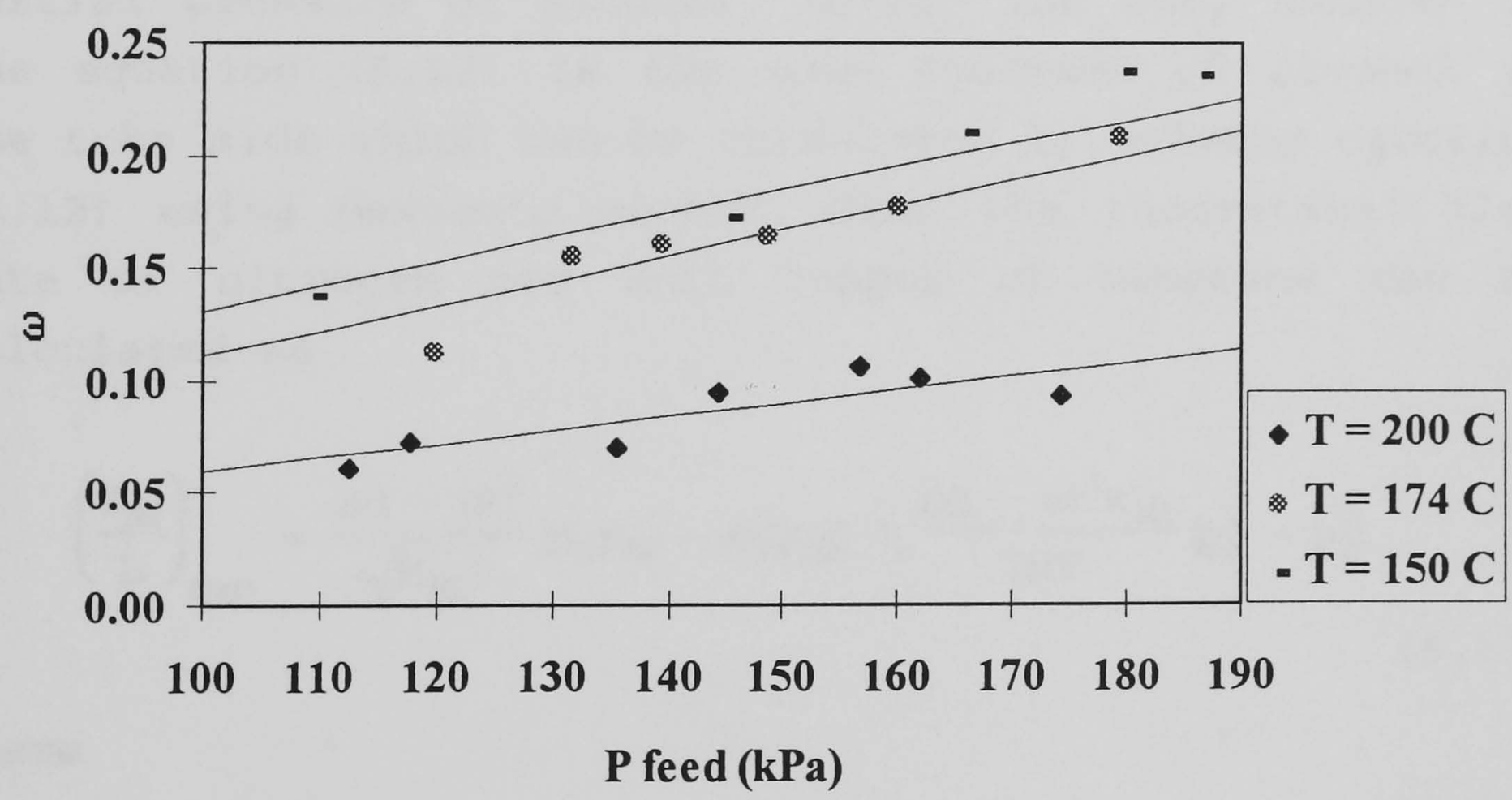


Figure 5.10 The relation between ω and feed pressure (From pure methanol vapour permeation through the membrane with 4 nm pore size)

In order to verify the proposed model, a set of experiments between the nonadsorbed nitrogen gas and alcohol were performed. The flow rate of nitrogen gas obtained from the experiment was compared to that

predicted from the model. The flow rate of alcohol per unit length of membrane can be expressed as

$$\frac{F_{alc}}{L} = \frac{a(1-\omega)^3}{\sqrt{M_{alc}T}}(p_1x_{alc} - p_2y_{alc}) + \frac{b(1-\omega)^4x_{alc}}{2\mu T}(p_1^2 - p_2^2) \qquad (5.12)$$

As experiments in this study were carried out in 'dead-end' operation, the concentration of each component in the feed side was unknown. However the following parameters were known, flow rate and composition (permeate side), pressure (feed side) and also the Knudsen and viscous parameters of the gas phase flow. The only three unknowns were mole fraction of alcohol and nitrogen in the feed side (x_{alc} and x_{N2}) and the parameter (ω). The values of the parameter ω have been found from the experiment of pure components as a function of partial pressure of alcohol. Hence, the only unknown in the equation (5.12) is the mole fraction of alcohol in the tube side which can be calculated by solving equation (5.12) using Newton's method. Then the theoretical flow rate of nitrogen per unit length of membrane can be calculated as

$$\left(\frac{F_{N2}}{L}\right)_{theo} = \frac{a(1-\omega)^3}{\sqrt{M_{N2}T}}(p_1x_{N2} - p_2y_{N2}) + \frac{b(1-\omega)^4x_{N2}}{2\mu T}(p_1^2 - p_2^2) \qquad (5.13)$$

where

$$x_{N2} = 1 - x_{alc} \quad \text{and} \quad y_{N2} = 1 - y_{alc} \qquad (5.14)$$

The flow rate per unit length of nitrogen gas from the calculation is plotted against the real values from the experiment of N_2-ethanol and N_2-methanol mixtures as shown in Figure 5.11 - Figure 5.14.

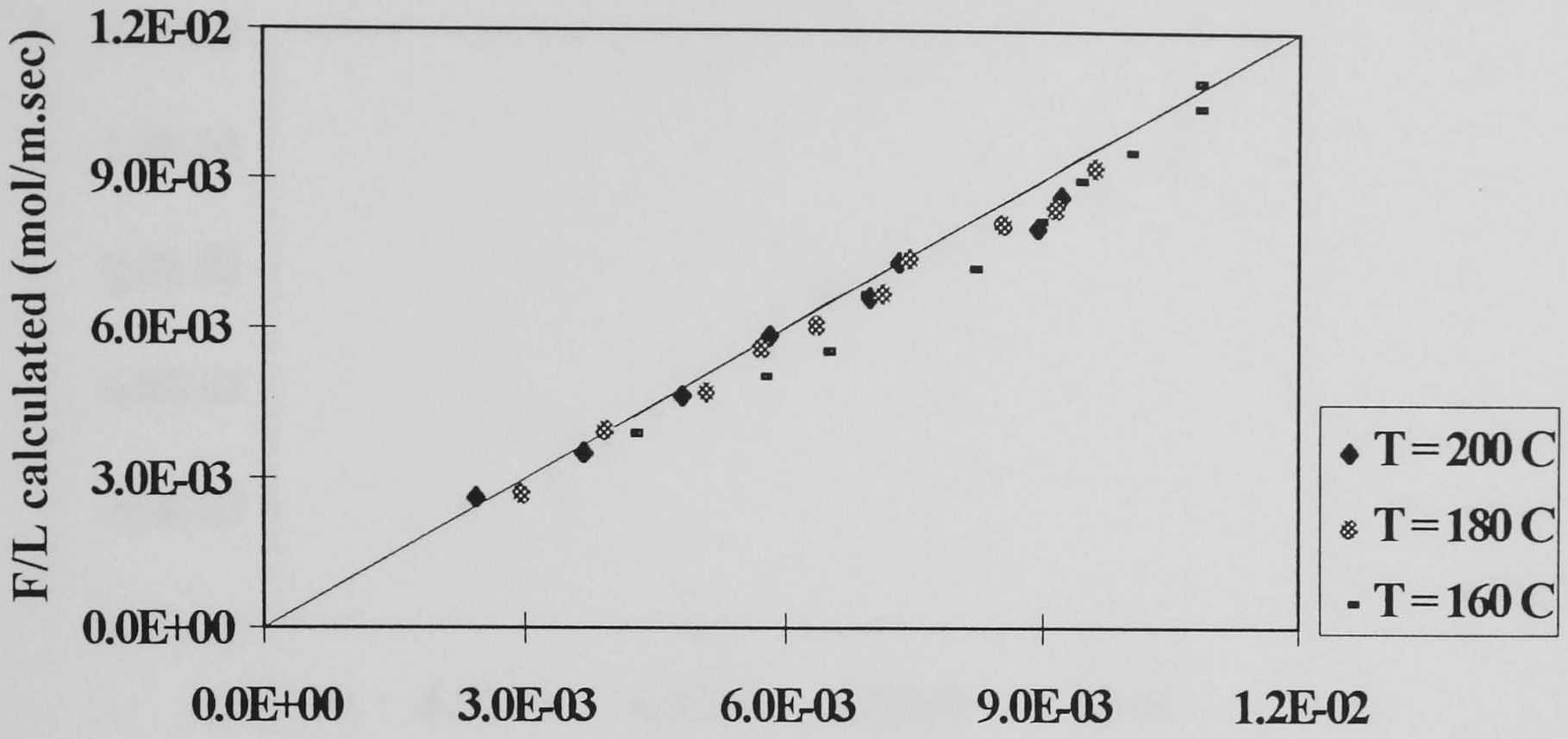


Figure 5.11 Experimental results from the mixtures of nitrogen gas and ethanol vapour through the membrane with 10 nm pore size

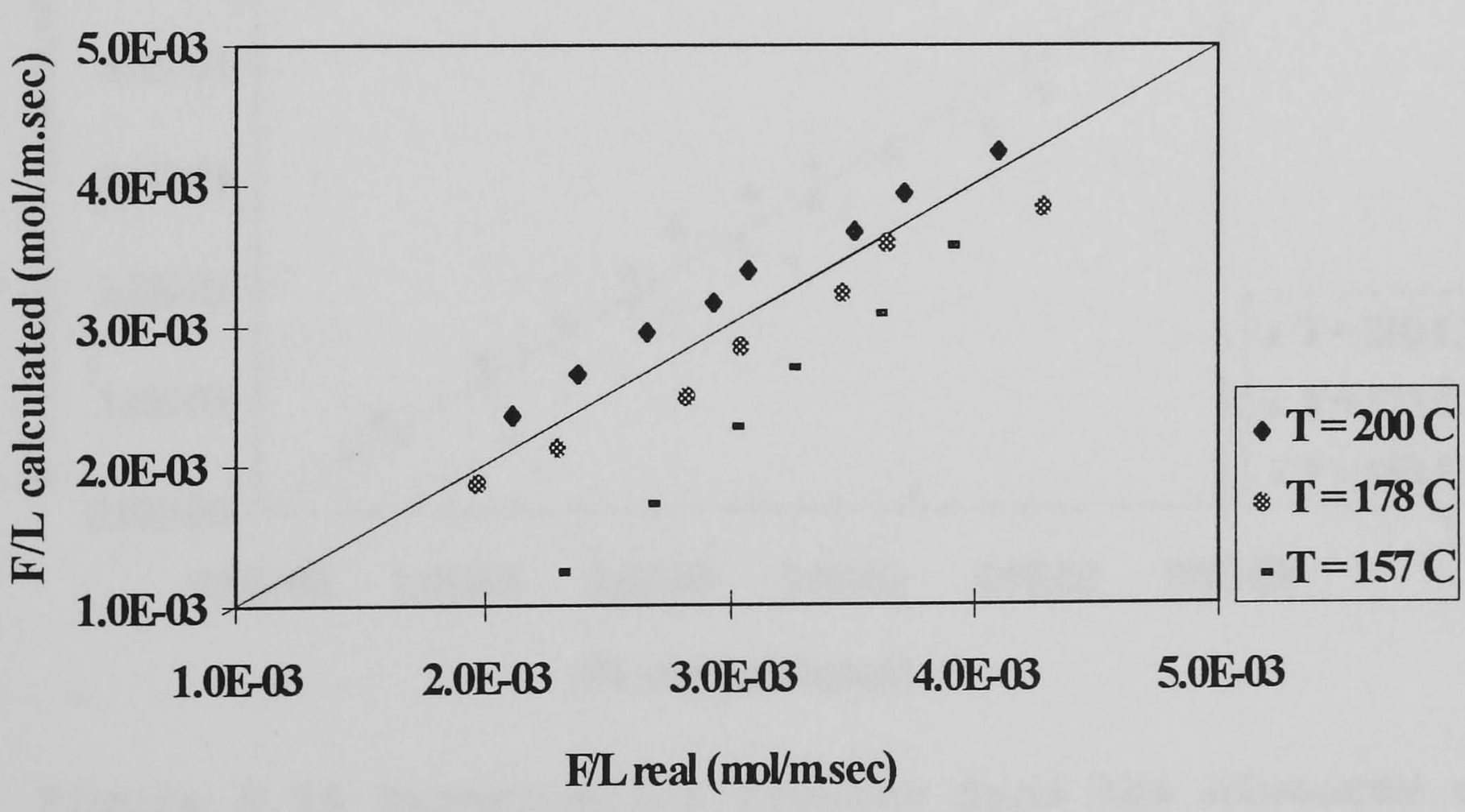


Figure 5.12 Experimental results from the mixtures of nitrogen gas and ethanol vapour through the membrane with 4 nm pore size

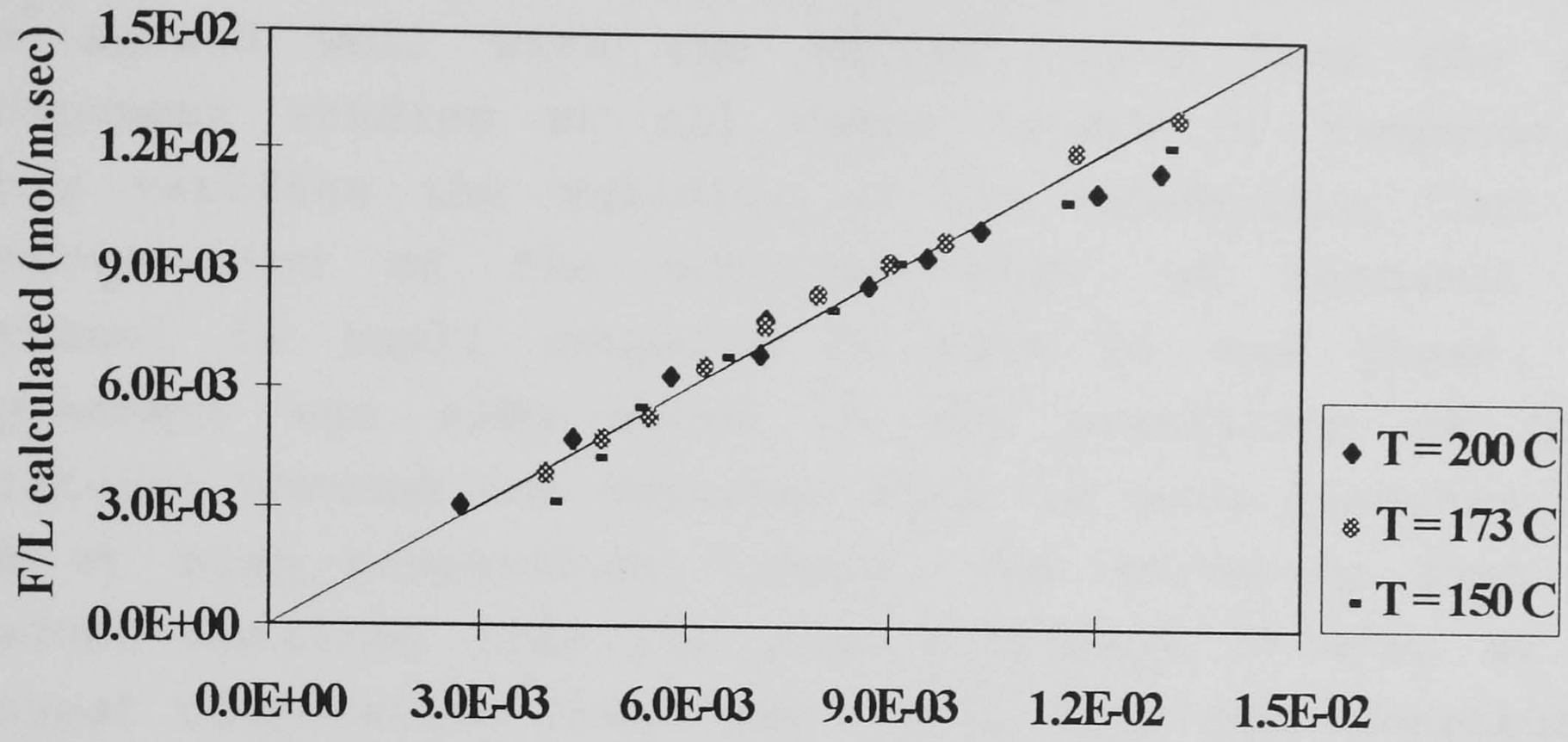


Figure 5.13 Experimental results from the mixtures of nitrogen gas and methanol vapour through the membrane with 10 nm pore size

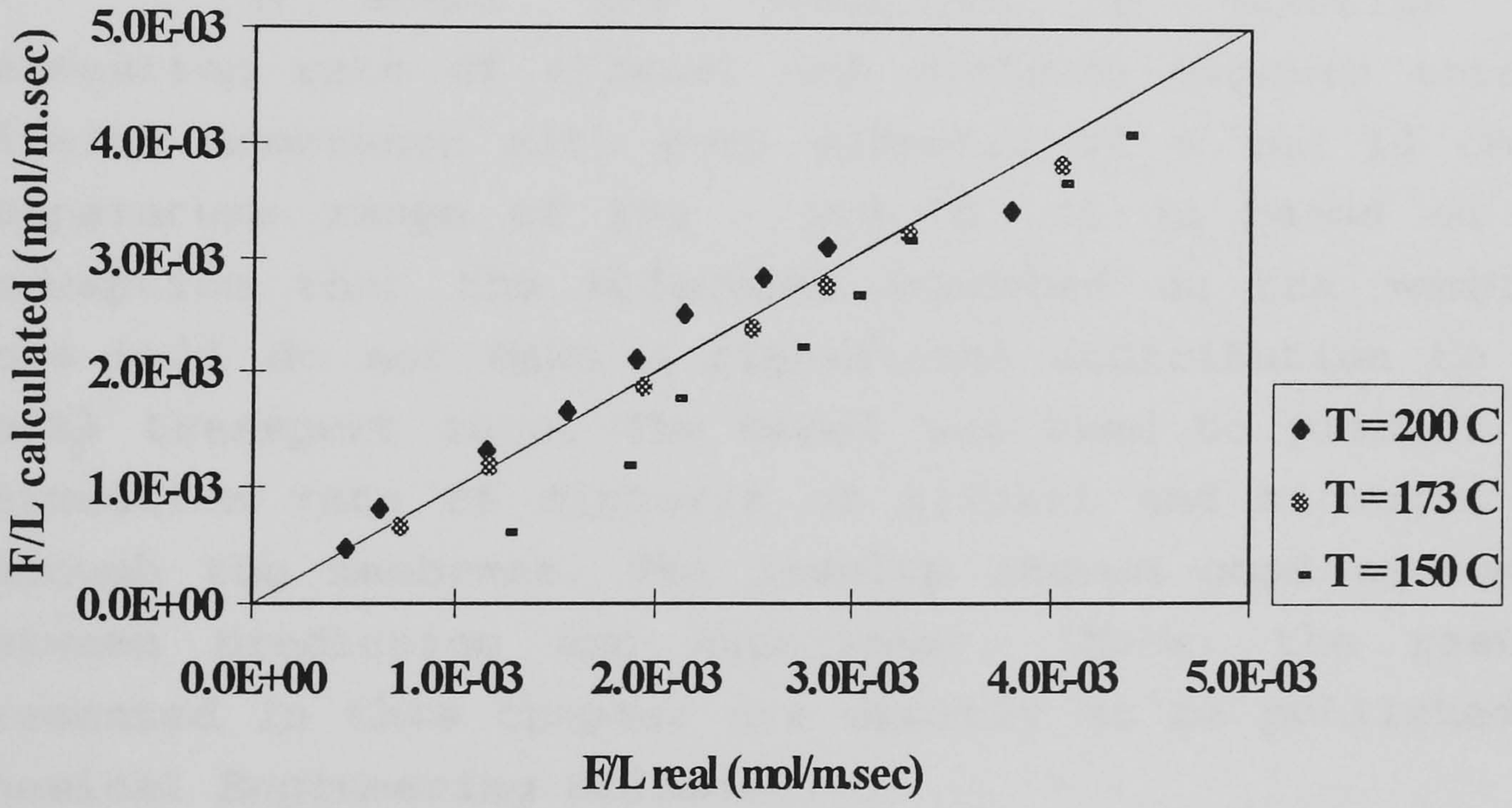


Figure 5.14 Experimental results from the mixtures of nitrogen gas and methanol vapour through the membrane with 4 nm pore size

The continuous lines in each graph show the case where the values from the experiment are equal to those predicted from the pure alcohol permeation. It is obvious that both the permeation of N_2-ethanol and N_2-methanol

mixture through the membrane with the pore diameter of 10 nm agreed well with the values found from the pure component studies at all three levels of temperature. This verifies the validity of the assumption that the contribution of the adsorbed phase of methanol and ethanol is small compared to that of gas phase. The agreement was also found in the permeation of those mixtures through the membrane with the pore diameter of 4 nm at high temperature levels. The deviation from the values obtained from the pure component studies at the lowest temperature level may result from the contribution of the adsorbed phase becoming significant or that the adsorption of alcohol at this temperature level is beyond monolayer adsorption.

5.5 Conclusion

A model was developed to describe the permeation rate of ethanol and methanol vapours through alumina membranes with pore diameter of 4 and 10 nm at temperature range of 150 - 200 ^{o}C. It is based on the assumption that the molecules adsorbed on the membrane pore wall do not make a significant contribution to the total transport rate. The model was used to predict the permeation rate of mixtures of alcohol and nitrogen gas through the membrane. The results showed good agreement between prediction and experiment. (Note: the results presented in this chapter are shortly to be published in Chemical Engineering Science.)

CHAPTER 6

EXPERIMENTAL STUDIES OF ACETONE AND ISOPROPANOL PERMEATION

6.1 Introduction

6.2 Description of Experimental System

6.3 Model Development

6.4 Results and Discussion

6.5 Prediction of Permeation of Pure Isopropanol and Acetone Vapours

6.6 Prediction of Mixture of Organic Vapour Permeation

6.7 Conclusions

CHAPTER 6

EXPERIMENTAL STUDIES OF ACETONE AND ISOPROPANOL PERMEATION

6.1 Introduction

This chapter presents the results of vapour permeation of acetone and isopropanol through a commercially available 'Membralox' membrane with pore diameter of 4 nm at three temperature levels; 160, 180 and 200 ^{o}C. Three main mechanisms involved in the vapour permeation are Knudsen diffusion, viscous bulk flow and surface diffusion. Two surface diffusion models; namely Fick's law and H.I.O. (Higashi, Ito and Oishi) models, were considered. Results from pure component permeation studies were fitted with the models and the validity of the models were checked with experimental results of mixture between the organic vapour and nitrogen gas. The study was further extended to the case of mixtures of acetone and isopropanol vapours.

6.2 Description of Experimental System

The experimental procedures for the permeation studies of pure acetone and isopropanol through the membrane and of mixtures of the organic vapour with nitrogen were exactly the same as those described before in Section 5.2. For the permeation studies of mixtures of two vapours, the procedure was similar to the studies with pure component. However, instead of only using a feed of pure component, a mixture with a known concentration was used. It should be noted that since some of isopropanol and acetone may be catalytically

converted to other species on the alumina membranes, the composition of the liquid outlet condensed by liquid nitrogen was checked by using a gas chromatograph with an FID (Flame Ionisation Detector) detector and the conversion of both species was found less than 5 % in all experiments.

6.3 Model Development

When surface diffusion becomes important in gas transport through a porous membrane, the total gas flow rate per unit length of membrane can be expressed as the combination of flows from gas phase and adsorbed phase as follows,

$$\left(\frac{F_i}{L}\right)_{total} = \left(\frac{F_i}{L}\right)_g + \left(\frac{F_i}{L}\right)_s \tag{6.1}$$

where F_i is the molar flow rate of component i and L is the axial length of a membrane. The subscript g refers to the gas flow and s is the surface flow. The gas phase flow is the contribution of Knudsen diffusion and viscous bulk flow. By assuming that the adsorption isotherm follows Henry's law, the expression of gas phase flow rate of component i per unit length of membrane developed before for the case of mixture of nitrogen gas and alcohol vapour in Chapter 5 can be modified and given as

$$\left(\frac{F_i}{L}\right)_g = \frac{a(1-\omega)^3}{\sqrt{M_i T}}(p_1 x_i - p_2 y_i) + \frac{b(1-\omega)^4 x_i}{2\mu T}(p_1^2 - p_2^2) \tag{6.2}$$

where $\omega = \chi_{org}\, p_1 x_{org}$ (6.3)

and $\chi_{org} = \dfrac{2K'_{org}\, V_{t org}}{S_t d_o}$ (6.4)

where a and b are Knudsen and viscous parameters. p_1 is the feed side pressure, p_2 is the permeate side pressure, x_i and y_i are molar fraction of species i in the feed and permeate side respectively, T is the operating temperature, K' is the parameter in the adsorption isotherm, d_o is the membrane pore diameter, μ is gas viscosity, V_t is the specific volume of the adsorbed phase, and S_t is the membrane specific surface area. The subscript org denotes the organic component. It should be noted that in these expressions the blockage of gas phase transport is due to the adsorption of organic components on the pores of the membrane.

There have been a number of models developed to describe the surface diffusion. In this study two models were used, Fick's law and the H.I.O. model. The surface flux expressions are given as follows

Fick's law model:

$$J_{s,i} = -\frac{\rho_{app} D_{s,i}}{\tau_s}\left(\frac{dq_i}{dp_i}\right)\left(\frac{dp_i}{dr}\right) \qquad (6.5)$$

H.I.O. model (Higashi *et al.*, 1963):

$$J_{s,i} = -\frac{\rho_{app} D_{s,i}}{(1-\theta_i)\tau_s}\left(\frac{dq_i}{dp_i}\right)\left(\frac{dp_i}{dr}\right) \qquad (6.6)$$

where

$$D_{s,i} = D^{o}_{s,i} \exp(-E_{s,i} / RT) \qquad (6.7)$$

In the expressions, $J_{s,i}$ is the surface flux of species i, ρ_{app} is the apparent density of membrane, $D_{s,i}$ is the surface diffusivity of species i, $D^{o}_{s,i}$ is a constant, $E_{s,i}$ is an activation energy of surface diffusion of component i, q_i is the amount of species i adsorbed in mol/kg, τ_s

is the tortuosity factor for surface flow, θ_i is the surface coverage due to species i and r is the radial distance along the membrane.

Because the membrane is cylindrical in shape, the surface flow rate through the membrane $(F_i)_s$ can be given by

Fick's law model:

$$(F_i)_s = -\frac{2\pi r L \rho_{app} D_{s,i} K'_i}{\tau_s} \frac{d}{dr} p_i \qquad (6.8)$$

H.I.O. model:

$$(F_i)_s = -\frac{2\pi r L \rho_{app} D_{s,i} K'_i}{(1 - K_i p_i)\tau_s} \frac{d}{dr} p_i \qquad (6.9)$$

It is further assumed that the surface diffusivity is constant within the Henry's law region. Even though this diffusivity is generally found to be concentration dependent, the dependency is suggested to arise largely from the nonlinearity of the equilibrium relationship (Ruthven, 1984). Integration of Equation (6.8) and (6.9) with respect to the boundary condition that at a distance r_1 (on the inner side of the membrane) the partial pressure is $p_1 x_i$ and at a distance r_2 (on the outer side of the membrane) the partial pressure is $p_2 y_i$ give,

Fick's law model:

$$\left(\frac{F_i}{L}\right)_s = D_{F,i}(p_1 x_i - p_2 y_i) \qquad (6.10)$$

where

$$D_{F,i} = \frac{2\pi \rho_{app} D_{s,i} K'_i}{\tau_s \ln(r_2 / r_1)} \qquad (6.11)$$

H.I.O. model:

$$\left(\frac{F_i}{L}\right)_s = D_{H,i} \ln\left(\frac{1 - K_i p_2 y_i}{1 - K_i p_1 x_i}\right) \tag{6.12}$$

where

$$D_{H,i} = \frac{2\pi\rho_{app} D_{s,i} K'_i}{\tau_s \ln(r_2 / r_1) K_i} \tag{6.13}$$

Thus the total flow rate of species i per unit length of membrane can be expressed as a sum of all three transport mechanisms as follows,

Fick's law model:

$$\left(\frac{F_i}{L}\right) = \frac{a(1-\omega)^3}{\sqrt{M_i T}}(p_1 x_i - p_2 y_i) + \frac{b(1-\omega)^4 x_i}{2\mu T}(p_1^2 - p_2^2) + D_{F,i}(p_1 x_i - p_2 y_i) \tag{6.14}$$

H.I.O. model:

$$\left(\frac{F_i}{L}\right) = \frac{a(1-\omega)^3}{\sqrt{M_i T}}(p_1 x_i - p_2 y_i) + \frac{b(1-\omega)^4 x_i}{2\mu T}(p_1^2 - p_2^2) + D_{H,i} \ln\left(\frac{1 - K_i p_2 y_i}{1 - K_i p_1 x_i}\right) \tag{6.15}$$

6.4 Results and Discussion

The permeability of isopropanol vapour through the alumina membrane with pore diameter of 4 nm were measured at 160, 180 and 200 °C, and the results are shown in Figure 6.1. The permeabilities at all temperature levels were found to be less than those predicted from pure nitrogen gas permeation.* This behaviour was seen previously in the permeation of ethanol and methanol through the same membrane in Chapter 5. The cause of the discrepancy was the blockage of membrane pore due to the adsorption of organic vapour.

* see Equation 2.15 for the predicted values

To verify this hypothesis, the results of permeation of pure isopropanol and mixture of isopropanol with nitrogen gas were calculated with the same procedures used in the interpretation of the ethanol and methanol data. These are described in section 5.4. The results of two fitting parameters, χ and K, from the data of pure component permeation are shown in Table 6.1 while the flow rate of nitrogen gas per unit length of membrane predicted from the data of pure component was compared with the experimental data as illustrated in Figure 6.2.

Table 6.1 Fitting parameters of gas phase flow model for the permeation of isopropanol

T (^{o}C)	$\chi * 10^{3}$ (kPa^{-1})	$K * 10^{3}$ (kPa^{-1})
160	1.0	0
180	0.8	0
200	0.6	0

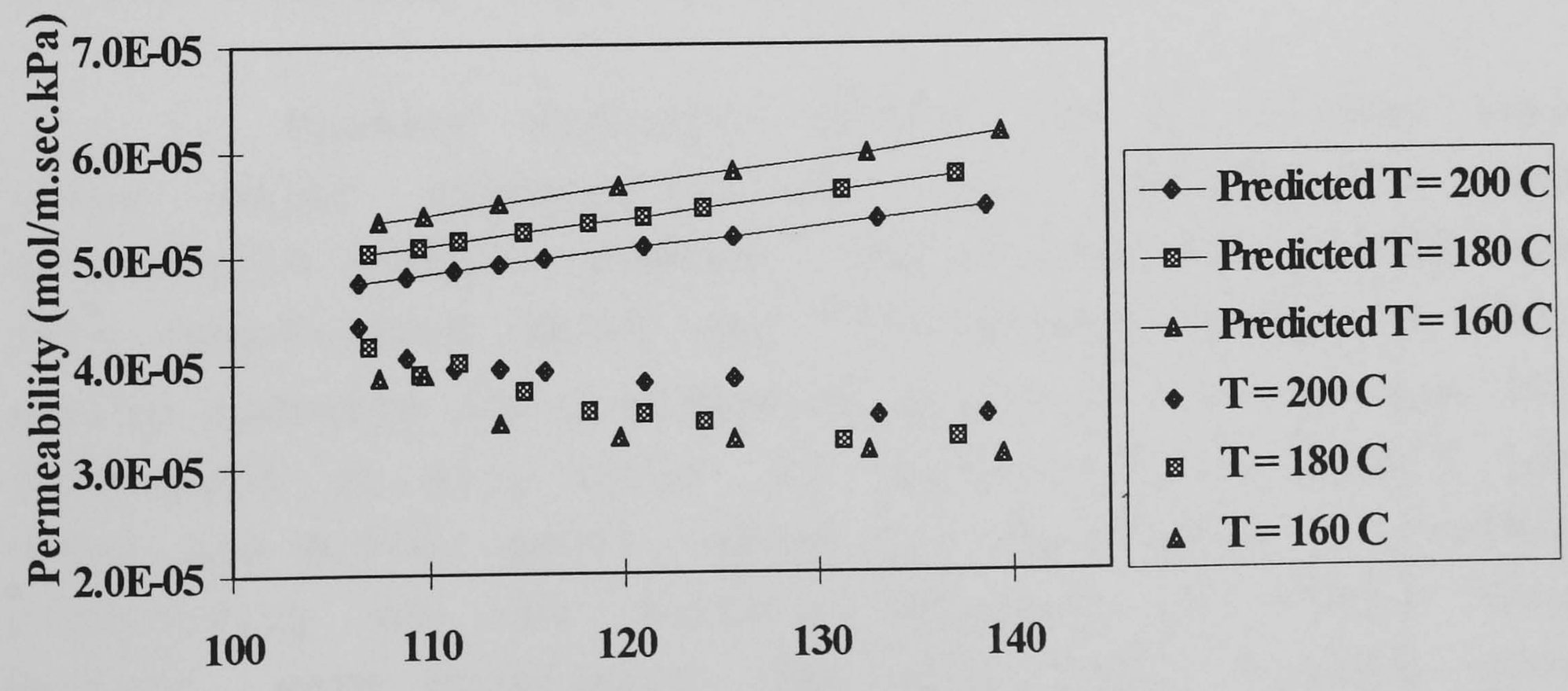


Figure 6.1 Permeability of pure isopropanol through the alumina membrane with 4 nm pore size

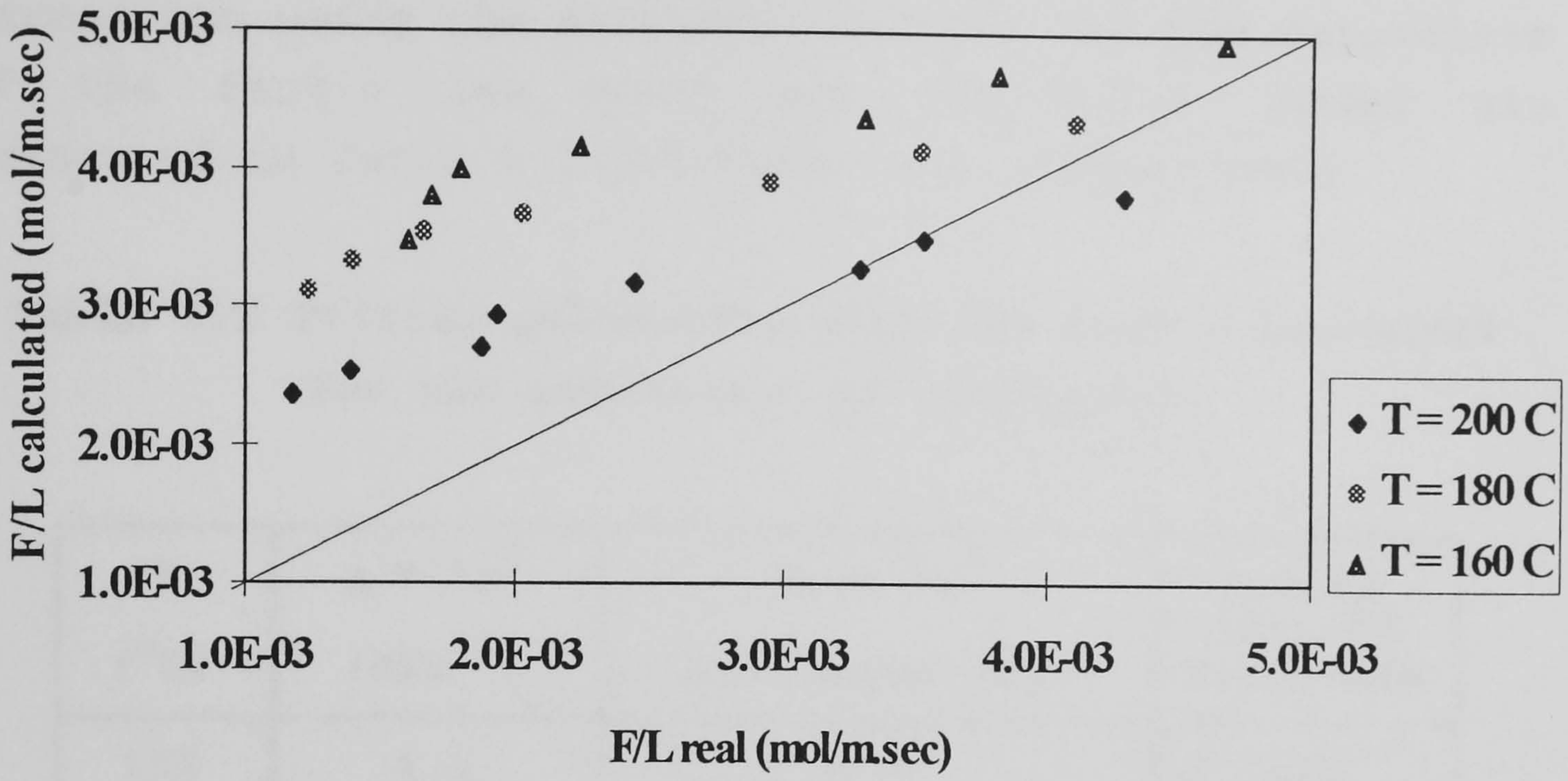


Figure 6.2 Experimental results from the mixtures of nitrogen gas and isopropanol vapour through the membrane with 4 nm pore size (gas phase flow model)

From Figure 6.2, it is obvious that the values calculated from the model are far from the real values from the experiments. This shows the failure of the assumption that the adsorbed phase does not make a contribution on the total flow rate. So for this case the contribution of surface diffusion must be taken into account.

Surface diffusion models can be divided into three major groups; Fick's law, hydrodynamic and mechanistic models. However, the mechanistic models are very complicated while the hydrodynamic model is only really suitable for a system at high surface coverage (θ) (Horiguchi *et al.*, 1971). In these studies, Fick's law model and H.I.O. model, where the dependency of surface diffusivity on the surface coverage is taken into account, were considered. The last model provides good agreement at surface coverage up to 60 % (Yang *et al.*, 1973).

Equations (6.14) and (6.15) were used to fit the experimental results of pure isopropanol vapour permeation using the software 'ORIGIN' and the parameters of the Fick's law model and the H.I.O. model are presented in Table 6.2 and Table 6.3, respectively.

Table 6.2 Fitting parameters with the Fick's law model for the permeation of isopropanol

T (^{o}C)	$\chi * 10^{3}$ (kPa^{-1})	$D_F * 10^{5}$ (mol/m.sec.kPa)	Sum of Squared Deviation
160	4.0	3.0	$7.0x10^{-10}$
180	3.3	2.8	$7.5x10^{-10}$
200	1.8	2.0	$9.7x10^{-10}$

Table 6.3 Fitting parameters with the H.I.O. model for the permeation of isopropanol

T (^{o}C)	$\chi * 10^{3}$ (kPa^{-1})	K $*10^{4}$ (kPa^{-1})	$D_H *10^{2}$ (mol/m.sec)	Sum of Squared Deviation
160	3.9	5.9	4.7	$1.1x10^{-9}$
180	2.9	4.9	5.2	$1.9x10^{-9}$
200	1.8	3.2	5.9	$1.3x10^{-9}$

By considering the values of sum of the deviation squared it is obvious that the Fick's law model can fit the results better than the H.I.O. model. However, the value of χ for both cases are similar. The adsorption parameters, K, from the H.I.O. model, in addition, allow the surface coverage of each experiment to be calculated. Since the maximum pressure in the feed side was around

180 kPa, the maximum surface coverage were 9, 8 and 5 % at 160, 180 and 200 ^{o}C, respectively. This proves the validity of the assumption that adsorption follows a Henry's law isotherm because the values of θ are low.

The Fick's law model was then checked with the results from the experiments with mixtures of isopropanol vapour and nitrogen gas and the similar procedure was used for the gas phase flow model. The results of the predicted nitrogen flow rate per unit length of membrane and the real values are shown in Figure 6.3. It is obvious that the prediction from the Fick's law model is much better than those from the gas phase flow model when the effect of surface diffusion is ignored.

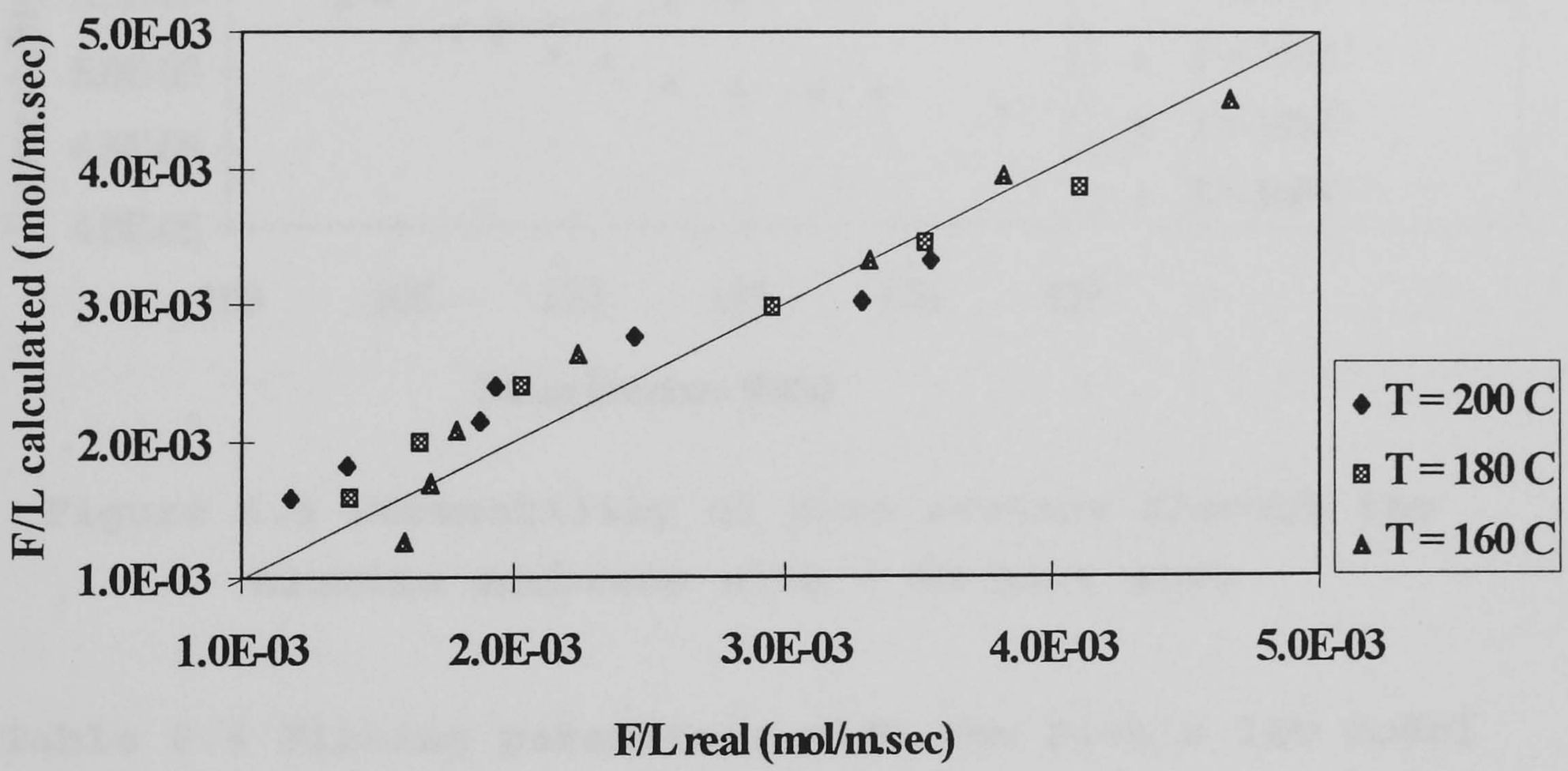


Figure 6.3 Experimental results from the mixtures of nitrogen gas and isopropanol vapour through the membrane with 4 nm pore size (Fick's law model)

The vapour permeation of acetone through the same membrane was carried out at the same temperature levels and the results are given in Figure 6.4. It can be seen that the permeability of acetone at some data points was higher than those predicted from the nitrogen permeation. So it is likely that the surface diffusion is one of the transport mechanisms. Capillary condensation

should not be of importance since the operating pressure is far below the saturation pressure (See Table A3.4 in Appendix 3). The Fick's law model was used to fit the results of the acetone permeation. The parameters calculated are given in Table 6.4. The model was also tested with the results from the experiment of mixtures between acetone vapour and nitrogen gas which is shown is Figure 6.5.

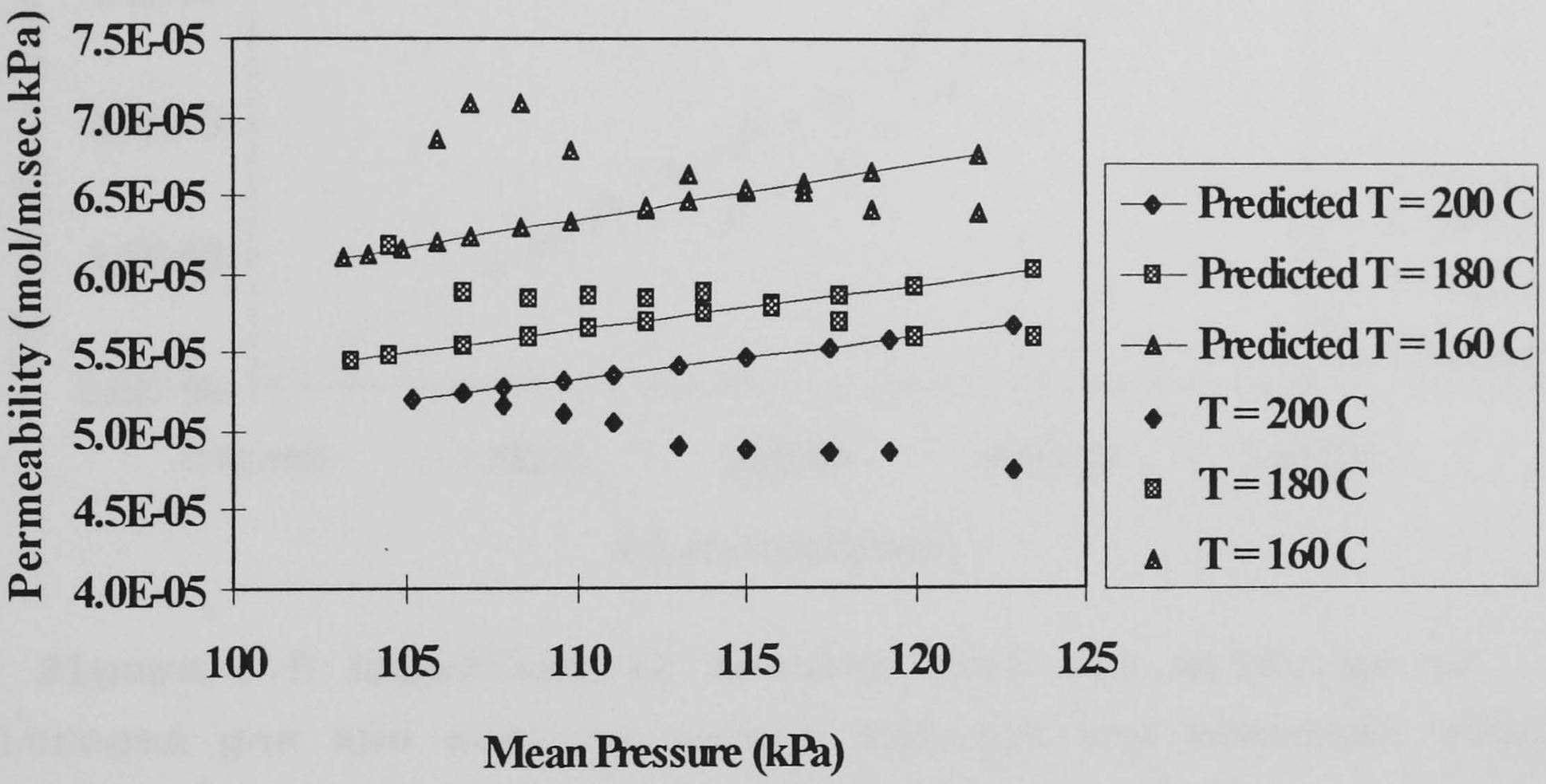


Figure 6.4 Permeability of pure acetone through the alumina membrane with 4 nm pore size

Table 6.4 Fitting parameters with the Fick's law model for the permeation of acetone

T (^{o}C)	$\chi * 10^{3}$ (kPa^{-1})	D_F*10^{5} (mol/m.sec.kPa)	Sum of Squared Deviation
160	3.4	5.7	$6.1x10^{-10}$
180	2.8	4.7	$3.4x10^{-10}$
200	1.7	2.8	$1.6x10^{-10}$

The flow rate of nitrogen gas per unit length predicted from the model was found in good agreement with those from experiment. However, at 160 °C the deviation is more pronounced. This may be due to deviation from Henry's law when the operating temperature is low.

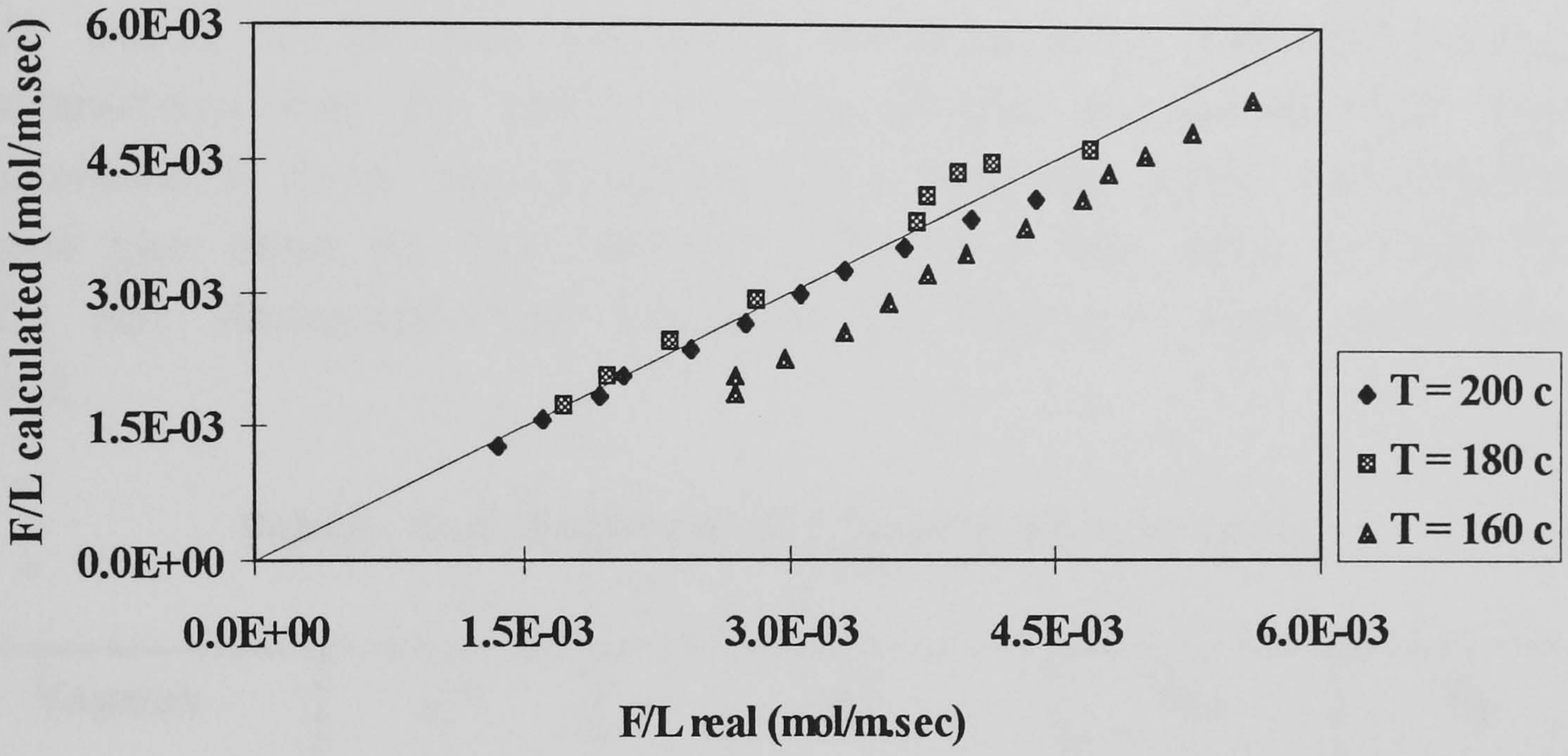


Figure 6.5 Experimental results from the mixtures of nitrogen gas and acetone vapour through the membrane with 4 nm pore size (Fick's law model)

6.5 Prediction of Permeation of Pure Isopropanol and Acetone Vapours

The model describing the surface diffusion of isopropanol and acetone vapours through the membrane contains two parameters χ and D_F. Since the parameter χ is proportional to the adsorption isotherm parameter (K') and the parameter D_F is proportional to the product of surface diffusivity (D_s) and the adsorption isotherm parameter (see Equation 6.4 and Equation 6.11), they can be described by the following expressions.

$$\chi = \chi^{\circ} \exp\left(\frac{Q_{st}}{RT}\right) \qquad (6.16)$$

$$D_F = D_F^{\circ} \exp\left(\frac{Q_{st} - E_s}{RT}\right) \qquad (6.17)$$

where Q_{st} is the heat of adsorption and E_s is the activation energy for surface diffusion. D_F° and χ° are constants. Plotting the values of $\ln(\chi)$ and $\ln(D_F)$ with 1/T where T is the absolute temperature, the following parameters can be obtained. It should be noted that the parameters from the studies with acetone were calculated from the data at 180 and 200 °C since the data at 160 °C did not describe the results of mixture with nitrogen well.

Table 6.5 Surface diffusion parameters

Vapour	χ° (kPa^{-1})	D_F° (mol/m.sec.kPa)	Q_{st} (kJ/mol)	E_s (kJ/mol)
Isopropanol	3.6×10^{-7}	2.4×10^{-7}	34	16
Acetone	1.6×10^{-8}	2.9×10^{-10}	46	1

It is known that the activation energy of surface diffusion is proportional to the heat of adsorption (Suzuki, 1990). The ratio of activation energy of surface diffusion and the heat of adsorption can vary from zero to one, depending on the size of the energy barrier to surface flow. The result from the experiment of isopropanol shows that the activation energy of surface diffusion (E_s) is approximately a half of the heat of adsorption (Q_{st}). This value has been often determined experimentally in other systems (Okubo and Inoue, 1987). However, for the case of acetone, the activation energy for surface diffusion is very low. This low value of the activation energy (much lower than the heat of adsorption) indicates the mobility of the species

is not affected by change in temperature. An example of this system is the permeation of propane through 'Vycor' glass which showed that the activation energy of surface diffusion was only 0.7 kJ/mol (Weaver and Metzner, 1966).

6.5 Prediction of Organic Mixture Permeation

The aim of this section is to study the permeation of mixtures of isopropanol and acetone. This information is particularly important for the modelling of the dehydrogenation of isopropanol to acetone in an alumina membrane reactor where the system contains mixture of the two components and hydrogen gas. Since the experiment was performed at conditions where surface coverage is very small, it may be sensible to assume that the adsorption and surface diffusion of isopropanol and acetone are independent of each other. The effect of both components affects pore blockage and the value of ω can be expressed as follows

$$\omega = \chi_{iso} p_1 x_{iso} + \chi_{ace} p_1 x_{ace} \qquad (6.18)$$

where x_{iso} and x_{ace} denote composition of isopropanol and acetone in the feed side.

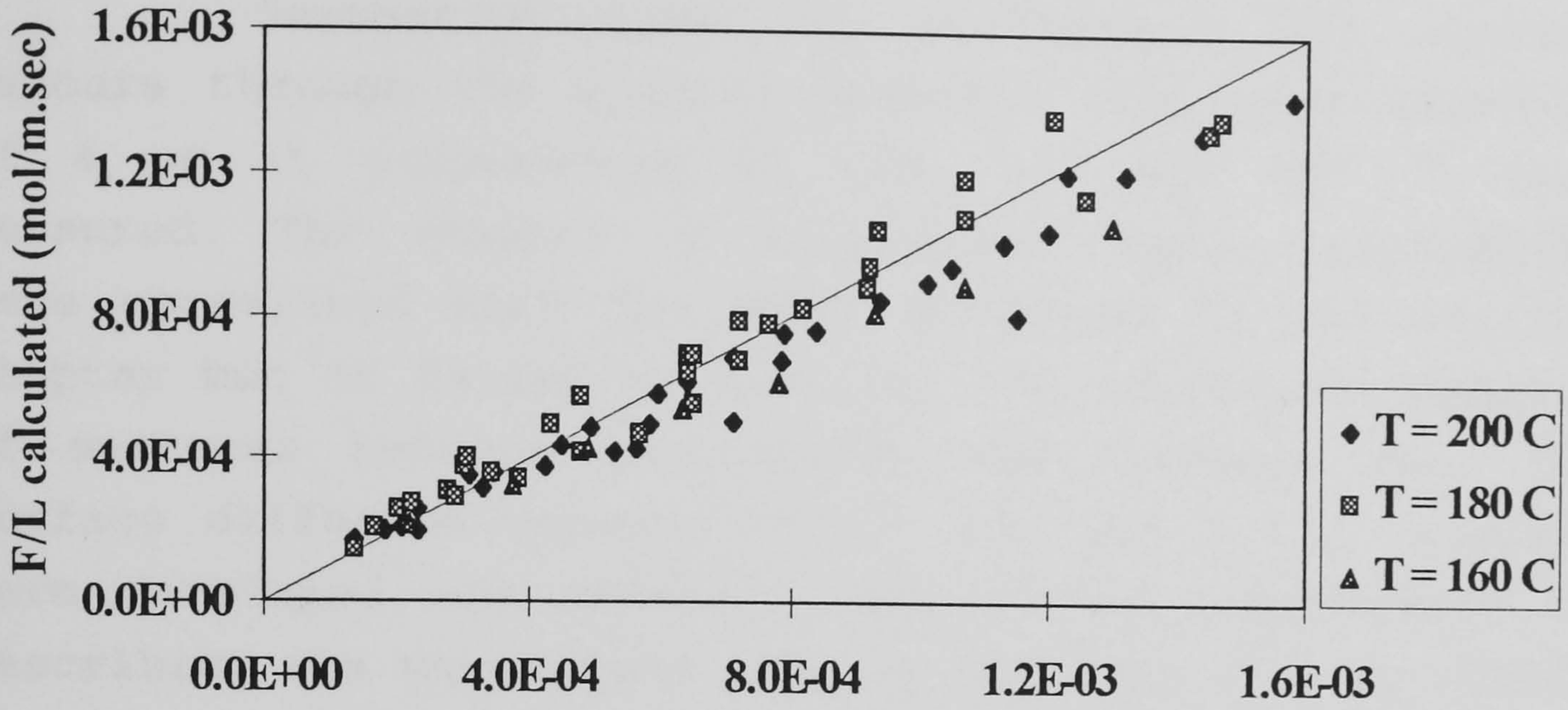


Figure 6.6 Experimental results from the mixtures of isopropanol and acetone vapours through the membrane with 4 nm pore size

To verify the assumption, another set of experiment with the mixtures of isopropanol and acetone vapours were carried out at the same temperature levels. In this study concentrations of 25, 50 and 75 % by volume of isopropanol were used. The volume fraction data was converted to mole fraction data for the calculation. The way to interpret the results were the same as those used to correlate data on organic vapour and nitrogen gas mixtures as described in section 5.4. In this case the composition of isopropanol (x_{iso}) in the tube side was calculated and then the predicted value of flow rate per unit length of acetone was calculated and compared with the real value from experiment. The comparison between those two values are given in Figure 6.6. It can be seen that the model can predict the behaviour of mixtures of the two organic components well. Seventy two data points can be predicted with an average deviation of 11 %. The data at 160 ^{o}C was not as well correlated as the higher temperature data.

6.6 Conclusions

Permeation rate of isopropanol and acetone vapours through the alumina membrane with pore diameter of 4 nm at temperature of 160, 180 and 200 ^{o}C were measured. The results of isopropanol vapour permeation were correlated with the model developed in the earlier chapter but it failed to describe the permeation results of mixtures between isopropanol and nitrogen gas. Two surface diffusion models; Fick's law and H.I.O. models, were developed and showed a significant improvement on describing the permeation rate of mixtures of isopropanol vapour and nitrogen gas. The results from both models were in good agreement with experiment. The Fick's law model was satisfactorily used to describe the results of acetone vapour. The model was further extended to predict the permeation of mixtures between the two organic vapours through the membrane. It could predict the experimental results well especially at high operating temperature.

CHAPTER 7

APPLICATION ON THE DEHYDROGENATION OF ISOPROPANOL TO ACETONE IN AN ALUMINA MEMBRANE REACTOR

7.1 Introduction
7.2 Modelling of a Membrane Reactor
7.3 Solving the Rate Equations
7.4 Results and Discussion
7.5 Conclusion

CHAPTER 7

APPLICATION ON THE DEHYDROGENATION OF ISOPROPANOL TO ACETONE IN AN ALUMINA MEMBRANE REACTOR

7.1 Introduction

Simulation studies were carried out for the dehydrogenation of isopropanol to acetone in an alumina membrane reactor using the permeation model outlined in the previous chapters. This reaction is of commercial importance since this represents the largest single use of isopropanol. The chemical reaction is given as follow

$$CH(CH_3)_2OH \longleftrightarrow (CH_3)_2CO + H_2$$

In industrial operation, the reaction is carried out at 325 ^{o}C under atmospheric pressure and 97 % conversion of isopropanol is theoretically possible. The main purpose of this chapter is to investigate whether the concept of a membrane reactor is applicable to this system. Operating a reactor at lower temperature can reduce energy consumption, catalyst deactivation and by-product problems. In modelling the transport of nitrogen, hydrogen gases, isopropanol and acetone vapours through the alumina membrane with pore diameter of 4 nm were obtained before in Chapter 4 and 6 whereas the reaction kinetic data was obtained from the literature. The performance of the membrane reactor was compared with that of a plug flow reactor. The effects of operating pressure, reactor diameter, sweep flow rate, mode of operation, operating

temperature, rate of reaction and membrane selectivity were considered.

7.2 Modelling of a Membrane Reactor

The membrane reactor in this study is a double tubular reactor; the inner tube is made of an alumina inorganic membrane, and the outer shell of an impermeable one. The catalyst is packed in the shell side where a mixture of nitrogen, hydrogen and isopropanol is introduced. While the reaction takes place, the gases, nitrogen, hydrogen, acetone and isopropanol, diffuse through the membrane into the tube side and flow out at the end. The model can be simplified by the following assumptions.

1. The flow in the system is at steady state.
2. The reaction is operated at isothermal conditions.
3. The ideal gas law can be used to determine gas properties.
4. There is constant pressure in both the shell and the tube side.
5. The interfacial mass transfer resistance between the gas and the surface of membrane is small compared with the internal mass transfer resistance in the membrane.
6. Axial diffusion is negligible.
7. The membrane is not catalytically active.

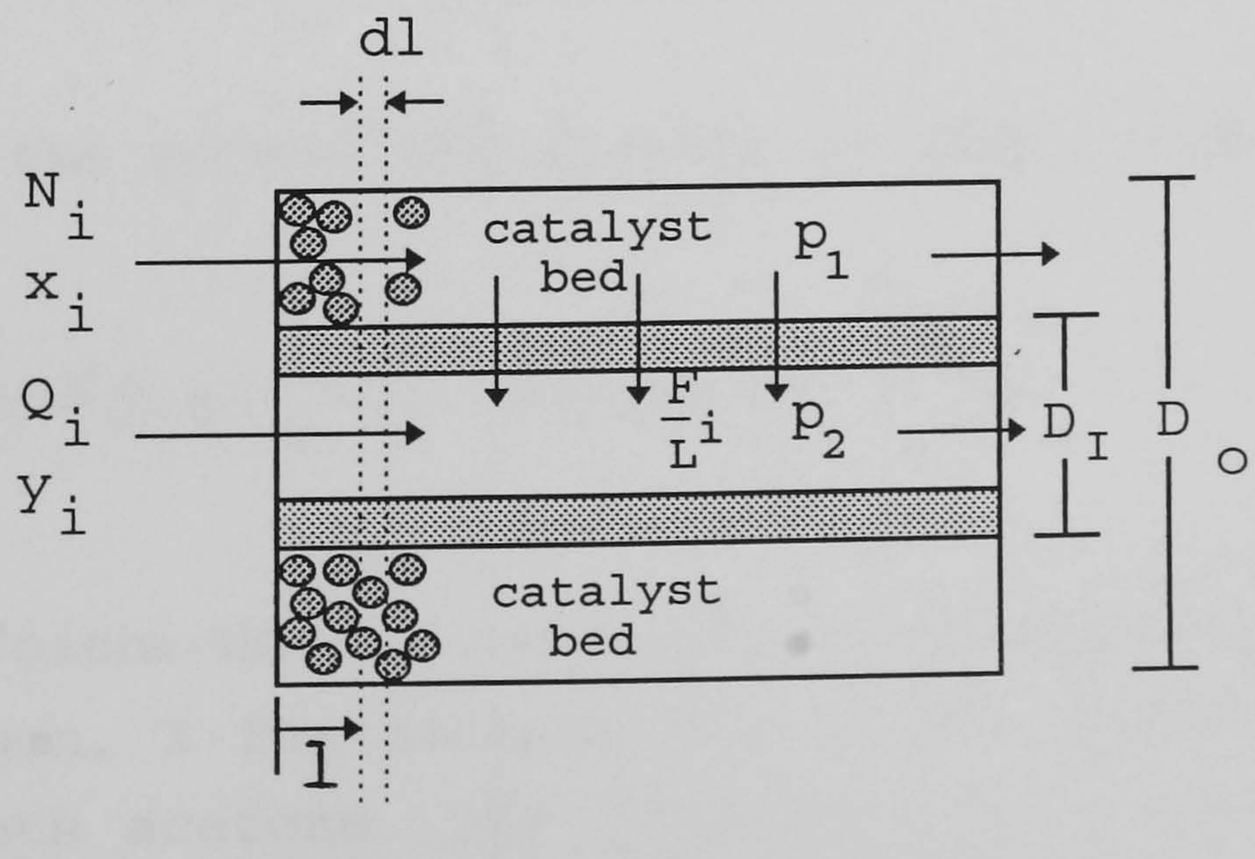


Figure 7.1 The membrane reactor configuration

Figure 7.1 illustrates the membrane configuration used in this study. For cocurrent operation, the molar flow rate of species i in the shell side is $N_{i|l}$ and mole fraction $x_{i|l}$. The diameter of the shell tube is D_o and the outer diameter of the membrane tube is D_I. The dehydrogenation reaction occurs in a small element of length dl with a rate of reaction r_i and the gases diffuse through the membrane to the tube side. The molar flow rate of species i is $Q_{i|l}$ and its composition $y_{i|l}$. The pressure in the shell side is p_1 and in the tube side is p_2. Gas flows out of the small element with the molar flow rate of each species of $N_{i|l+dl}$. The composition of species i in the shell is $x_{i|l+dl}$ and in the tube it is $y_{i|l+dl}$. $Q_{i|l+dl}$ and $\left(\frac{F_i}{L}\right)$ are the molar flow rate down the tube and the rate of permeation of species i per unit length of membrane respectively. The analytical procedure follows that of a previous paper (Assabumrungrat and White, 1996).

Performing the material balance, a set of equations can be obtained. For flow in the permeate side chamber (tube side)

$$Q_{i|l}-Q_{i|l+dl}+\left(\frac{F_i}{L}\right)dl = 0 \qquad (7.1)$$

The subscripts, l and l+dl, represent the position of interest and i refers to each species.

For flow in the packed bed chamber or shell side is

$$N_{i|l}-N_{i|l+dl}+\frac{\pi}{4}(D_o^2 - D_I^2)\nu_i r_{ace}\,dl - \left(\frac{F_i}{L}\right)dl = 0 \qquad (7.2)$$

ν_i is the stoichiometric coefficient of species i, namely 1 for hydrogen, 1 for acetone and -1 for isopropanol, and ace represents acetone. The equations (7.1) and (7.2) can be written in the differential forms as shown below.

$$\frac{d}{dl} Q_i = \left(\frac{F_i}{L}\right) \tag{7.3}$$

and

$$\frac{d}{dl} N_i = \frac{\pi}{4} (D_o^2 - D_I^2) \nu_i r_{ace} - \left(\frac{F_i}{L}\right) \tag{7.4}$$

For countercurrent operation, the material balance can be carried out in the same manner. The differential equation of the feed side is the same as the one obtained from cocurrent mode while in the permeate side it is

$$\frac{d}{dl} Q_i = -\left(\frac{F_i}{L}\right) \tag{7.5}$$

For the molar flow rate of species i per unit length of membrane, it is assumed that the expressions obtained from Chapter 4 and 6 can describe the permeation from the shell side to the tube side. They were given before in Equations (6.14) and (6.18) and can be described as

$$\left(\frac{F_i}{L}\right) = \frac{a(1-\omega)^3}{\sqrt{M_i T}} (p_1 x_i - p_2 y_i) + \frac{b(1-\omega)^4 x_i}{2\mu T} (p_1^2 - p_2^2) + D_{F,i}(p_1 x_i - p_2 y_i) \tag{7.6}$$

where

$$\omega = \chi_{iso} p_1 x_{iso} + \chi_{ace} p_1 x_{ace} \tag{7.7}$$

The first two terms in equation (7.6) are the contribution of gas phase flow due to Knudsen diffusion and viscous bulk flow, respectively. The last term considers the surface diffusion of an adsorbed phase. It should be noted that this expression takes into account the effect of pore blockage due to the presence of adsorbed species. The values of the parameter a (Knudsen parameter) and b (viscous flow parameter) were given in Chapter 4 as 4.8×10^{-3} $(mol.g.K)^{1/2}/sec.kPa$ and 1.0×10^{-12} mol.K/m.kPa, respectively. Subscripts iso and ace denote isopropanol

and acetone. R is the gas constant, T is operating temperature, μ is gas viscosity, M_i is molecular weight, x_i is the molar fraction of species i in the reaction side and y_i is the molar fraction of species i in the permeation side. These are given by the following expressions

$$x_i = \frac{N_i}{\sum N_i} \tag{7.8}$$

and

$$y_i = \frac{Q_i}{\sum Q_i} \tag{7.9}$$

The parameters χ in kPa^{-1} and D_F in mol/m.sec.kPa of hydrogen and nitrogen are zero while those of isopropanol and acetone were given in Table 6.5 in Chapter 6.

The rate expression of the dehydrogenation of isopropanol to acetone on a catalyst with a composition of $La_{1.6}Sr_{0.4}CuO_{3.8}$, given by Jeyalakshmi *et al.* (1990), was used in the simulations through out this chapter and can be expressed as

$$r_{ace} = \frac{k_o K_a \rho_b (p_{iso} - p_{ace}\, p_{H2} / Kp)}{RT(1 + K_a\, p_{iso})^2} \tag{7.10}$$

where

$$k_o = 4.0x10^{7} exp(-10756/T) \tag{7.11}$$

$$K_a = 4.4x10^{-1} exp(1991/T) \tag{7.12}$$

k_o, K_a and K_p are the reaction rate constant in m^3.kPa/(kg.sec), the adsorption parameter in kPa^{-1} and the equilibrium constant in kPa, respectively. ρ_b is density of the catalyst bed. Subscript H2 denotes hydrogen and the equilibrium constant is defined as

$$K_p = \frac{p_{ace}\, p_{H2}}{p_{Iso}} \tag{7.13}$$

Stull *et al.* (1969) provided the equilibrium constant data for this reaction which can be correlated to the following form

$$K_p = 2.8x10^8 \exp(-7048/T) \qquad (7.14)$$

7.3 Solving the Rate Equations

After doing the material balance, a system of ordinary differential equations are obtained. Each mode of operation; i.e. cocurrent or countercurrent, needs different mathematical techniques. The former one is an initial value problem while the latter one is a two point boundary problem. In this study the Runge-Kutta method is used to integrate the initial value case with the following boundary conditions

$$\text{at} \quad l = 0 \qquad N_i = N_i^o$$

$$\text{and} \quad \text{at} \quad l = 0 \qquad Q_i = Q_i^o$$

For the two point boundary problem, a successive substitution method was used with the following boundary conditions.

$$\text{at} \quad l = 0 \qquad N_i = N_i^o$$

$$\text{and} \quad \text{at} \quad l = L \qquad Q_i = Q_i^L$$

When the boundary conditions are specified, the membrane reactor mass balance can be achieved by an iterative calculation until the mass balance converges. First, the flow rate of permeate outlet of each component (Q_i^o) are guessed. Then the set of ordinary equations can be integrated using the same technique as the initial value problem over the whole length of membrane reactor until the flow rate of permeate stream (Q'^L_i) is obtained. The process can now be repeated by changing the guess for the

permeate stream outlet as $Q_i^o + (Q_i^L - Q'^L_i)\xi$ where ξ is a relaxation constant. The process is repeated until convergence is achieved.

7.4 Results and Discussion

Various operating conditions are considered in this section and comparisons are made between membrane reactor performance and plug flow reactor performance by considering the conversions.

Table 7.1 Summary of input parameters used for membrane reactor model

Mode of operation	Cocurrent
Molar feed rate (mmol/sec)	0.2
Composition of hydrogen in feed inlet	0.1
Composition of isopropanol in feed inlet	0.45
Composition of nitrogen in feed inlet	0.45
Molar flow rate of nitrogen sweep gas (mmol/sec)	0.3
Feed side pressure (kPa)	131.3
Permeate side pressure (kPa)	101.3
Inner diameter of reactor (m)	0.01
Outer diameter of reactor (m)	0.04
Operating temperature (^oC)	200
Catalyst bed density (kg/m^3)	1500

Table 7.1 summarises the operating conditions used in this study. Deviation from these conditions will be stated at the appropriate time. It should be noted that hydrogen was added in the feed in order to reduce the catalyst fouling. This was also done by a number of membrane reactor studies such as the dehydrogenation of propane to propene (Uemiya *et al.*, 1991b).

- **Effect of Feed Side Pressure**

Figure 7.2 illustrates the effect of feed side pressure on the performance of the membrane reactor. The conversion is plotted against the length of membrane reactor. The conversion is defined as follows

$$\% \quad \text{conversion} = 100 * \left(1 - \frac{Q_{iso} + N_{iso}}{N^{o}_{iso}}\right) \quad \% \qquad (7.15)$$

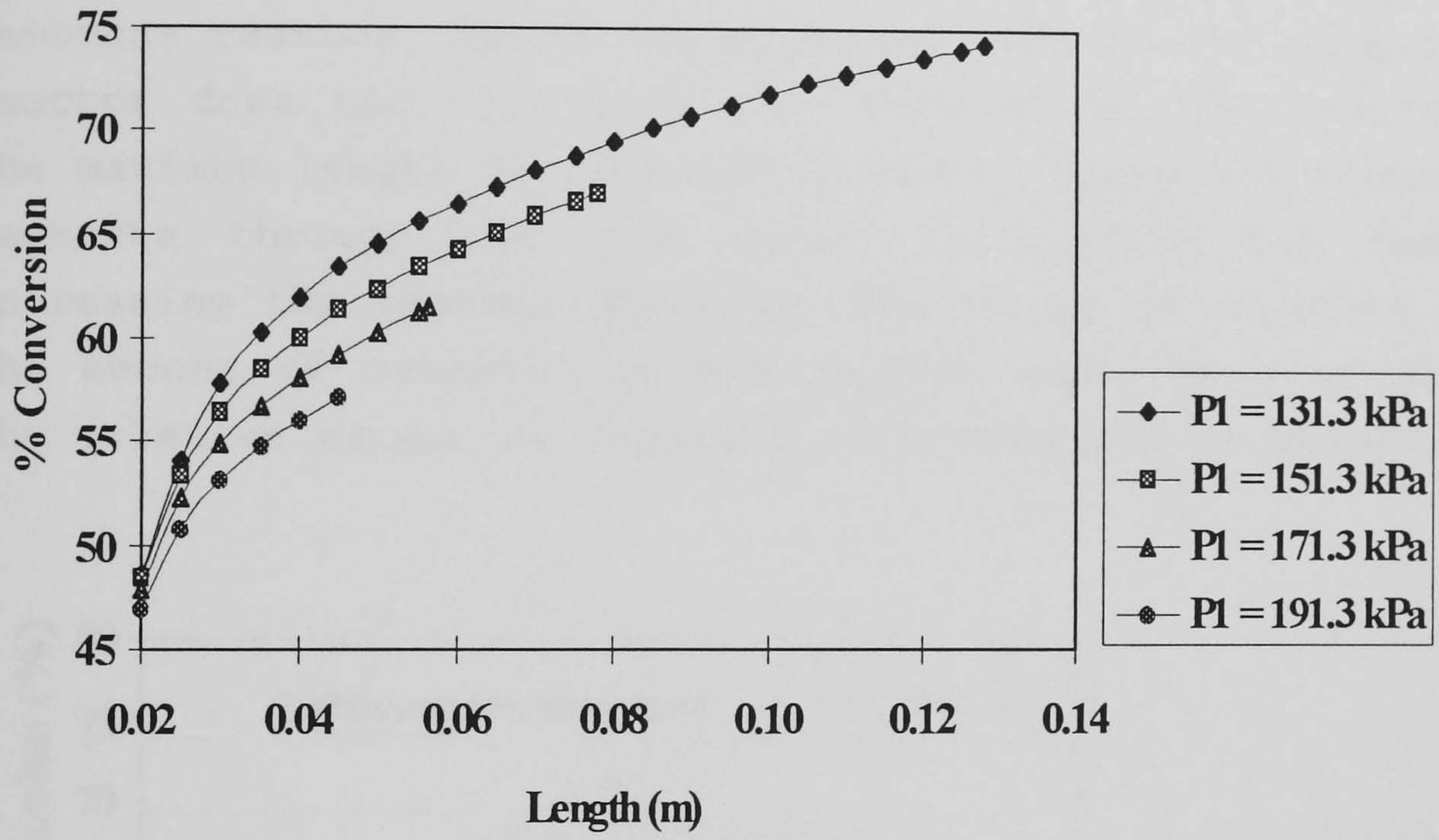


Figure 7.2 Effect of reaction side pressure on the performance of membrane reactor

Four values of feed pressures were considered. From the graph it can be seen that as the reactor length increases, and thus the residence time in the reactor increases, the conversion is higher. It should be noted that there is an end point for each curve in the graph. This corresponds to the condition where all species pass through the membrane to the permeate side. As the reactor length increases, the output flow rate on the feed side decreases and approaches zero and at this condition the maximum conversion is achieved because the reacting species has the highest contacting time with the

catalyst. When the feed side pressure is high, the maximum reactor length and the maximum conversion is lowered. This is because the loss of reactant to the permeation side is faster as the pressure driving force is high.

- **Effect of Reactor Diameter**

Figure 7.3 shows the effect of the reactor diameter on the maximum conversion achievable in the membrane reactor. Since the membrane tube in the membrane reactor does not vary with the diameter of the reactor, the maximum length of membrane reactor, where all species permeate through the tube side, is roughly the same. Increasing the reactor diameter results in an increase of the amount of catalyst in the reactor and, as a result, the relative extent of reaction to permeation is higher.

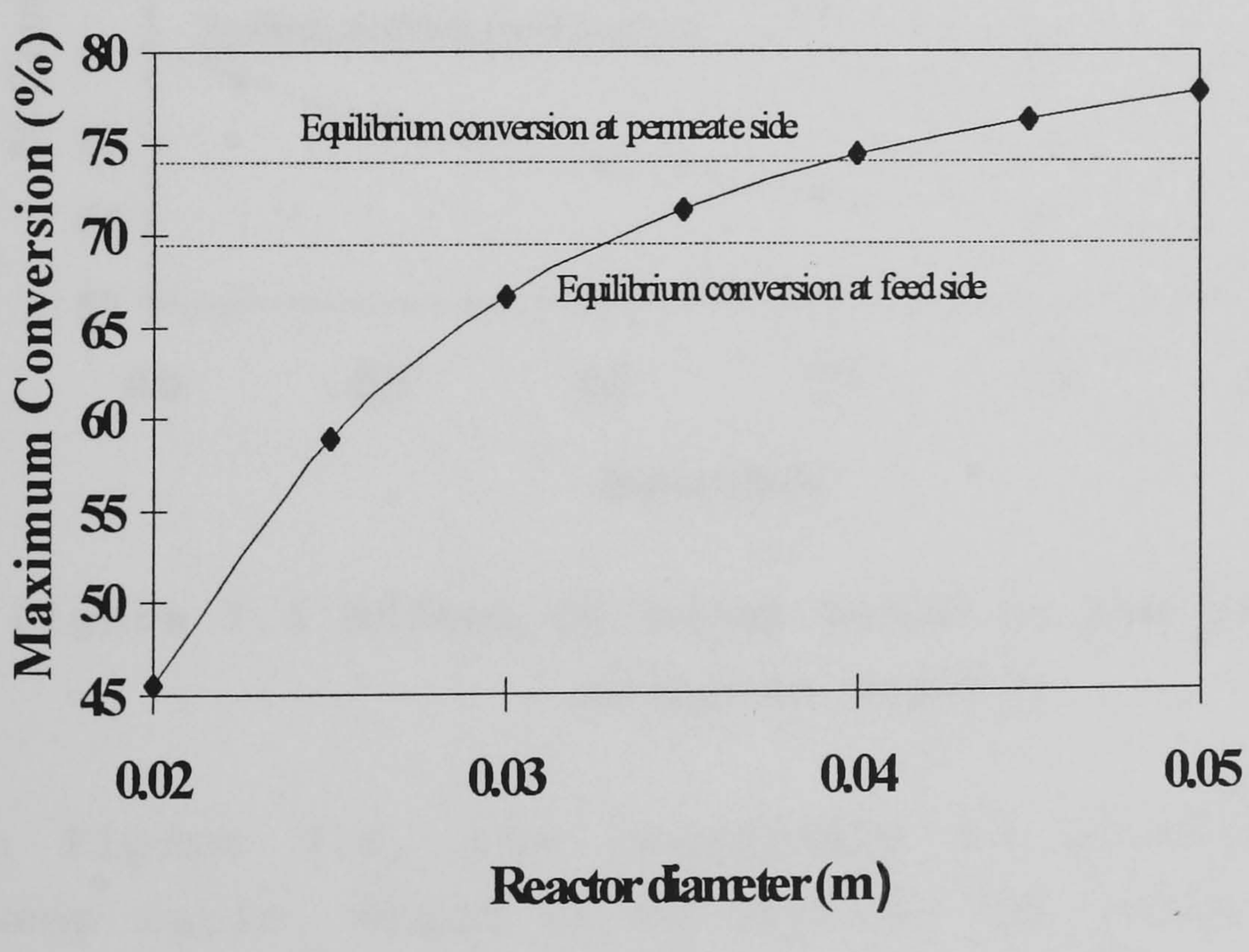


Figure 7.3 Effect of reactor diameter on the performance of membrane reactor

In the graph, two horizontal dotted lines show the equilibrium conversions of plug flow reactors operated at permeate side pressure of 101.3 kPa and at feed side

pressure of 131.3 kPa. It is obvious that maximum conversion increases with increase of the reactor diameter, and when the reactor diameter is large, the membrane reactor can provide higher conversion than the plug flow reactors.

- **Effect of Sweep Flow Rate**

The main purpose of introducing sweep gas to a permeate side in membrane reactor operation is to reduce the partial pressure of products in the permeate side and, hence, the removal of the products such as hydrogen gas is increased.

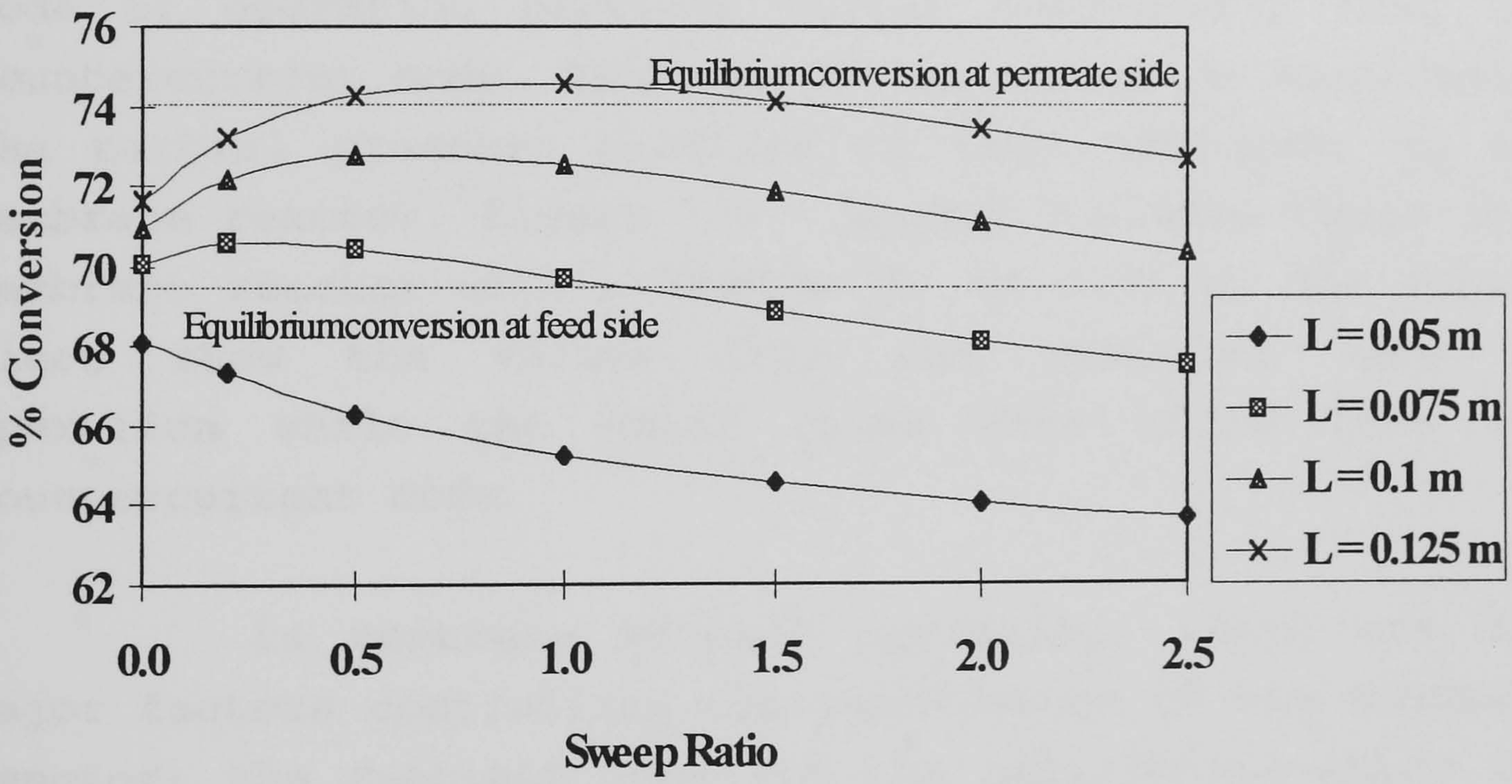


Figure 7.4 Effect of sweep ratio on the performance of membrane reactor

In Figure 7.4, the conversion is plotted against the sweep ratio, which is defined as the ratio of sweep flow rate to feed flow rate, for four lengths of membrane reactor (L). In general, when the sweep ratio increases, the conversion is higher due to the removal of hydrogen gas. However, in the graph after a certain value of sweep ratio, the conversion declines. This can be explained by the fact that the reactant, isopropanol, can also

permeate through the membrane. Increasing the sweep flow rate can also increase the reactant loss from the reaction side and lower the reaction conversion. In addition, nitrogen sweep gas can also permeate through the membrane and dilute the reactant. Consequently, the rate of reaction decreases.

- **Effect of Mode of Operation**

Membrane reactor can be operated in cocurrent or countercurrent modes of operation. Figure 7.5 shows the results of membrane reactor with reactor lengths of 0.05 and 0.10 m operated at both modes of operation as a function of sweep ratio. It is obvious that the cocurrent mode of operation provides better performance than the countercurrent mode. This can be described by considering the partial pressure profiles of each component in the membrane reactor. Figure 7.6 - Figure 7.8 show those in a membrane reactor with a length (L) of 0.05 m. The dotted lines show the values from the cocurrent mode of operation while the solid lines show those from the countercurrent mode.

In membrane reactor operation, there are two major factors controlling the performance of the membrane reactor; the reactant loss and the equilibrium shift due to the removal of products from the reaction chamber. In general, the conditions at the feed end are very important since most of the reaction occurs near this end where the rate of reaction is high. From Figure 7.7, it can be seen that the partial pressure of isopropanol in the reaction chamber decreases rapidly near the feed inlet in both modes of operation. The decrease can be caused by reactant loss to the permeate side or from the reaction itself. However, the partial pressure of isopropanol in the permeate side in both types of operation does not show marked difference. So the effect of reactant loss to the permeation side for both modes of

operation should not be significantly different. Considering the partial pressure profiles of hydrogen in Figure 7.6, it is obvious that, near the feed end the partial pressure in the reaction side from countercurrent operation is much higher than that from cocurrent operation and, therefore, the removal of hydrogen from the reaction chamber is lower in the countercurrent operation. This is because in countercurrent operation the partial pressure of the product near the feed end is high. This is also found in Figure 7.8 which shows the partial pressure of acetone. However, the partial pressure profile of acetone in the reaction side in the countercurrent operation is not significantly higher than that in the cocurrent mode.

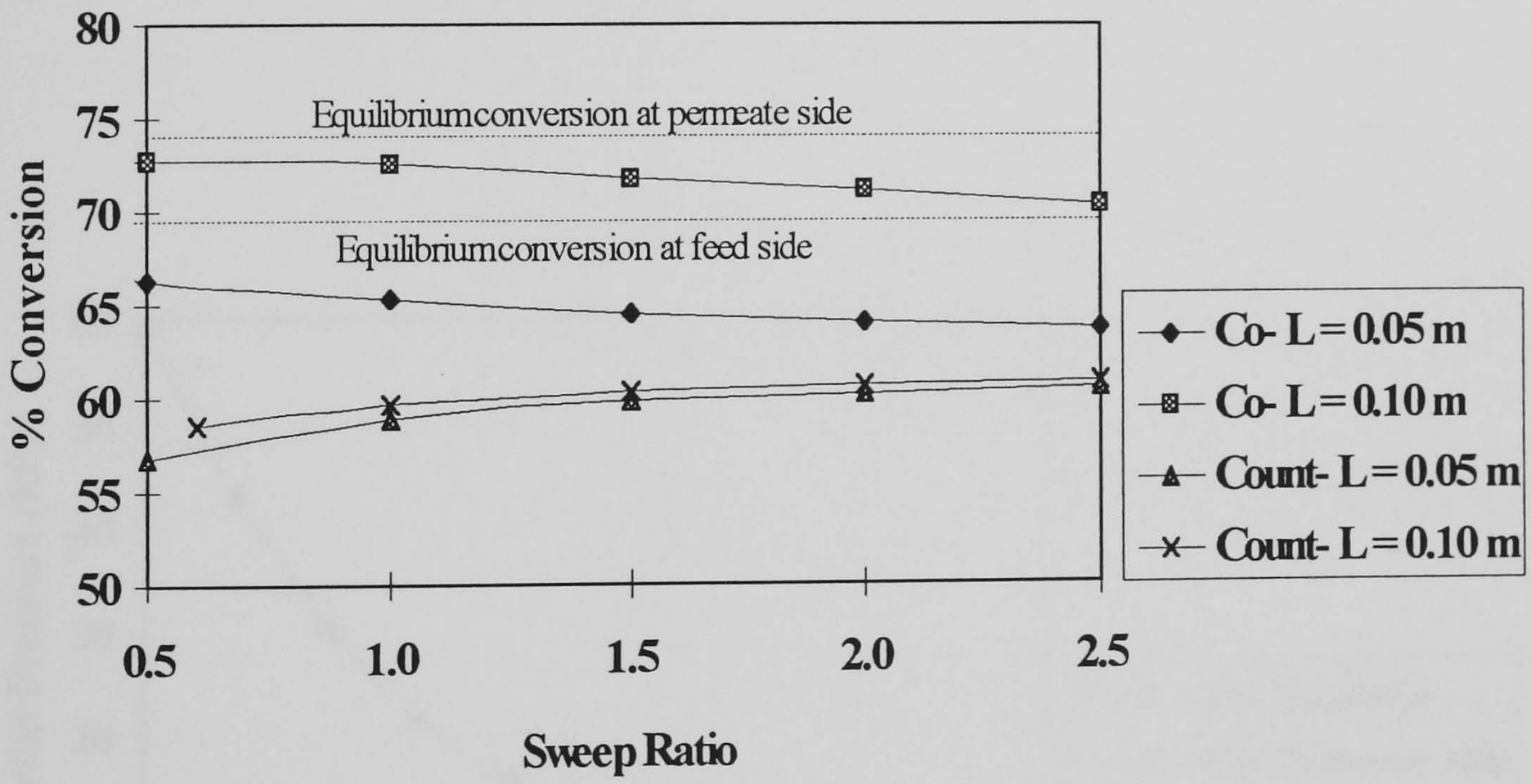


Figure 7.5 Effect of mode of operation on the performance of membrane reactor

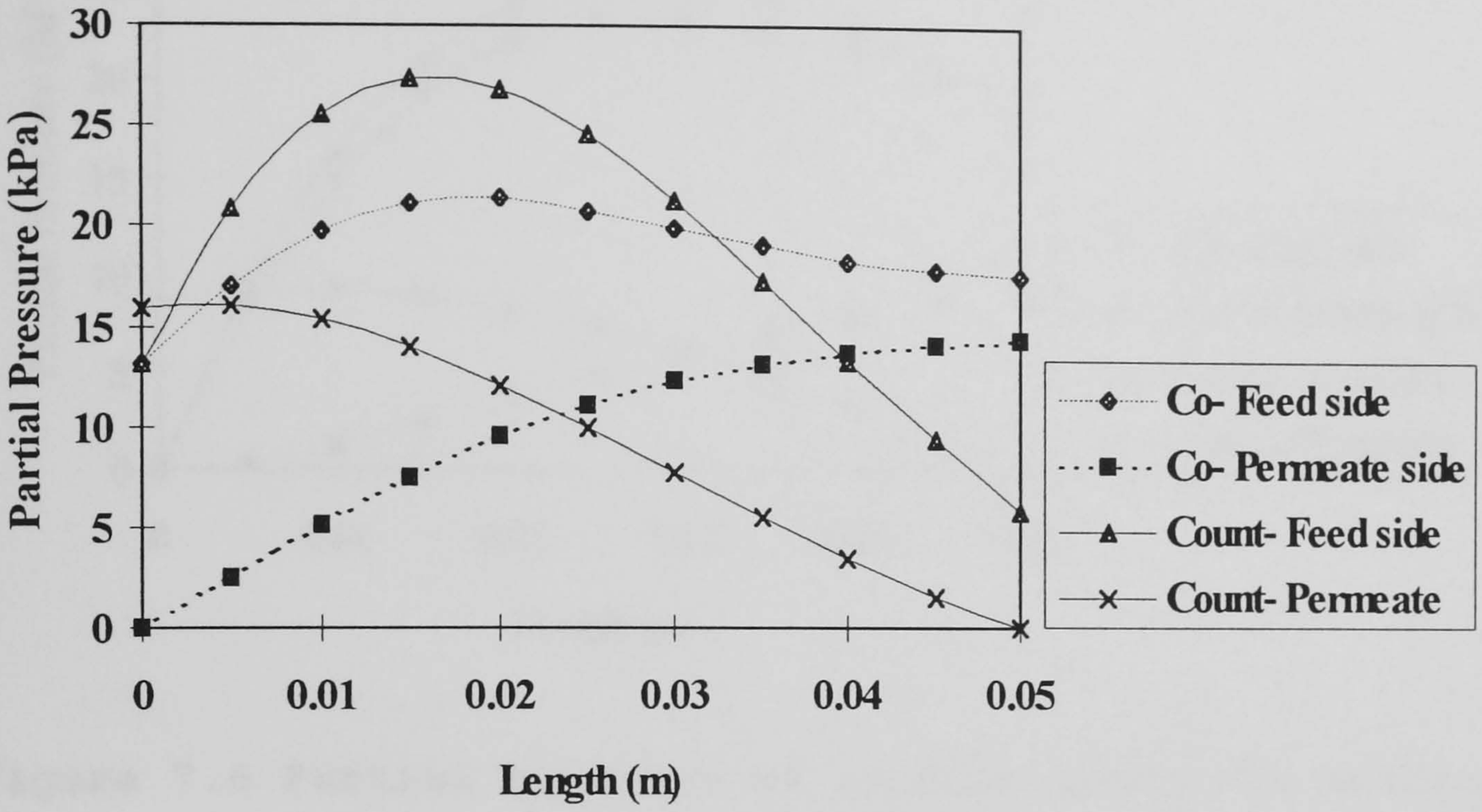


Figure 7.6 Partial pressure of hydrogen along the membrane

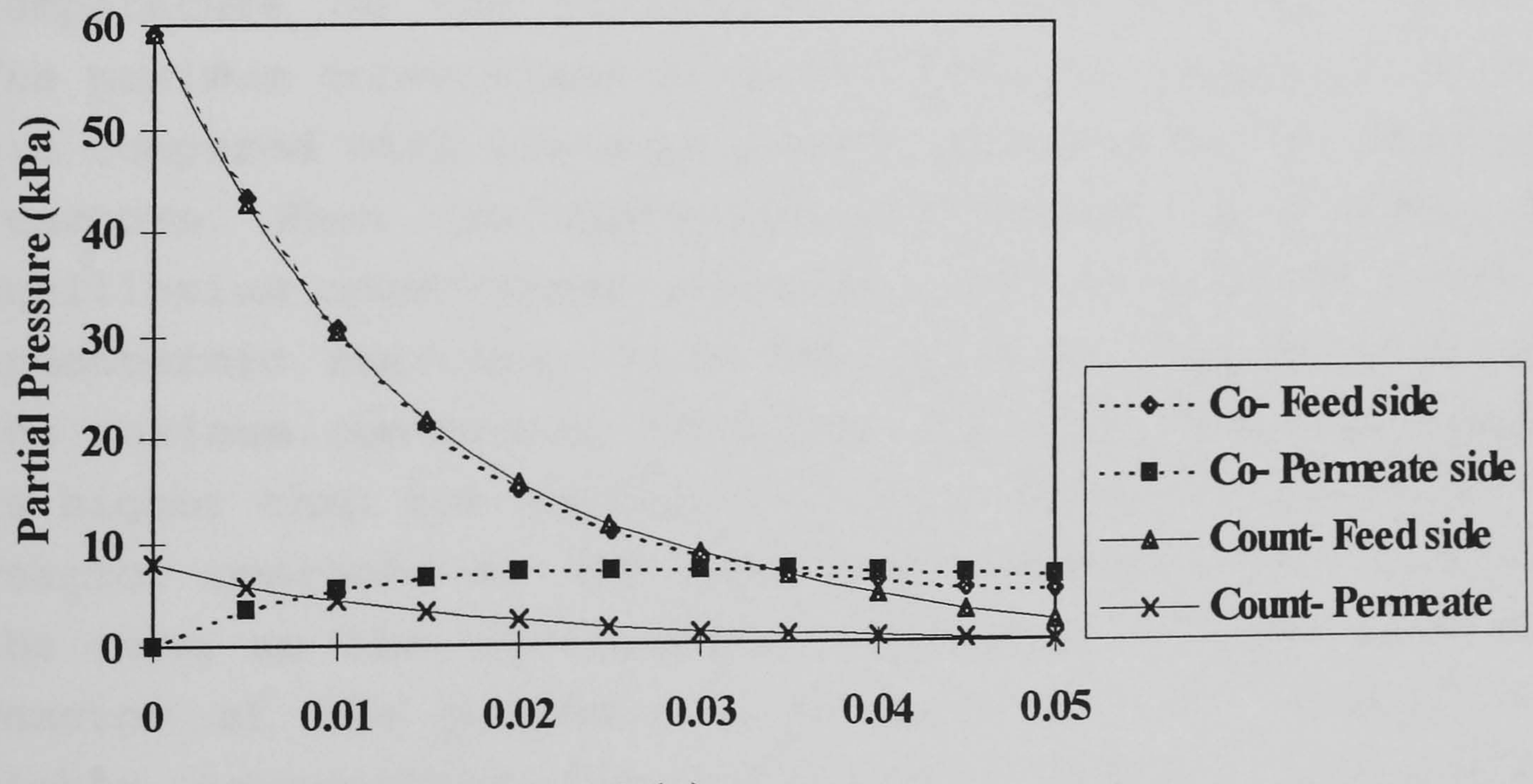


Figure 7.7 Partial pressure of isopropanol along the membrane

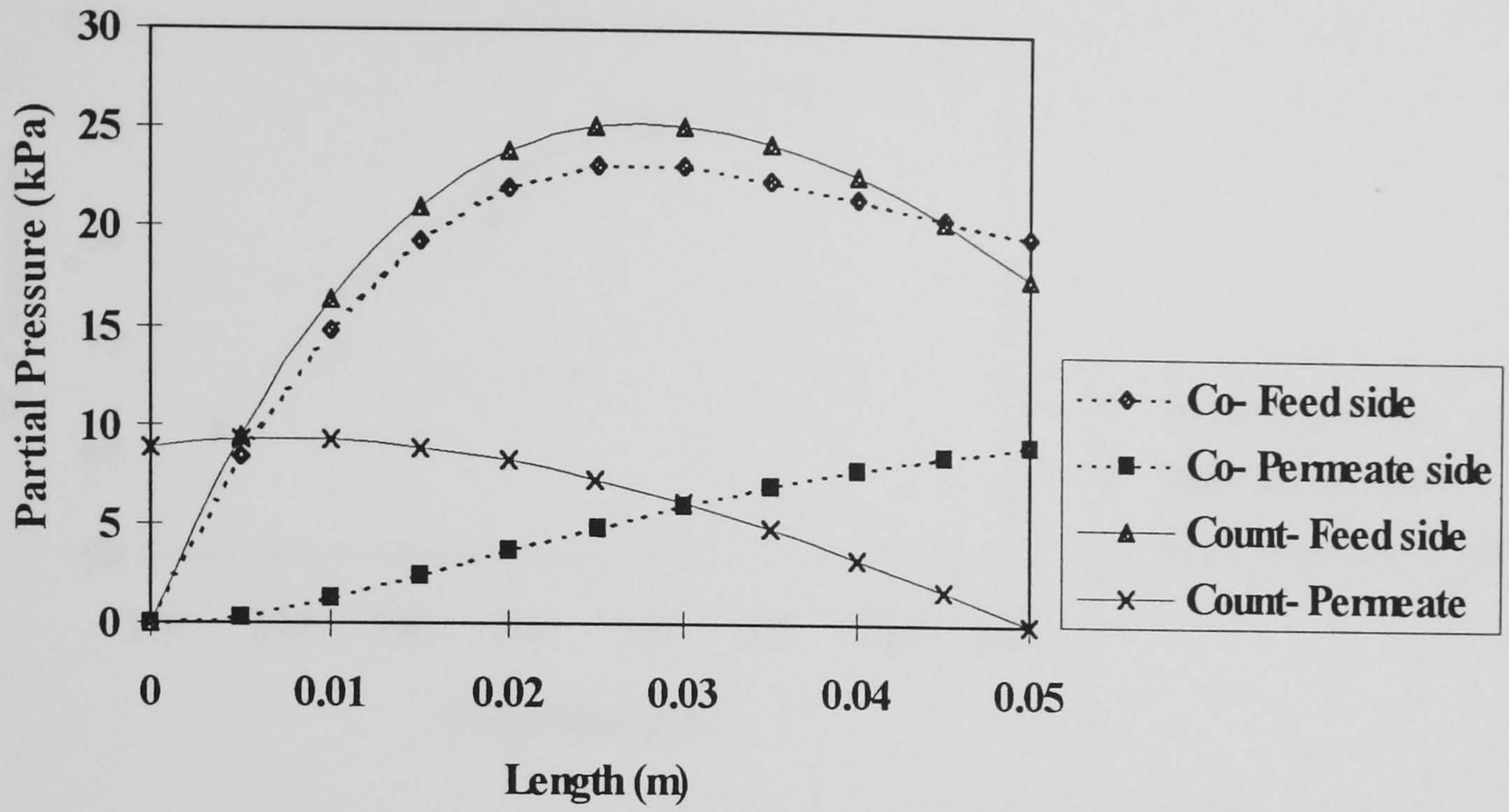


Figure 7.8 Partial pressure of acetone along the membrane

- **Effect of Operating Temperature**

Figure 7.9 shows the effect of operating temperature on the performance of the membrane reactor. The maximum conversions obtained from the membrane reactor are compared with the equilibrium conversions in plug flow reactors. When the operating temperature is higher, the equilibrium conversions increase. This is because it is an endothermic reaction. From the graph it can be seen that the maximum conversion obtained from the membrane reactor is higher than the equilibrium conversion of the plug flow reactor operated at the feed side pressure. It is almost the same as the equilibrium conversion of the plug flow reactor at the permeate side pressure. In addition, at higher temperature the difference between the maximum conversion from the membrane reactor and the equilibrium conversion under the feed side pressure becomes smaller. This means the improvement in conversion in the membrane reactor is less noticeable at a higher operating temperature.

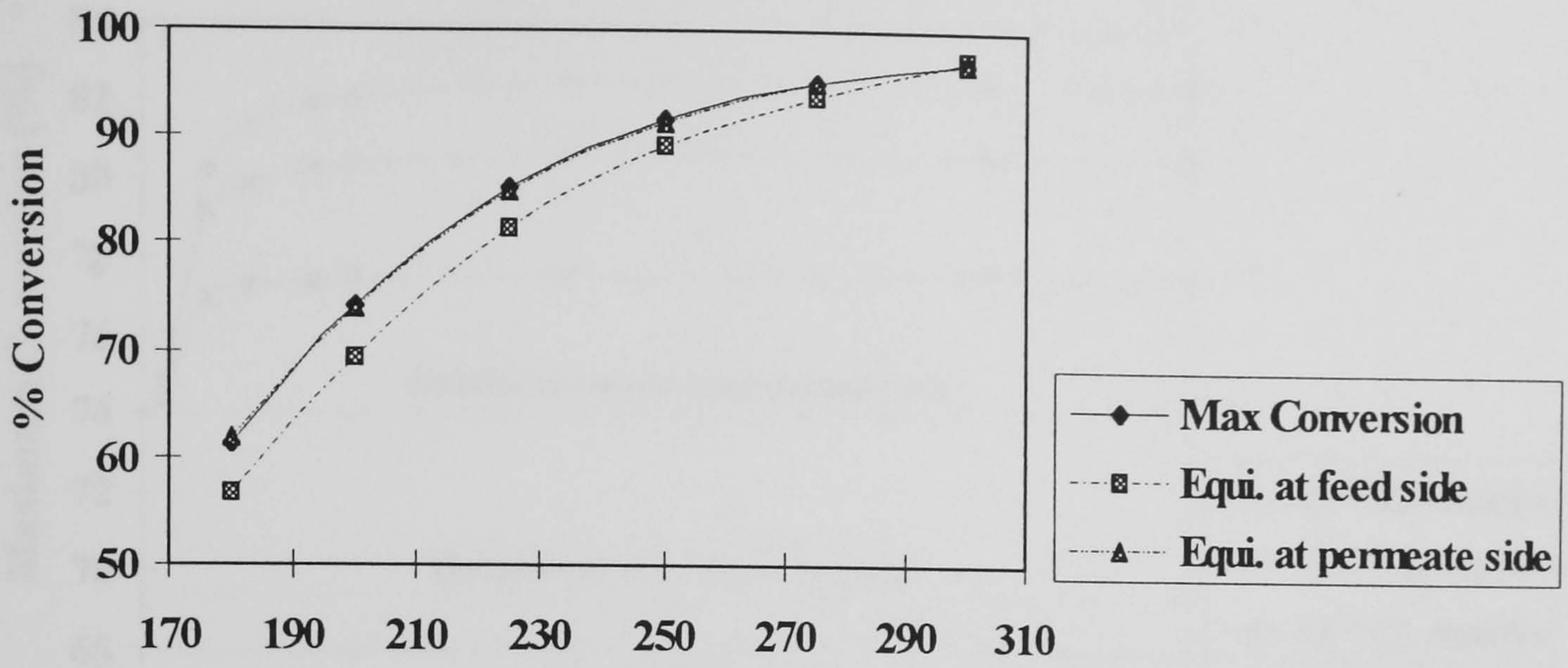


Figure 7.9 Effect of operating temperature on the performance of membrane reactor

Since the results from simulations discussed so far do not show substantial improvement over a conventional plug flow reactor, the following sections are aimed at investigating the limiting factors on the performance of the membrane reactor.

- **Effect of Rate of Reaction**

This section is to investigate the effect of rate of reaction on the performance of the membrane reactor. The value of reaction rate constant k_o is varied from 1 to 50 times of the value used in this study. Three values of sweep flow rate of 0.1, 0.2 and 0.3 mmol/s were considered. Figure 7.10 shows that the maximum conversion obtained from the membrane reactor is higher when the rate constant increases; however, it gradually levels off and further increase of rate constant does not improve the performance of the membrane reactor. The improvement is more pronounced when the sweep flow rate is high. From these results, it implies that the membrane reactor can perform better if a more active catalyst is used.

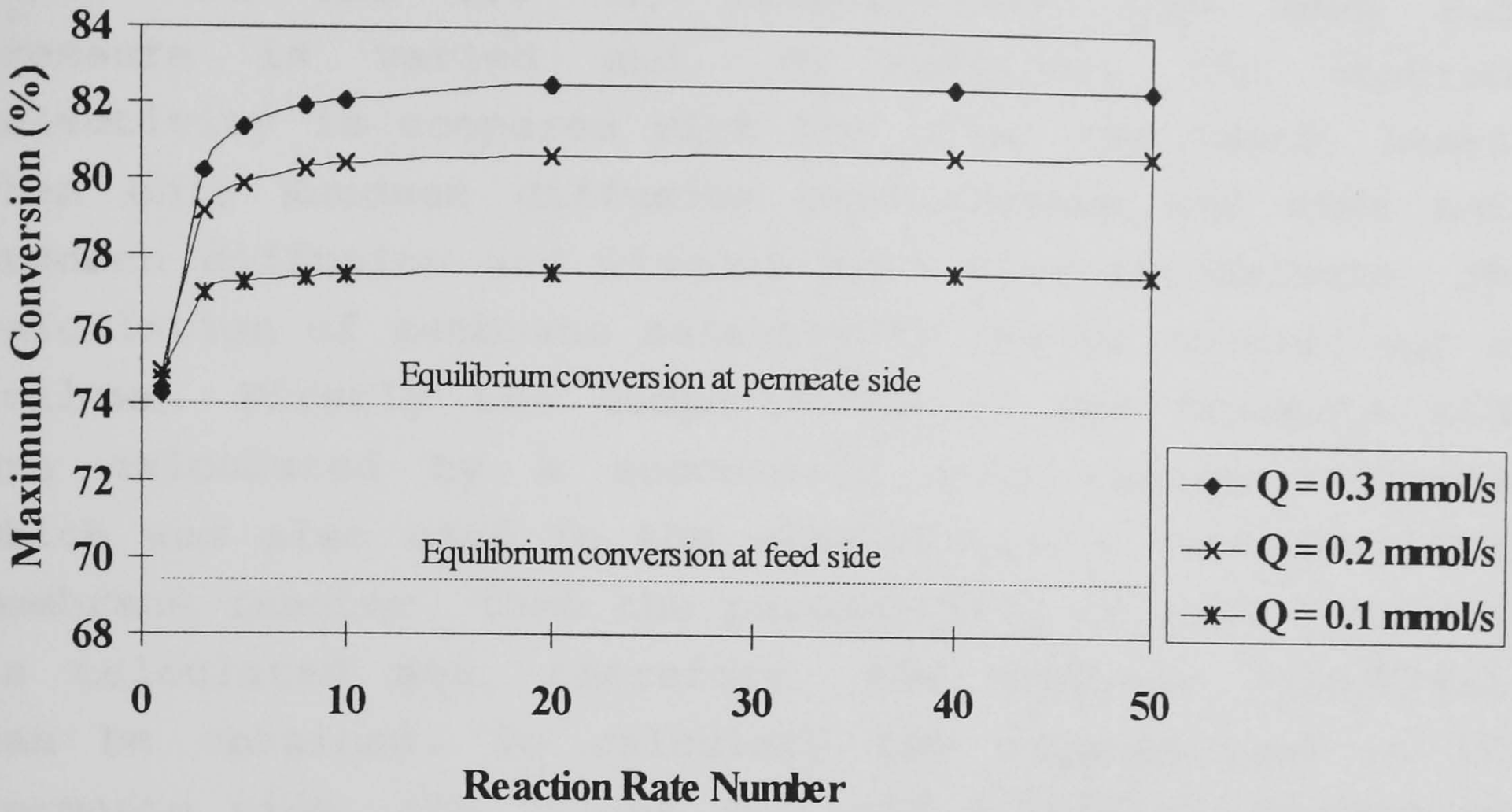


Figure 7.10 Effect of rate of reaction on the performance of membrane reactor

- **Effect of Surface Diffusion on the Membrane Selectivity**

When there is no significant interaction between permeating gases and a membrane surface, Knudsen diffusion and viscous flow denominate the transport rate through a porous membrane. For the alumina membrane with pore size of 4 nm, Knudsen diffusion is the major flow mechanisms and the membrane selectivity is roughly equal to the square root of the molecular weights of the gases in the mixture. However, when surface diffusion becomes important, separation becomes more complicated. In this section the selectivity of the membrane for a mixture containing equimolar quantities of hydrogen, acetone and isopropanol is investigated. The ratio of the permeabilities of two components of interest is used to show the membrane selectivity.

Figure 7.11 - Figure 7.13 show the membrane selectivities of hydrogen/isopropanol, hydrogen/acetone and acetone/isopropanol at the condition where the permeate side pressure and operating temperature are

101.3 kPa and 200 °C, respectively. The feed side pressure is varied and, in addition, the membrane selectivity is compared with the other two cases; namely when only Knudsen diffusion predominates and when both Kundsen diffusion and viscous bulk flow predominate. The calculation of membrane selectivity can be carried out as follows. Firstly the compositions in the permeate side are calculated by a successive substitution technique which was also used in the simulations of countercurrent membrane reactor. Then the permeability of each component is calculated and, therefore, the membrane selectivity can be obtained. To calculate the compositions in the permeate side, the values (y_i) are initially guessed and then the molar flow rate per unit length of membrane can be calculated. For example, for the case where only Knudsen diffusion predominates, the molar flow rate per unit length of membrane is

$$\left(\frac{F_i}{L}\right) = \frac{a}{\sqrt{M_i T}}\left(p_1 x_i - p_2 y_i\right) \tag{7.16}$$

Then the compositions in the permeate side are calculated by the following expression.

$$y'_i = \frac{\left(F_i/L\right)}{\sum_i \left(F_i/L\right)} \tag{7.17}$$

The differences between the guessed values and the calculated values are used to adjust the new initial guesses. Then the process is repeated until convergence is achieved.

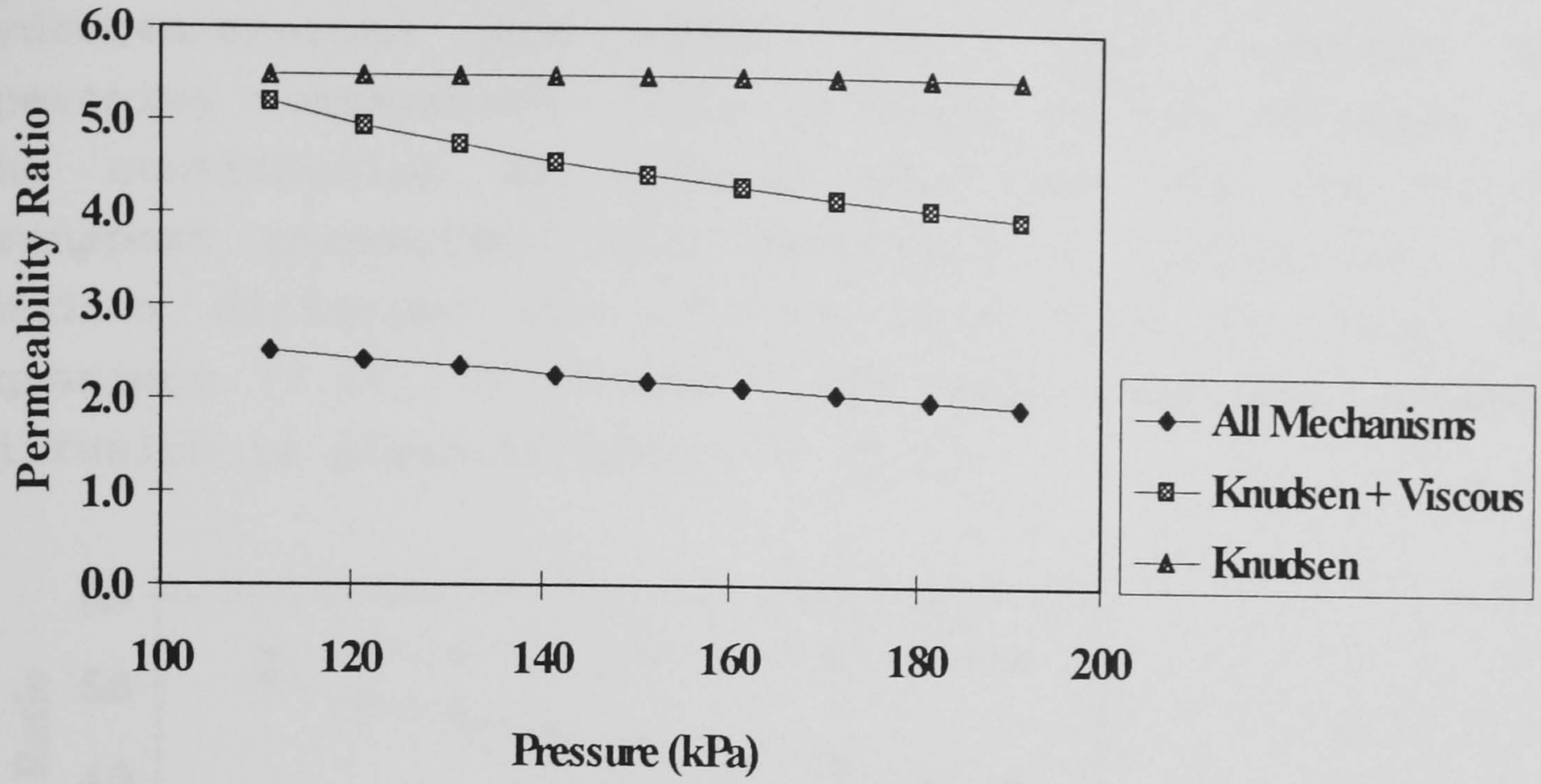


Figure 7.11 Effect of pressure on permeability ratio of hydrogen and isopropanol

From the graphs it can be seen that when Knudsen diffusion predominates, the selectivity is independent of feed side pressure while when the transport mechanisms are due to the combination between the Knudsen diffusion and viscous bulk flow, the selectivity decreases with increase of feed pressure. This is because the contribution of non separative viscous flow becomes more significant as the pressure is higher. However, in the presence of surface diffusion, the selectivities for hydrogen/isopropanol and hydrogen/acetone become much lower to be around 2.5 and 2 respectively. The low selectivities are caused from both the higher permeation rate of the organic vapours due to the surface diffusion and the lower hydrogen permeation rate due to the pore blocking by the presence of an adsorbed phase of organic vapour on the membrane pore surface. In Figure 7.13, the selectivity of acetone/isopropanol is higher than that of Knudsen diffusion. However, the increase is rather small.

The effect of operating temperature on the membrane selectivity is shown in Figure 7.14. The

membrane selectivities of hydrogen/isopropanol and hydrogen/acetone are higher with the increase of operating temperature. This is owing to the decrease of the contribution of surface diffusion to the total transport mechanisms. The variation of temperature for Knudsen diffusion and viscous bulk flow is given by Equations (7.6), (7.7) and (6.16) while that for surface diffusion is given by Equation (6.17).

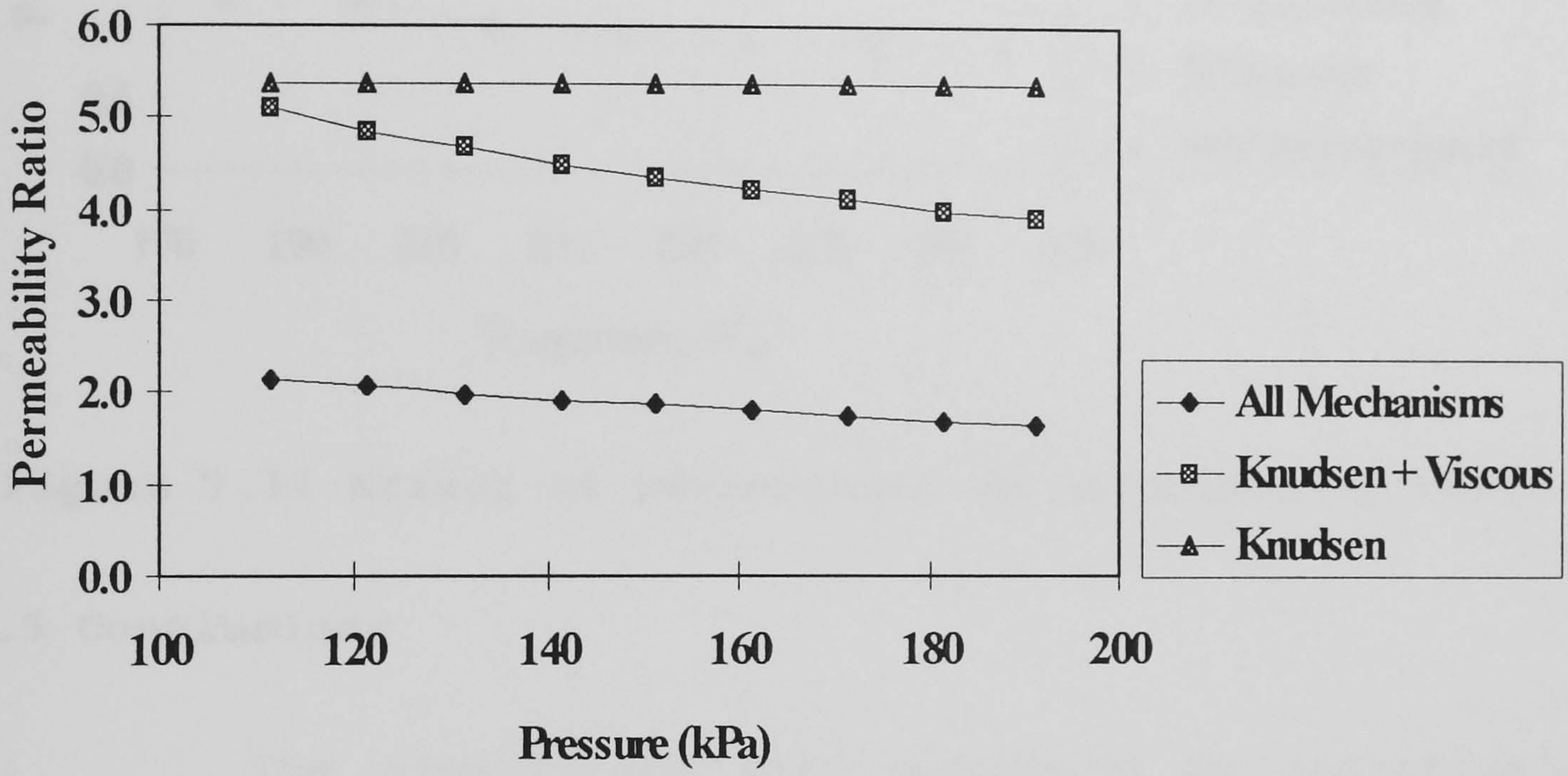


Figure 7.12 Effect of pressure on permeability ratio of hydrogen and acetone

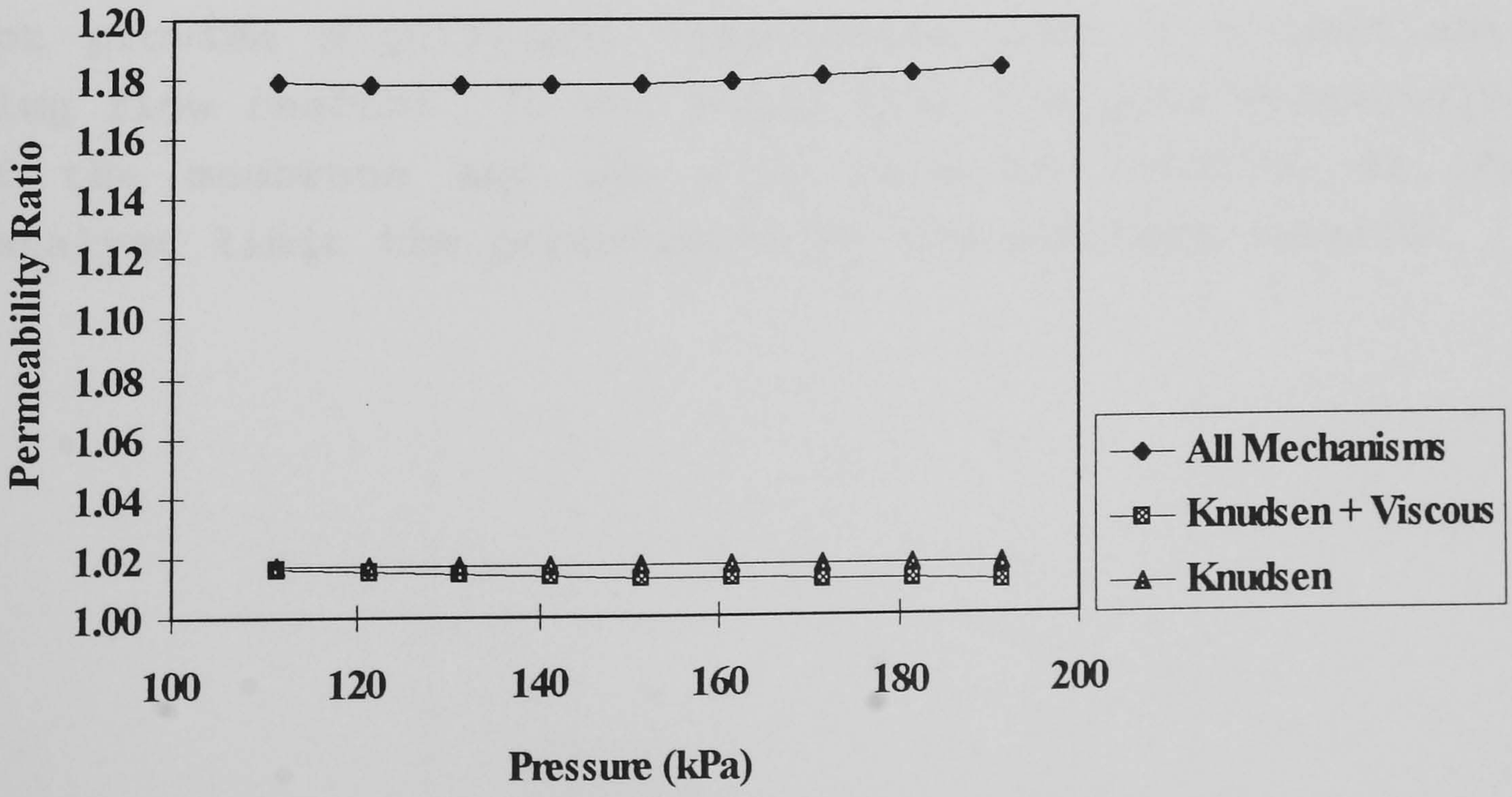


Figure 7.13 Effect of pressure on permeability ratio of acetone and isopropanol

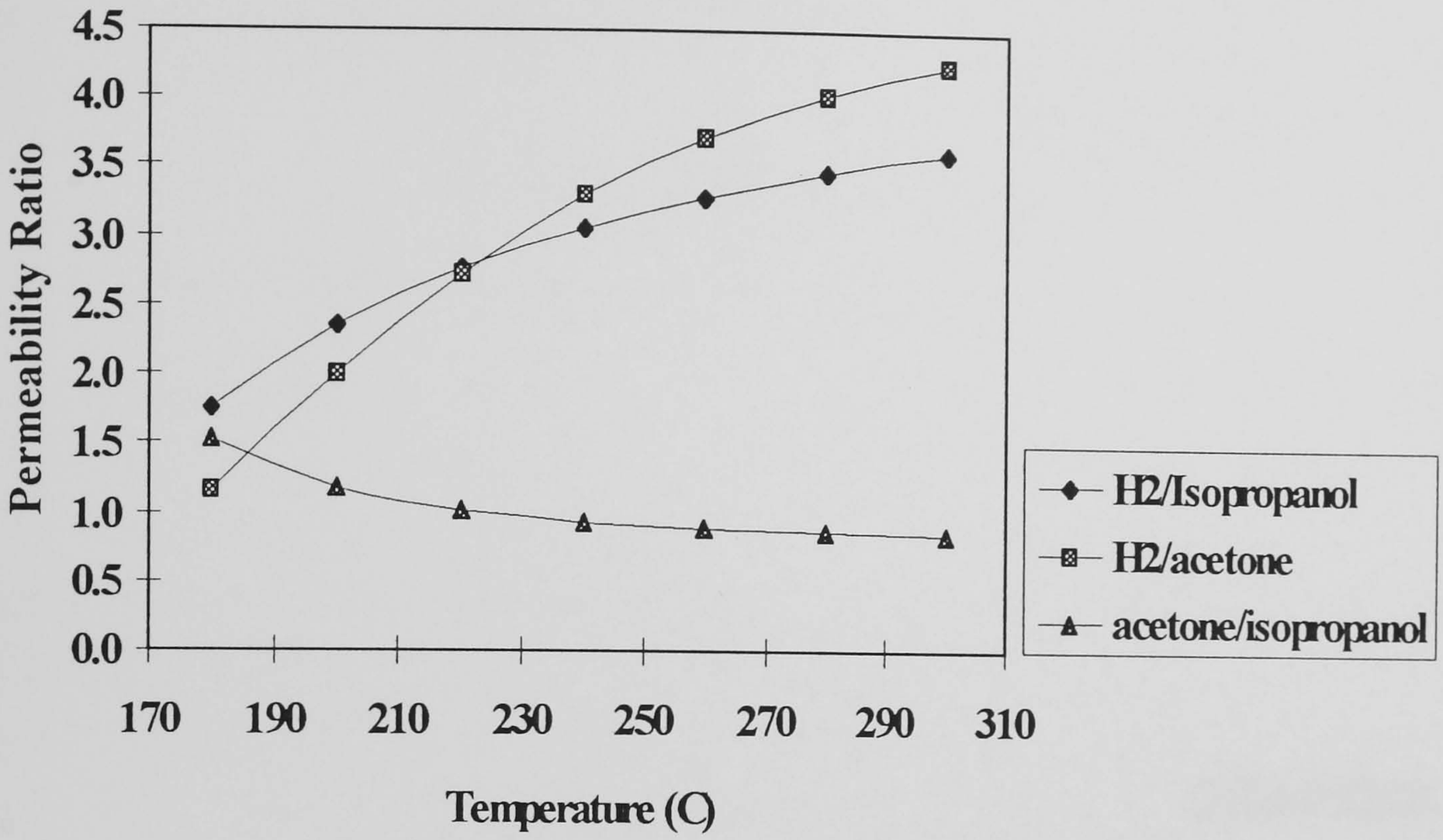


Figure 7.14 Effect of temperature on permeability ratio

7.5 Conclusions

The simulations were performed to investigate the performance of the dehydrogenation of isopropanol to acetone in an alumina membrane with pore size of 4 nm. Cocurrent mode of operation showed superior performance to countercurrent mode. However, the membrane reactor did not provide significant improvement over a conventional plug flow reactor. It was found that the poor selectivity of the membrane and the slow rate of reaction of the catalyst limit the performance of the membrane reactor.

CHAPTER 8

CONCLUSIONS AND SUGGESTIONS FOR FUTURE WORK

8.1 Conclusions

8.2 Suggestions for Future Work

CHAPTER 8

CONCLUSIONS AND SUGGESTIONS FOR FUTURE WORK

8.1 Conclusions

The aim of this thesis was to investigate the transport mechanisms of some gases and organic vapours through commercially available alumina membranes with pore diameter of 4 and 10 nm at conditions which are suitable for chemical reactions. The following are conclusions drawn from this work.

1) The transport of hydrogen and nitrogen through the membranes can be described by the contribution of Knudsen diffusion and viscous bulk flow. When gas permeability is plotted against mean pressure across the membrane, a linear relationship is obtained. The intersection and slope of the curve provide the contributions of Knudsen diffusion and viscous bulk flow, respectively. The expressions obtained are useful for prediction gas phase flow of the same gas at different operating condition, such as temperature, or for prediction of other gases where their molecular weight and viscosity are known.

2) From the permeation studies of ethanol and methanol vapours, the permeabilities are less than the values predicted from gas phase permeation. A model was developed to describe the results. It was found that the discrepancy from the theoretical values is because of the pore blockage due to the presence of the adsorbed alcohol. It was further found that the contribution of the adsorbed phase does not make significant contribution on the total permeation rate.

3) From the permeation studies of isopropanol and acetone vapours, even though the permeabilities of isopropanol vapour were lower than the predicted values (as was found in the case of ethanol and methanol vapour permeation), the model developed for the ethanol and methanol cases failed to describe the results. A surface diffusion model based on Fick's law was considered and included in the model and it can describe the results for both isopropanol and acetone fairly well. The model was then extended to predict the permeation rate of mixtures of isopropanol and acetone vapours using the results from pure component studies. It can predict the results with an average deviation of 11 %.

4) The studies of an alumina membrane reactor for the dehydrogenation of isopropanol to acetone showed that the concept does not significantly improve the performance of a conventional plug flow reactor.

It is believed that all the organic vapour permeation results in this work are novel. Most previous work was performed in the capillary condensation regime, which is useful for solvent recovery, or at significantly higher temperatures. It is also the first time an alumina membrane has been considered for the dehydrogenation of isopropanol to acetone.

8.2 Suggestions for Future Work

1) The apparatus designed for this study is based on the forced flow measurement where one side of the membrane is closed. The pressure in the permeation side is fixed at one atmosphere while pressure in the feed side is recorded with the feed flow rate. Hence, the equipment is only suitable for the study of permeation rate under pressure gradients. In order to study the case where total pressure is the same on both sides of the

membrane, some equipment modifications are necessary, such as introducing the feed outlet stream to create a cross-flow device, and connecting all streams to an on-line gas chromatograph to allow their compositions to be measured. It should be noted that the way to connect both ends of the membrane to the module is rather difficult since the membrane is very fragile. Since the maximum operating temperature in these studies is limited by the oven at 200 ^{o}C, the module should be further modified to fit into a furnace in order to allow the study to be performed at higher temperature levels.

2) Experimental studies of other organic vapours such as methyl formate and formaldehyde through the same membrane are suggested. Since formaldehye is available in a mixture with other components, the modified apparatus which was suggested in (1) is necessary. With the results of methanol permeation the data will be useful for modelling of the dehydrogenation of methanol in an alumina membrane reactor. The experiment should also cover the case of mixture of those organics.

3) Recently a number of new membranes such as a silicalite membrane have been made with pores of molecular dimensions of around 0.4 nm. With this kind of membrane it is expected that separation factor will be very high and, therefore, the membrane will be suitable for a membrane reactor where small molecular size products are exclusively removed from the reaction side to the permeate side. Hence, it is worthy investigating the permeation of gases and vapours, for example, hydrogen gas and isopropanol and acetone vapours, through the membrane.

4) The experimental studies on a membrane reactor is also suggested to be done in order to compare with results from simulation. When the model can describe

the experimental results well, the simulation study can be extended to find an optimum condition for the membrane reactor.

APPENDICES

APPENDIX 1

CHARACTERISTICS OF THE MONOTUBE MEMBRALOX MULTILAYER ALUMINA MEMBRANES

Brand : ALCOA-SCT (France)
Designation : 7/10 Monotube, type G
Support Composition : α - alumina
Membrane Composition: γ - alumina
Available Pore Size : 4 and 10 nm
Length : 0.25 m
Internal Diameter : 0.007 m
Outside Diameter : 0.010 m
Surface Area : 0.005 m^2
Bursting Pressure : > 3000 kPa

Table A1.1 Characteristics of a membrane with 4 nm pore size

Layer	Thickness (m)	Porosity	Pore Size (m)
Support 1	1.5E-03	0.45	1.5E-05
Support 2	5.0E-05	0.53	8.0E-07
Support 3	3.0E-05	0.53	2.0E-07
Separative layer	5.0E-06	0.53	4.0E-09

The following table compares the nitrogen permeability of the three support layers with that of the separative layer. The calculation is based on the condition where

temperature (T) and mean pressure across the membrane ($\bar{p}$) are 298 K and 101.3 kPa, respectively.

Table A1.2 Permeability of each membrane layer

Layer	Permeability ($mol/m^2.sec.kPa$)	Permeability Ratio
Support 1	2.5E+00	171
Support 2	5.6E-01	39
Support 3	1.5E-01	10
Separative layer	1.4E-02	1

The expression for the gas permeability can be developed as follows.

From Equations (2.1) and (2.2) the total flux across the membrane is

$$J = -\left(\frac{\pi n d_p^3}{12RT\tau}\sqrt{\frac{8RT}{\pi M}} + \frac{\pi n d_p^4 p}{128\tau\mu RT}\right)\frac{dp}{dz} \qquad (A1.1)$$

since the porosity (ε) of the membrane is defined as the volume of the pores in the membrane divided by the total volume of the membrane, it can be expressed as

$$\varepsilon = \frac{\pi}{4} n d_p^2 \qquad (A1.2)$$

Hence,

$$J = -\left(\frac{d_p}{3RT}\left(\frac{\varepsilon}{\tau}\right)\sqrt{\frac{8RT}{\pi M}} + \frac{d_p^2 p}{32\mu RT}\left(\frac{\varepsilon}{\tau}\right)\right)\frac{dp}{dz} \qquad (A1.3)$$

Equation (A1.3) can be integrated with respect to the boundary condition where the pressure on one side of the

membrane is p_1 and the other side of the membrane is p_2. This gives the permeability (P) as

$$P = \frac{J}{\Delta p} = \left(\frac{d_p}{3RT} \left(\frac{\varepsilon}{\tau} \right) \sqrt{\frac{8RT}{\pi M}} + \frac{d_p^2}{32 \mu RT} \left(\frac{\varepsilon}{\tau} \right) \bar{p} \right) \frac{1}{\Delta z} \qquad \text{(A1.4)}$$

where Δp is p_1-p_2 and Δz is thickness of the membrane. In the calculation for nitrogen gas permeability even though the value of bed tortuosity (τ) is unknown, it is known to be inversely proportional to the membrane porosity (ε) (Ash *et al*, 1976). Hence in this calculation it is assumed to be equal to the reciprocal of the porosity. It should be noted that the permeability defined in this Appendix is in molar flux per unit pressure drop.

APPENDIX 2

MOLECULAR DIAMETER AND MEAN FREE PATH OF SOME GASES AND VAPOURS

In Table A2.1 the molecular diameter of nitrogen and hydrogen gases are given from both viscosity and van der Waal while the molecular diameter of organic liquid is calculated from their densities with the assumption that each molecule is square in shape.

Table A2.2 shows the mean free path of the same gases and vapours at pressure of 101.3 kPa and 4 levels of temperature. The mean free path is calculated from the following expression (Jeans, 1946).

$$\lambda = \frac{3\mu}{p}\sqrt{\frac{\pi RT}{8M}} \qquad \text{(A2.1)}$$

where λ is a mean free path, μ is gas viscosity, p is an operating pressure, R is the gas constant and M is a molecular weight.

Table A2.1 Molecular diameter of some gases and vapours

Gas/Vapour	Molecular Diameter (nm)		
	From Viscosity	From van der Waal	From the Above Assumption
H_2	0.24	0.23	-
N_2	0.32	0.32	-
Methanol	-	-	0.41
Ethanol	-	-	0.46
Isopropanol	-	-	0.50
Acetone	-	-	0.50

Table A2.2 Mean free path of some gases and vapours

Gas/Vapour	Mean Free Path (nm)			
	T = 20 °C	T = 160 °C	T = 180 °C	T = 200 °C
H_2	145	227	239	252
N_2	88	143	152	160
Methanol	-	62	66	71
Ethanol	-	46	49	53
Isopropanol	-	45	48	51
Acetone	-	45	48	51

APPENDIX 3

SATURATION PRESSURE OF SOME ORGANIC VAPOURS

Saturation vapour pressure in a capillary pore is smaller than that in normal condition. This is due to the effect of surface tension. The saturation pressure in the capillary pore can be predicted by the Kelvin equation as follows

$$\frac{\rho RT}{M} \ln \frac{p_p}{p_o} = -\frac{4\sigma \cos \psi}{d_p} \qquad \text{(A3.1)}$$

where p_o is saturation pressure at normal surface, p_p is saturation pressure in a membrane pore, M is molecular weight, σ is surface tension, ρ is density of liquid in the pore, d_p is pore diameter, ψ is the contact angle of the condensed liquid on the solid, R is the gas constant and T is operating temperature.

By assuming that a density of liquid in a pore can be estimated by the density of liquid at room temperature and the contact angle (ψ) is zero, the saturation pressure inside the membrane pore can be calculated. Table A3.1 and A3.2 shows the saturation pressure of ethanol and methanol, respectively, in the membranes with pore diameter of 4 and 10 nm. While Table A3.3 and Table A3.4 gives those values of isopropanol and acetone, respectively, in the membrane with pore diameter of 4 nm.

Table A3.1 Saturation pressure of ethanol

T (^{o}C)	Saturation Pressure * 10^{-3} (kPa)	Saturation Pressure in Membrane * 10^{-3} (kPa)	
		4 nm	10 nm
160	1.2	0.9	1.1
180	1.8	1.4	1.6
200	2.8	2.2	2.5

Table A3.2 Saturation pressure of methanol

T (^{o}C)	Saturation Pressure * 10^{-3} (kPa)	Saturation Pressure in Membrane * 10^{-3} (kPa)	
		4 nm	10 nm
150	1.3	1.1	1.2
175	2.3	1.9	2.1
200	3.8	3.1	3.4

Table A3.3 Saturation pressure of isopropanol

T (^{o}C)	Saturation Pressure * 10^{-3} (kPa)	Saturation Pressure in 4 nm Membrane pore * 10^{-3} (kPa)
160	1.2	0.8
180	1.8	1.3
200	2.8	2.0

Table A3.4 Saturation pressure of acetone

T (^{o}C)	Saturation Pressure * 10^{-3} (kPa)	Saturation Pressure in 4 nm Membrane Pore * 10^{-3} (kPa)
160	1.4	1.0
180	2.0	1.5
200	2.8	2.1

APPENDIX 4

ERROR ANALYSIS FOR EXPERIMENTAL DATA

The experimental work of this thesis is mainly concerned with gas permeability. The main sources of instrumental error are the pressure measurement and the flow measurement. The corresponding accuracy of the instrument are as follows

Instruments	**Accuracy**
Rotameters	0.04
Pressure Gauge	0.04

Accidental and indeterminate errors were avoided as much as possible by developing methods and procedures of analysis that were performed all the time. It is believed that this source of error was of minor importance compared with the errors due to instrumental analysis.

The error due to pressure and flow measurement are mainly related with the gas permeability determination. The permeate flux equation is represented by:

$$P = \frac{a}{\sqrt{MT}} + \frac{b}{\mu T}\bar{p} \qquad \text{(A4.1)}$$

and

$$P = \frac{Q}{\Delta p} \qquad \text{(A4.2)}$$

where P is the gas permeability, Q is the flow rate per unit length, Δp is the pressure difference across the membrane.

Taking natural logarithmic of both sides on equation (A4.2) gives

$$\ln(P) = \ln(Q) - \ln(\Delta p) \tag{A4.3}$$

or

$$\frac{dP}{P} = \frac{dQ}{Q} \pm \left|\frac{d\Delta p}{\Delta p}\right| \tag{A4.4}$$

The error due to pressure measurement is of the following order:

$$\frac{\Delta p}{p} = 0.04 \tag{A4.5}$$

and the error associated with the measurement of flow Q is

$$\frac{\Delta Q}{Q} = 0.04 \tag{A4.6}$$

Since the error in the determination of the Kundsen parameter (a) is mainly functions of the flow and pressure measurement, the maximum possible error should be 0.04 + 0.04 or 0.08. The error in the determination of viscous parameter b should be around 0.12.

Table A4.1 shows the mean, standard deviation and coefficient of variation of the experimental results of nitrogen gas permeation through the alumina membrane with pore size of 4 and 10 nm (in Chapter 4). It can be seen from the values in Table A4.1 that the precision given by the coefficient of variation is of the order of 0.031 for the coefficient a and 0.068 for the coefficient b. At 90 % probability level the error is equal to twice the coefficient of variation, giving 0.06 and 0.14 for the error in a and b respectively. These values agree with the values of 0.08 and 0.12 reported earlier.

Table A4.1 Error analysis of parameters a and b for the membrane with pore size of 4 and 10 nm

Membrane	T (K)	a x 10^{-3} Run 1	Run 2	Mean	Standard Deviation	Coefficient of variation	b x 10^{-12} Run 1	Run 2	Mean	Standard Deviation	Coefficient of variation
4 nm	292	4.64	4.72	4.78	0.11	0.02	1.12	1.08	1.00	0.06	0.06
	364	4.90	4.99				1.06	1.00			
	396	4.84	4.88				0.92	0.91			
	425	4.72	4.81				0.96	0.95			
	457	4.72	4.62				0.99	1.04			
	474	4.77	4.69				1.00	1.01			
	Average	4.77	4.79				1.01	1.00			
Membrane	T (K)	a x 10^{-2} Run 1	Run 2	Mean	Standard Deviation	Coefficient of variation	b x 10^{-12} Run 1	Run 2	Mean	Standard Deviation	Coefficient of variation
10 nm	292	1.38	1.24	1.29	0.04	0.031	2.23	2.66	2.65	0.18	0.068
	364	1.22	1.28				2.98	2.66			
	396	1.27	1.27				2.75	2.79			
	425	1.30	1.30				2.53	2.58			
	457	1.31	1.30				2.54	2.65			
	474	1.27	1.28				2.76	2.67			
	Average	1.29	1.28				2.63	2.67			

REFERENCES

REFERENCES

Altena, F.W., et al. 'Some comments on the applicability of gas permeation methods to characterise porous membranes based on improved experimental accuracy and data handling', *J. Mem. Sci. 12 (1983) 313-322*

Althainz, P., et al. 'Reception tuning of gas - sensor microsystems by selective coatings', *Sensors and Actuator, B: Chemical B25 (1995) 366-369*

Anderson, M.A., et al. 'Titania and alumina ceramic membranes', *J. Mem. Sci. 39 (1988) 243-258*

Armor, J.N. 'Catalysis with permselective inorganic membranes', *App. Cat. 49 (1988) 1-25*

Ash, R., et al. 'Flow of adsorbable gases and vapours in a microporous medium I. Single sorbates', *Proc. Roy. 271 A (1962a) 1-18*

Ash, R., et al. 'Flow of adsorbable gases and vapours in a microporous medium II. Binary mixtures', *Proc. Roy. 27I A (1962b) 19-33*

Ash, R., Baker, R.W. and Barrer, R.M. 'Sorption and surface flow in graphitezed carbon membranes I. The steady state', *Proc. Roy. 299 A (1966) 434-453*

Ash, R., Barrer, R. and Sharma, P. 'Sorption and flow of carbon dioxide and some hydrocarbons in a microporous carbon membrane', *J. Mem. Sci. 1 (1976) 17-32*

Assabumrungrat, S. and White, D.A. 'Modelling endothermic reactions in a compound membrane reactor', *Gas. Sep. & Puri. 10 (1996) 47-52*

Ballew, H.W. 'Basis of filtration and separation', *Nuclepore Corp., Pleasanton, CA, 1978*

Barrer, R. M. 'Fluid flow in porous media', *Disc. Faraday Soc. 3 (1948) 61-72*

Barrer, R.M. and Barrier, J.A. 'Sorption and surface diffusion in porous glass', *Pro. Roy. A213 (1952) 250-265*

Bernstein, L.A. and Lund, C.R.F. 'Membrane reactors for catalytic series and series-parallel reactions', *J. Mem. Sci. 77 (1993) 155-164*

Berg, D., et al. 'Gas permeability through alumina membrane produced by sol-gel technique', *J. of Non. Cry. Sol. 94 (1987) 160-162*

Bird, R.B., et al. 'Transport and Phenomena', *Wiley International Edition, John Wiley & Sons, Inc. (1960)*

Brunauar, S. 'The adsorption of gases and vapours Vol.1 Physical adsorption', *Oxford University Press (1944) 19*

Cannon, K.C. and Hacskaylo, J.J. 'Evaluation of palladium-impregnation on the performance of a Vycor glass catalytic membrane reactor', *J. Mem. Sci. 65 (1992) 259-268*

Capannelli, G. et al. 'Comparison of the catalytic performance of $V_2O_5/\gamma\text{-}Al_2O_3$ in the oxidehydrogenation of propane to propylene in different reactor configurations: i) packed-bed reactor, ii) monolith-like reactor and iii) catalytic membrane reactor', *Chem. Eng. Sci. 51 (1996) 1817-1826*

Carman, P.C. and Malherbe, P.R. 'Diffusion and flow of gases and vapours through micropores II. Surface flow', *Proc. Roy. A203 (1950) 165-178*

Carman, P.C. and Raal, F.A. 'Diffusion and flow of gases and vapours through micropores III. Surface diffusion coefficients and activation energies', *Proc. Roy. A209 (1951) 38-58*

Chai, M., et al. 'Promotion of methane steam reforming using ruthenium-dispersed microporous alumina membrane reactor', *Chem. Let. 1993, 41-44*

Champagnie, A.M., et al. 'A high temperature catalytic membrane reactor for ethane dehydrogenation', *Chem. Eng. Sci. 45 (1990) 2423-2429*

Chen, Y.D. and Yang, R.T. 'Predicting binary Fickian diffusivities from pure-component Fickian diffusivities for surface diffusion', *Chem. Eng. Sci. 47 (1992) 3895-3905*

Ciordano, N., et al. 'Pulse flow gas chromatographic technique in heterogeneous catalysis', *Z. Phys. Chem. (Leipzig) 262 (1981) 996-1008*

Collins, J.P. and Way, J.D. 'Catalytic decomposition of ammonia in a membrane reactor', *J. Mem. Sci. 96 (1994) 259-274*

Flerov, G.N. 'Synthesis of superheavy elements and application of the nuclear physics methods in adjacent field', *Vestn. Akad. Nauk SSSR 4 (1984) 35*

Gilliland, E.R., Baddour, R.F. and Russell, J.L. 'Rates of flow through microporous solids', *AIChE J. 4 (1958) 90-96*

Gilliland, E.R., et al. 'Diffusion on surfaces. I. Effect of concentration on the diffusivity of physically adsorbed gases', *Ind. Eng. Chem. Fundam. 13 (1974) 95-99*

Gobina, E. and Hughes, R. 'Ethane dehydrogenation using a high-temperature catalytic membrane reactor', *J. Mem. Sci. 90 (1994) 11-19*

Gobina, E., Hou, K. and Hughes, R. 'Ethane dehydrogenation in a catalytic membrane reactor coupled with a reactive sweep gas', *Chem. Eng. Sci. 50 (1995) 2311-1319*

Gobina, E. and Hughes, R. 'Reaction coupling in catalytic membrane reactors', *Chem. Eng. Sci. 51 (1996) 3045-3050*

Higashi, K., et al. 'Surface diffusion phenomena in gaseous diffusion I) Surface diffusion of pure gas', *J. Atomic Energy Soc. Jpn. 5 (1963) 846*

Horiguchi, Y. , Hudgins, R.R. and Silveston, P.L. 'Effect of surface heterogeneity on surface diffusion in microporous solids', *Can. J. Chem. Eng. 49 (1971) 76-87*

Hsieh, H.P. 'Inorganic membrane reactors - A review', *AIChE Symp. Ser. 268 (1989) 1*

Huang, T-C and Chen, H-I 'Permeation of gases through aa supported alumina membrane', *J. of Chin. Int. Chem. Eng. 26 (1995) 47-56*

Itoh, N., et al. 'Simulation of a reaction accompanied by separation', *Int. Eng. Chem. 25 (1985) 138*

Itoh, N. 'Simulation of bifunctional palladium membrane reactor', *J. Chem. Eng. Jpn. 23 (1990) 81-87*

Jeans, J.H. 'An introduction to the kinetic theory of gases' *University press, Cambridge (1946)*

Jeyalakshmi, R., et al. 'Kinetics of dehydrogenation of 2-propanol on $La_{2-x}Sr_xCuO_{4-y}$', *Bull. Chem. Soc. Jpn.* *63* *(1990) 2970-2974*

Jia, M.D, et al. 'Ceramic-zeolite composite membranes and their application for separation of vapour/gas mixtures', *J. Mem. Sci.* *90* *(1994) 1-10*

Julbe, A., et al. 'The sol-gel approach to prepare candidate microporous inorganic membranes for membrane reactors', *J. Mem. Sci.* *77* *(1993) 137-153*

Kammermeyer, K. and Wyrick, D.D. 'Effect of adsorption in barrier separation' *Ind. Eng. Chem.* *50* *(1958) 1309-1310*

Lin, Y.S., et al. 'Microporous and dense ceramic membranes prepared by CVD and EVD', *Inorganic Membranes ICIM2-91 Proc 2 Int. Conf. Inorg. Membr. ICIM2 91., 1991, No.1991, 465-468*

Litinskii, A.O., et al. 'Study of different forms of alcohol chemisorption on γ-Al_2O_3 (alumina) with the scope of an obitial-stiochiometric cluster model', *Kinet. Katal.* *22* *(1981) 1423-6*

Liu, A.G. et al. 'Permeation of ethylbenzene and hydrogen through untreated and catalytically-treated alumina membrane', *Sep. Sci. Pur.* *25* *(1990) 1511-1521*

Lonsdale, H.K. 'The Growth of Membrane Technology', *J. Mem. Sci.* *10* *(1982) 81-181*

Matson, S.L., Lopez J. and Quinn J.A. 'Review Article Number 13: Separation of gases with synthetic membranes', *Chem. Eng. Sci.* *38* *(1983) 503-524*

Megiris, C.E. and Glezer, J.H.E. 'Preparation of silicon dioxide films by low-pressure chemical vapour deposition

on dense and porous alumina substrates', *Chem. Eng. Sci.* *47* *(1992) 3925-3934*

Mohan, K. and Govind, R. 'Analysis of a cocurrent membrane reactor', *AIChE J.* *32* *(1986) 2083*

Mohan, K. and Govind, R. 'Studies on a membrane reactor', *Sep. Sci. & Tech.* *23* *(1988) 1715-1733*

Nozaki, T., et al. 'Selective oxidative coupling of methane with membrane reactor', *Chem. Eng. Sci.* *47* *(1992) 2745-2950*

Okazaki, M., Tamon, H. and Toei, R. 'Interpretation of surface flow phenomenon of adsorbed gases by hopping model', *AIChE J.* *27* *(1981) 262-270*

Okubo, T. and Inoue, H. 'Surface diffusion on modified surface of porous glass', *J. Chem. Eng. Jpn.* *20* *(1987) 590-597*

Okubo, T. and Inoue, H. 'Analysis of surface diffusion of adsorptive gases through porous glass by a square-pulse method', *Int. Chem. Eng.* *29* *(1989) 539-546*

Okubo, T. et al. 'Equilibrium shift of dehydrogenation at short space-time with hollow fibre ceramic membrane', Ind. Eng. Chem. Res. 30 (1991) 614-616

Omata, K., et al. 'Oxidative coupling of methane using a membrane reactor', *App. Cat.* *52* *(1989) L2-L5*

Ponzi, M., et al. 'On the surface diffusion of adsorbable gases through porous media', *AIChE J.* *23* *(1977) 347-352*

Qiu, M.M. and Hwang, S.T. 'Continuous vapour-gas separation with a porous membrane permeation system', *J. Mem. Sci.* *59* *(1991) 53-72*

Rao, M.B. and Sircar, S. 'Nanoporous carbon membranes for separation of gas mixtures by selective surface flow', *J. Mem. Sci. 85 (1993) 253-264*

Ruthven, D.M. 'Principles of adsorption and adsorption processes', *John Wiley & Sons, Inc. NEW YORK (1984)*

Shelekhin, A.B., et al. 'Gas separation properties of a new polymer/inorganic composite membrane', *J. Mem. Sci. 66 (1991) 129-141*

Shinji, O., et al. 'The dehydrogenation of cyclohexane by the use of a porous-glass reactor', *Bull. Chem. Soc. Jpn. 55 (1982) 2760-2764*

Shu, J., et al. 'Catalytic palladium-based membrane reactors: A review', *Can. J. Chem. Eng. 69 (1991) 1036-1060*

Shu, J., et al. 'Simultaneous deposition of Pd and Ag on porous stainless steel by electroless plating', *J. Mem. Sci. 77 (1993) 181-195*

Sircar, S. and Rao, M.B. 'Estimation of surface diffusion through porous media', *AIChE J. 36 (1990) 1249-1254*

Sladek, K.J., Gilliland, E.R. and Baddour, R.F. 'Diffusion on surfaces. II. Correlation of diffusivities of physically and chemically adsorbed species', *Ind. Eng. Chem. Fundam. 13 (1974) 100-105*

Sloot, H.J., et al. 'Surface diffusion of hydrogen sulphide and sulphur dioxide in alumina membranes in the continuum regime', *J. Mem. Sci. 74 (1992a) 263-278*

Sloot H.J., et al. 'High-temperature membrane reactor for catalytic gas-solid reactions', *AIChE J. 38 (1992b) 887-900*

Smith, R.K. and Metzner, A.B. 'Rates of surface migration of physically adsorbed gases', *J. Phy. Chem. 68 (1964) 2741-2747*

Struis, R.P.W.J., et al. 'A membrane reactor for methanol synthesis', *J. Mem. Sci. 113 (1996) 93-100*

Stull, D.R. et al. 'The chemical thermodynamics of organic compounds', *John Wiley & Sons, Inc. NEW YORK (1969)*

Sun, Y.M. and Khang, K.J. 'Catalytic membrane for simultaneous chemical reaction and separation applied to a dehydrogenation reaction', *Ind. Eng. Chem. Res. 27 (1988) 1136-1142*

Sun, Y.M. and Khang, K.J. 'A catalytic membrane reactor: Its performance in comparison with other types of reactors', *Ind. Eng. Chem. Res. 29 (1990) 232-238*

Suzuki, M. 'Adsorption Engineering', *Elsevier Science Publishers B.V. TOKYO (1990)*

Tekic, M.N., et al. 'Applicability of two membranes for improving performance of a membrane reactor', *J. Mem. Sci. 96 (1994) 213-222*

Tomlinson, R.H. and Flood, A.E. 'Flow of gases and vapours through adsorbing porous media' *Can. J. Res. B 26* (1948) 38-53

Tonkovich, A.L.Y., et al. 'Inorganic membrane reactors for the oxidative coupling of methane', *Chem. Eng. Sci. 51 (1996) 3051-3056*

Uemiya, S., et al. 'Steam reforming of methane in a hydrogen-permeable membrane reactor', *App. Cat. 67 (1991a) 223-230*

Uemiya, S., et al. 'Promotion of the conversion of propane to aromatics by use of a palladium membrane', *App. Cat. 76 (1991b) 171-181*

Uhlhorn, R.J.R., et al. 'Gas and surface diffusion in modified γ - alumina systems', *J. Mem. Sci. 46 (1989) 225-241*

Uhlhorn, R.J.R., et al. 'Gas transport and separation with ceramic membranes. Part I. Multilayer diffusion and capillary condensation', *J. Mem. Sci. 66 (1992) 259-269*

van den Berg, G.B. and Smolders, C.A. 'Diffusional phenomena in membrane separation processes', *J. Mem. Sci. 73 (1992) 103-118*

Weaver, J.A. and Metzner, A.B. 'The surface transport of adsorbed molecules', *AIChE J. 12 (1966) 655-661*

White, D.A., et al. 'Modelling gas separations through alumina-based membranes', *Gas. Sep. & Purif. 6 (1992) 197-200*

Wicke, E. and Kallenbach, R. 'Surface diffusion of carbon dioxide in activated charcoal', *Kolloid Z. 97 (1941) 135*

Winston Ho, W.S. and Sirkar, K.K. 'Membrane Handbook', *VAN NOSTRAND REINHOLD NEW YORK (1990)*

Wu, J.C.S., et al. 'Dehydrogenation of ethylbenzene to styrene using commercial ceramic membranes as reactors', *Sep. Sci. & Tech. 25 (1990) 1489-1510*

Yamasaki, A. and Inoue, H. 'Surface diffusion of organic vapour mixtures through porous glass', *J. Mem. Sci. 59 (1991) 233-248*

Yang, R.T., et al. 'Modification to the Higashi model for surface diffusion', *AIChE J. 19 (1973) 1052-1053*

Zaman, J. and Chakma, A. 'Inorganic membrane reactors', *J. Mem. Sci. 92 (1994) 1-28*

Zaspalis, V.T., et al. 'Reactions of methanol over alumina catalytically active membranes modified by silver', *App. Cat. 74 (1991a) 235-248*

Zaspalis, V.T., et al. 'Reactor studies using vanadia modified titania and alumina catalytically active membranes for the reduction of nitrogen oxide with ammonia', *App. Cat. 74 (1991b) 2349-160*

Ziaka, Z.D., et al. 'Propane dehydrogenation in a packed-bed membrane reactor', *AIChE J. 39 (1993) 526-529*

BIBL. LOUVAIN. UCL.